Copernicus Marine Service

QUALITY INFORMATION DOCUMENT

Mediterranean Sea Production Centre
MEDSEA_ANALYSISFORECAST_BGC_006_014

Issue: 3.1

Contributors: L. Feudale, A. Teruzzi, S. Salon, G. Bolzon, P. Lazzari, G. Coidessa, V. Di Biagio, E. Álvarez, C. Amadio, G. Cossarini

Approval date by the CMEMS product quality coordination team: 15/11/2023

CHANGE RECORD

When the quality of the products changes, the QuID is updated and a row is added to this table. The third column specifies which sections or sub-sections have been updated. The fourth column should mention the version of the product to which the change applies.

Issue	Date	§	Description of Change	Author	Validated By
1.0	31/08/2017	All	Release of V3.2 version of the Med-biogeochemistry at 1/24° resolution	G.Cossarini, S. Salon, G. Bolzon, A. Teruzzi, P. Lazzari, L. Feudale	
1.1	30/04/2018	All	Release of V4.1 version of the Med-biogeochemistry at 1/24° resolution	G.Cossarini, S. Salon, G. Bolzon, A. Teruzzi, P. Lazzari, L. Feudale	
1.2	27/01/2019	All	Release of version at Q2/2019 of the Med-biogeochemistry at 1/24° resolution with BFM version 5 and open boundary at Dardanelles	A. Teruzzi, G.Cossarini, S. Salon, G. Bolzon, P. Lazzari, L. Feudale	Mercator Ocean
1.3	06/12/2019	All	Release of version Q1/2020 of the Med-biogeochemistry at 1/24° resolution with BGC-Argo float assimilation	A. Teruzzi, G. Cossarini, L. Feudale, G. Bolzon, S. Salon	Mercator Ocean
2.0	15/01/2021	All	Release of version Q2/2021 of the Med-biogeochemistry with new products (silicate, ammonium and biomass of zooplankton) and new boundary condition in Atlantic	L. Feudale, A. Teruzzi, S. Salon, G. Bolzon, P. Lazzari, G. Coidessa, Di Biagio V., G. Cossarini	Emanuela Clementi (Med-MFC Deputy Leader)
2.1	03/09/2021	All	Release of version Q4/2021 of the Med-biogeochemistry with the addition of the daily discharges of nutrients and carbonate system variables for the Po River (Adriatic Sea)	L. Feudale, A. Teruzzi, S. Salon, G. Bolzon, P. Lazzari, G. Coidessa, Di Biagio V., G. Cossarini	Emanuela Clementi (Med-MFC Deputy Leader)
3.0	31/08/2022	All	Release of version Q4/2022 of the Med-biogeochemistry with the new optical component (OASIM atmospheric irradiance model and new BFM with multispectral radiative component), and assimilation of BGC-Argo oxygen	L. Feudale, A. Teruzzi, S. Salon, G. Bolzon, P. Lazzari, G. Coidessa, Di Biagio V., E. Álvarez, C. Amadio, G. Cossarini	Anna Chiara Goglio (Med-PQ responsible)

Issue	Date	§	Description of Change	Author	Validated By
3.1	15/06/2023	All	Release of version Q4/2023 of the Med-biogeochemistry with tuning of the bio-optical component and addition of PFTs chlorophyll and carbon biomass of 4 Phytoplankton Functional Types.	L. Feudale, A. Teruzzi, S. Salon, G. Bolzon, P. Lazzari, G. Coidessa, Di Biagio V., E. Álvarez, C. Amadio, G. Cossarini	Anna Chiara Goglio (Med-PQ responsible)

TABLE OF CONTENTS

I. EXECUTIVE SUMMARY

I.1. Products covered by this document

This document describes the quality of the product MEDSEA_ANALYSISFORECAST_BGC_006_014, the nominal product for the analysis and forecast of the biogeochemical state of the Mediterranean Sea. The MED Biogeochemistry product includes 2D and 3D daily and monthly fields at 1/24° horizontal resolution (which for the Mediterranean basin is about 4 km) of 15 variables grouped into 6 datasets:

PFTC: total chlorophyll, total phytoplankton carbon biomass, zooplankton carbon biomass, and chlorophyll and carbon biomass of 4 phytoplankton functional types (PFTs)

NUTR: phosphate, nitrate, ammonium and silicate;

BIOL: oxygen and primary production;

CARB: pH (reported on Total Scale), dissolved inorganic carbon and alkalinity;

CO2F: surface partial pressure of CO2 and surface CO2 flux.

OPT: light attenuation coefficient at 490 nm wavelength (Kd490)

This Copernicus Marine Service product can be acknowledged using the following citations:

Feudale, L., Bolzon, G., Lazzari, P., Salon, S., Teruzzi, A., Di Biagio, V., Coidessa, G., Álvarez, E., Amadio, C., & Cossarini, G. (2023). Mediterranean Sea Biogeochemical Analysis and Forecast (CMEMS MED-Biogeochemistry, MedBFM4 system) (Version 2) [Data set]. Copernicus Marine Service. https://doi.org/10.25423/CMCC/MEDSEA_ANALYSISFORECAST_BGC_006_014_MEDBFM4

Salon, S., Cossarini, G., Bolzon, G., Feudale, L., Lazzari, P., Teruzzi, A., Solidoro, C., Crise, A., 2019. Marine Ecosystem forecasts: skill performance of the CMEMS Mediterranean Sea model system. Ocean Sci. Discuss. 1–35. https://doi.org/10.5194/os-2018-145

I.2. Summary of the results

The quality of the product MEDSEA_ANALYSISFORECAST_BGC_006_014 for Mediterranean Sea biogeochemistry analysis and forecasts has been assessed over the period 1/1/2019-31/12/2019 by means of a comparison with observational in-situ datasets, semi-independent data (satellite and BGC-Argo float datasets used in the assimilation) and literature estimates. A detailed and scientific description of the MedBFM model system and of the validation framework can be found in Salon et al. (2019). The main results of the present quality product assessment are summarized in the following points:

Chlorophyll: Given as the mass concentration of chlorophyll a in sea water in the Copernicus Marine Service catalogue, with units [mg m^{-3}]. Results give evidence of the model capability of reproducing spatial patterns, seasonal cycles (surface winter bloom period), and the related vertical properties at mesoscale and weekly temporal scale. At the surface, the western open sea sub-basins are generally characterized by higher uncertainty and variability (estimated by RMSD) than the eastern ones, with a basin-averaged RMSD of 0.06 (0.01) mg m^{-3} in winter (summer). In coastal areas, the basin-averaged uncertainty increases to 0.30 (0.27) mg m^{-3} in winter (summer), with higher values in regions of

freshwater influence (ROFIs) and in areas affected by shelf dynamics. Overall, the model tends to underestimate the observed chlorophyll maxima. Comparisons with BGC-Argo float data demonstrate the model skill in reproducing the key physico-biogeochemical coupling mechanisms at mesoscale and the vertical dynamics. The mean RMSD of chlorophyll vertical profiles computed between model and BGC-Argo float observations is 0.06 mg m^{-3}. Further, to quantify the model skill to reproduce the chlorophyll key dynamic key properties we used some novel metrics: averaged chlorophyll content in the photic layer (0-200 m), depth of the deep chlorophyll maximum (DCM) and thickness of the winter bloom layer (WBL). In areas with a sufficiently high number of available float profiles per month, the RMSDs for averaged chlorophyll content in the photic layer, DCM and WBL are 0.03 mg m^{-3}, 8 m, andf 27 m, respectively.

Primary production: Provided as the net primary production of carbon per unit of volume in sea water with units of [mg m^{-3} day^{-1}]. Comparisons with available peer-reviewed publications show that the simulation consistently reproduces basin-scale and sub-basin-scale patterns and estimates.

Phytoplankton carbon biomass: Provided as carbon mole concentration of phytoplankton in sea water in the Copernicus Marine Service catalogue with units of [mmol m^{-3}]. It represents the sum of the carbon content of the four phytoplankton groups in the BFM model (diatoms, picophytoplankton, nanoflagellates and dinoflagellates). In this document, it is reported as [mgC/m^3] to facilitate direct comparisons with observations. Vertical profile shapes and values of particulate backscattering coefficient at 700 nm (bbp700) converted to carbon biomass provided by BGC-Argo optical data are reproduced satisfactorily by the model. The depth-averaged RMSD with respect to BGC-Argo data is 1.33 mg m^{-3} throughout the 0-200 m layer.

Zooplankton carbon biomass: Reported as the carbon mole concentration of zooplankton in sea water in the Copernicus Marine Service catalogue with units of [mmol m^{-3}]. It represents the sum of the carbon content of the four zooplankton groups in the BFM model (heterotrophic nano flagellates, microzooplankton, and 2 groups of mesozooplankton). In this document, the zooplankton carbon biomass is expressed as carbon mass per square meter for the layer 0-200 m [gC/m^2] to facilitate direct comparisons with observations. Observations tend to be scarce, offering sparse spatial coverage, and are typically reported as the integrated values in the layer 0-200 m. The model is able to reproduce the order of magnitude of this variable and the main spatial patterns inferred from estimates.

Phosphate: it is the mole concentration of phosphate expressed in [mmol m^{-3}]. RMSD at basin scale is 0.03 mmol m^{-3} in the upper 60 m and 0.03 mmol m^{-3} in the deeper layers. General basin-wide gradients and vertical profile shapes are simulated consistently with respect to observations, with model vertical profiles within the observed climatological variability.

Nitrate: Reported as the mole concentration of nitrate in units of [mmol m^{-3}]. The main horizontal spatial gradients (sub-basin wide patterns) and vertical patterns are well reproduced by the model: the sub-basin vertical profiles are within the observed climatological variability. RMSD at basin scale is 0.59 mmol m^{-3} in the upper 60 m and around 0.80 mmol m^{-3} in the deeper layers. Compared to BGC-Argo data the model consistently reproduces the key physico-biogeochemical coupling mechanisms at mesoscale and along the vertical dimension. Mean RMSD with respect to BGC-Argo vertical profiles is 0.44 mmol m^{-3}. Further, to quantify the model skill to reproduce key vertical characteristics we use 2 novel metrics: the averaged content of nitrate in the photic layer (0-200 m) and the depth of the nitracline. In areas with a sufficiently high number of available float profiles per month, RMSD for depth-averaged nitrate content is 0.22 mmol m^{-3} and RMSD for nitracline depth is 13 m.

Oxygen: Reported as the mole concentration of dissolved molecular oxygen in units of [mmol m^{-3}]. Compared to climatological vertical profiles, the basin-scale RMSD does not exceed 6 mmol m^{-3} in the first 100 m. Overall, model profiles are in fairly good agreement with climatologies (within the observed variability). Model outputs consistently reproduce the oxygen dynamics at the mesoscale and also the vertical properties, as shown by a comparison with BGC-Argo data. The overall RMSD is 5 mmol m^{-3}.

Ammonium: Reported as the mole concentration of ammonium expressed in [mmol m^{-3}]. The model successfully reproduces the orders of magnitudes of climatological vertical profiles used for comparisons, although surface horizontal patterns and some vertical profiles are not always well reproduced (the vertical mean RMSD is 0.32 mmol m^{-3}). This validation is affected by a limited availability of suitable observations.

Silicate: Reported as the mole concentration of silicate expressed in [mmol m^{-3}]. Basin vertical profiles are well simulated within the range of variability of the climatology, except in the western sub-basins where the model consistently overestimates surface concentrations.

pH: pH is reported in total scale, considering co-located conditions (i.e., of temperature, salinity and pressure). Averaged over all Mediterranean sub-basins, RMSD is 0.020, based on a comparison with reconstructed climatological vertical profiles.

Dissolved inorganic carbon (DIC): In the Copernicus Marine Service catalogue, DIC is reported in [mol m^{-3}], however, here we use units of [µmol kg^{-1}] to facilitate direct comparisons with in-situ observations (using sea water density for the unit conversion). Comparisons of model results with climatological vertical profile yield a basin-scale overall RMSD of around 18 µmol kg^{-1}.

Alkalinity: Alkalinity is reported in [µmol kg^{-1}] in this document, the common unit used to report in-situ observations. In the Copernicus Marine Service catalogue, alkalinity is expressed in [mol m^{-3}]. Overall RMSD is 19 µmol kg^{-1} with respect to reconstructed climatological vertical profiles in all Mediterranean sub-basins.

Surface partial pressure of CO2: This parameter is reported in units of Pascal [Pa] in the Copernicus Marine Service catalogue. Here, we report pCO2 in [µatm] using the conversion: 1 µatm = 101.325 kPa. RMSD is 23 µatm based on a comparison with climatological vertical profiles. With respect to the SPCAT dataset, RMSD of surface pCO2 is estimated as 42 µatm. Overall, the model is in good agreement with the observed seasonal cycles and spatial heterogeneities in all sub-basins.

Surface flux of CO2: This corresponds to the downward mass flux of carbon dioxide in units of [kg m^{-2} s^{-1}] (positive values representing a downward flux) in the Copernicus Marine Service catalogue. Here, report this variable in units of [mmol m^{-2} d^{-1}]. Based on a comparison with the climatology in von Schuckmann et al. (2018, Chapter 1.7) and other literature, the modelled CO2 flux estimates are consistent with spatial patterns seen in multi-decadal climatology .

Light attenuation coefficient at 490 nm (Kd490): This rate of attenuation is computed for the surface layer (first optical depth) and is provided in units of [m^{-1}]. RMSD with respect to Copernicus Marine Service Ocean Color estimates is 0.008 and 0.006 m^{-1} for winter and summer, respectively.

Phytoplankton functional types (PFTs): Chlorophyll is provided for 4 groups of phytoplankton (diatoms, nanophytoplankton, picophytoplankton, and dinoflagellates) in units of [mg CHLa m^{-3}]. Quality metrics

are estimated based on HPLC in situ data (i.e., pigment measurements). A visual comparison with the PTFs product derived from satellite data of Copernicus Marine Service Ocean Colour is also reported.

I.3. Estimated Accuracy Numbers

Tables I.1-5 report the estimated accuracy numbers (EANs) for the Mediterranean Biogeochemical modeling product. EANs are estimated as the overall RMSD for the entire Mediterranean Sea or as regional averages computed at the sub-basin level. EANs are computed for selected time periods (winter and summer) or spatial subdivisions (selected layers) when relevant. Further details of the validation can be found in Section IV.

Chlorophyll [mg/m³]		
	RMSD	
	winter	summer
OPEN SEA		
Mod-Sat	0.06	0.01
log_{10}(Mod)-log_{10}(Sat)	0.16	0.07
COASTAL AREAS		
Mod-Sat	0.30	0.27
log_{10}(Mod)-log_{10}(Sat)	0.23	0.22

Table I.1. *Mean RMSD of surface chlorophyll [mg m^{-3}] in open sea and coastal areas of the Mediterranean Sea. Winter corresponds to January to April and summer to June to September.*

	RMSD								
LAYERS (m)	**0-10**	**10-30**	**30-60**	**60-100**	**100-150**	**150-300**	**300-600**	**600-1000**	**Whole column (0-1000)**
PHOSPHATE [mmol/m³]	0.03	0.03	0.03	0.03	0.05	0.03	0.04	0.03	0.03
NITRATE [mmol/m³]	0.51	0.59	0.66	0.73	0.97	0.69	0.89	0.68	0.71
OXYGEN [mmol/m³]	5.53	5.15	5.63	3.76	6.11	5.68	6.88	5.98	5.59
AMMONIUM [mmol/m³]	0.38	0.19	0.15	0.24	0.31	0.32	0.43	0.55	0.32
SILICATE [mmol/m³]	0.65	0.69	0.55	0.51	0.81	0.83	0.72	0.65	0.68
DIC [µmol/kg]	34.0	30.6	24.1	16.4	14.3	8.2	11.0	4.1	17.86
Alkalinity [µmol/kg]	39.3	29.9	22.7	18.9	10.2	13.5	9.9	8.3	19.1
pH [-]	0.032	0.023	0.028	0.025	0.017	0.014	0.014	0.007	0.020

Table I.2. *Basin-scale mean RMSD for phosphate, nitrate, oxygen, ammonium, silicate, DIC, alkalinity and pH (based on in-situ condition) based on comparisons with reference vertical profile climatologies derived from in-situ observations.*

Variables	RMSD
Nitrate [mmol/m³] in the 0-200 m layer	0.43
Oxygen [mmol/m³] in the 0-150 m layer	5.2
Chlorophyll [mg/m³] in the 0-150 m layer	0.06
Phytoplankton carbon Biomass [mg/m3] for integral 0-200 m	1.33

Table I.3. *Basin-scale mean RMSD for nitrate, oxygen chlorophyll and phytoplankton carbon biomass estimated by comparing the model to vertical BGC-Argo profiles.*

Variables	RMSD [µatm]
EMODnet2018; pCO2 at 0-10 m	36.0
SOCAT v2; surface pCO2	42.4

Table I.4. *Basin-scale mean RMSD of partial pressure of carbon dioxide in seawater (pCO2) based on a comparison with a reference vertical profile climatology; surface basin-scale mean RMSD of pCO2 based on a comparison with SOCAT dataset.*

Light attenuation coefficient Kd490 [m^{-1}]		
OPEN SEA	**RMSD**	
	winter	**summer**
Mod-Sat	0.008	0.006
log_{10}(Mod)-log_{10}(Sat)	0.073	0.086

Table I.5. *Basin-scale mean RMSD of surface light attenuation coefficient at the 490 nm wavelength (Kd490) [m^{-1}] over the open sea of the Mediterranean Sea. Winter corresponds from January to April, summer corresponds from June to September.*

PFTs [mg m^{-3}]		
OPEN SEA data (vs HPLC)	**RMSD**	
0-150 m	**winter**	**summer**
Diatoms	0.07	0.06
Nanophytoplankton	0.10	0.06
Picophytoplankton	0.04	0.03
Dinoflagellates	0.01	0.02

Table I.6. *Basin-scale mean RMSD for chlorophyll a concentration [mg CHLa m^{-3}] in the top 150 m for each PFT compared with HPLC data over the open sea of the Mediterranean Sea. Winter corresponds to November- May; summer corresponds to June-October.*

II. PRODUCTION SYSTEM DESCRIPTION

II.1. Production centre details

Production centre: Istituto Nazionale di Oceanografia e di Geofisica Sperimentale - OGS (Italy) (Med-MFC; Production Unit: Med-BIO)
Production system name: Mediterranean Sea Biogeochemistry Analysis and Forecast (Copernicus Marine Service name: MEDSEA_ANALYSISFORECAST_BGC_006_014)

Description
The biogeochemical analysis and forecasts for the Mediterranean Sea at 1/24° horizontal resolution (ca. 4 km) are produced by means of the MedBFM4.0 model system. MedBFM4.0, which is run by OGS (IT), includes the transport model OGSTMv4.6 coupled with the biogeochemical flux model BFMv5.2, the variational data assimilation module 3DVarBio3.4, and the ocean-atmospheric spectral irradiance model OASIM. The biogeochemical MedBFM system, which is off-line coupled with the NEMO-OceanVar model (MEDSEA_ANALYSISFORECAST_PHY_006_013 product run by CMCC), produces seven days of analysis (weekly on Tuesday) with the assimilation of surface chlorophyll (CMEMS-OCTAC NRT product) and of vertical profiles of chlorophyll, nitrate and oxygen (BGC-Argo floats provided by CORIOLIS DAC). One day of hindcast and ten days of forecast are produced daily.
The analysis and forecast products are released after completion of the Med-PHY workflow (Fig II.1). On Tuesdays, the workflow consists of 7 days of analysis (-8 to -2), one day of hindcast (-1) and 10 days of forecast (0 to 9). From Wednesdays to Mondays, the workflow consists of one day of hindcast and 10 days of forecast. The data assimilation cycle (Tuesday run) uses the satellite chlorophyll (i.e., a composite average in the range of ±3 days) from 12:00 UTC of the Monday of the previous week (day -8) and the in situ vertical profiles of chlorophyll and nitrate from 12:00 UTC on day -8 to day -2. On day -8, independent satellite and float data assimilations are performed.

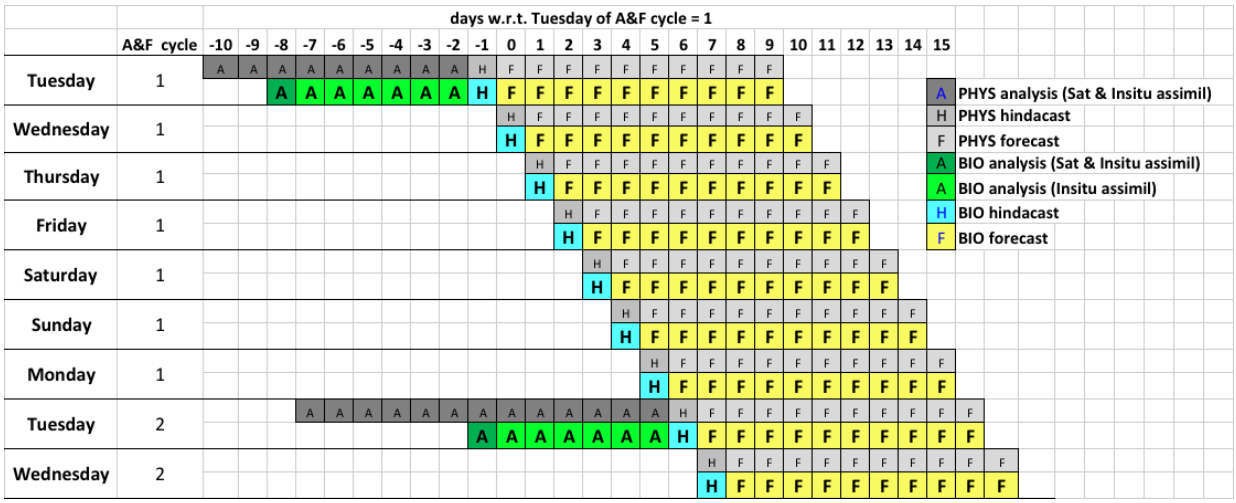

Figure II.1. *Schematic illustration of the Med-MFC-biogeochemistry system (Med-BIO) analysis and forecast workflow. Dark, intermediate, and light grey boxes represent the days of analysis, hindcast and forecast of the Med-PHY, respectively. Green, blue, and yellow boxes represent the days of analysis, hindcast and forecast of the Med-BIO workflow, respectively. The production week days when the workflow is executed are shown in the left column.*

II.2. Description of the MedBFM4.0 model system

The Med-biogeochemistry products are provided by the MedBFM version 4.0 model system. MedBFM4.0 consists of the coupled physical-biogeochemical OGSTM-BFM model, the ocean-atmospheric spectral irradiance model OASIM, and the 3DVarBio assimilation scheme (for more details, see Lazzari et al., 2010, 2012, 2016, 2021; Cossarini et al., 2015, 2019; Teruzzi et al., 2014, 2018, 2019; Salon et al., 2019; Álvarez et al., 2022). The OGSTM-BFM is designed with a transport model based on the OPA system and a biogeochemical reactor featuring the Biogeochemical Flux Model (BFM), while 3DVarBio is the data assimilation scheme for the correction of phytoplankton functional type and nutrient (i.e., nitrate and phosphate) variables using surface chlorophyll from satellite observations and vertical profiles of chlorophyll and nitrate from BGC-Argo floats (Fig.II.2).

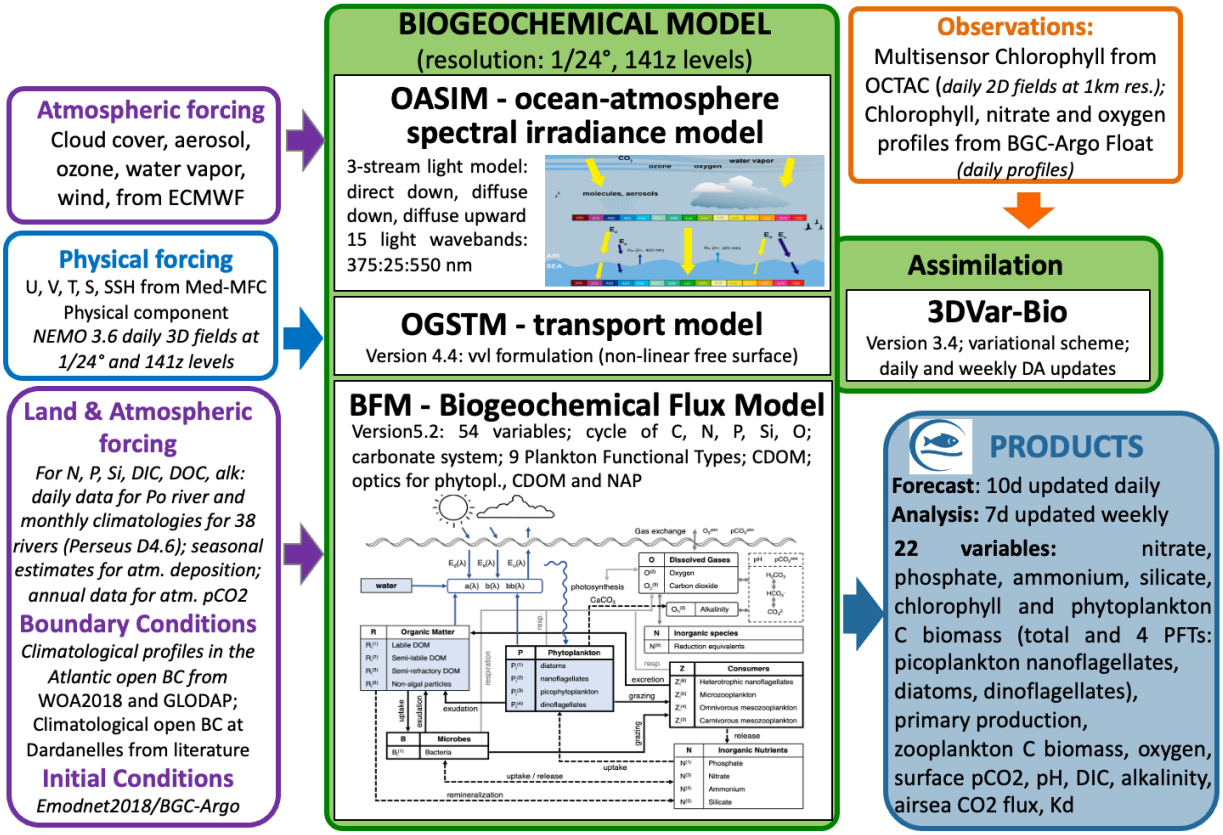

Figure II.2. *The MedBFM model system, dependencies, input data and interfaces with other components of the Copernicus Marine Service.*

The Ocean-Atmosphere Spectral Irradiance Model (OASIM; Gregg and Casey, 2009; Lazzari et al., 2021) resolves the propagation of the downward spectral radiance in the atmosphere and provides the direct and diffuse irradiance over the ocean surface. The novel bio-optical formulation in BFM includes a multispectral primary production module based on photosynthetic absorption and maximum quantum yield parameterization (Dutkiewicz et al., 2015; Álvarez et al., 2022; 2023). CDOM is separated in three pools, labile, semi-labile and semi-refractory, with specific production and degradation time scales, including photobleaching process (Lazzari et al., 2021). The three pools of CDOM have the same production and metabolization rates of the three corresponding DOC pools already present in BFM. Indeed, the CDOM is produced as a fixed quota of DOC, and CDOM is subject to photo-bleaching.

The OGSTMv4.6 is the physical model that resolves the transport of the tracers and the multispectral radiative transfer along the water column. The transport model is a modified version of the OPA 8.1 transport model (Foujols et al., 2000), which resolves the advection, the vertical diffusion and the sinking terms of tracers (biogeochemical variables). Details about horizonal and vertical resolution, coupling with Med-PHY physical forcings and main features of the biogeochemical reactor BFM (Fig. II.3) are provided in Salon et al. (2019).

The BFM model is also coupled to a carbonate system model (Cossarini et al., 2015, Melaku Canu et al., 2015), which consists of three prognostic state variables: alkalinity (ALK), dissolved inorganic carbon (DIC), and particulate inorganic carbon (PIC) which are driven by biological processes (i.e., photosynthesis, respiration, precipitation and dissolution of CaCO3, nitrification, denitrification, and uptake and release of nitrate, ammonia and phosphate by plankton) and physical processes (exchanges at air-sea interface and dilution-concentration due to evaporation minus precipitation process).

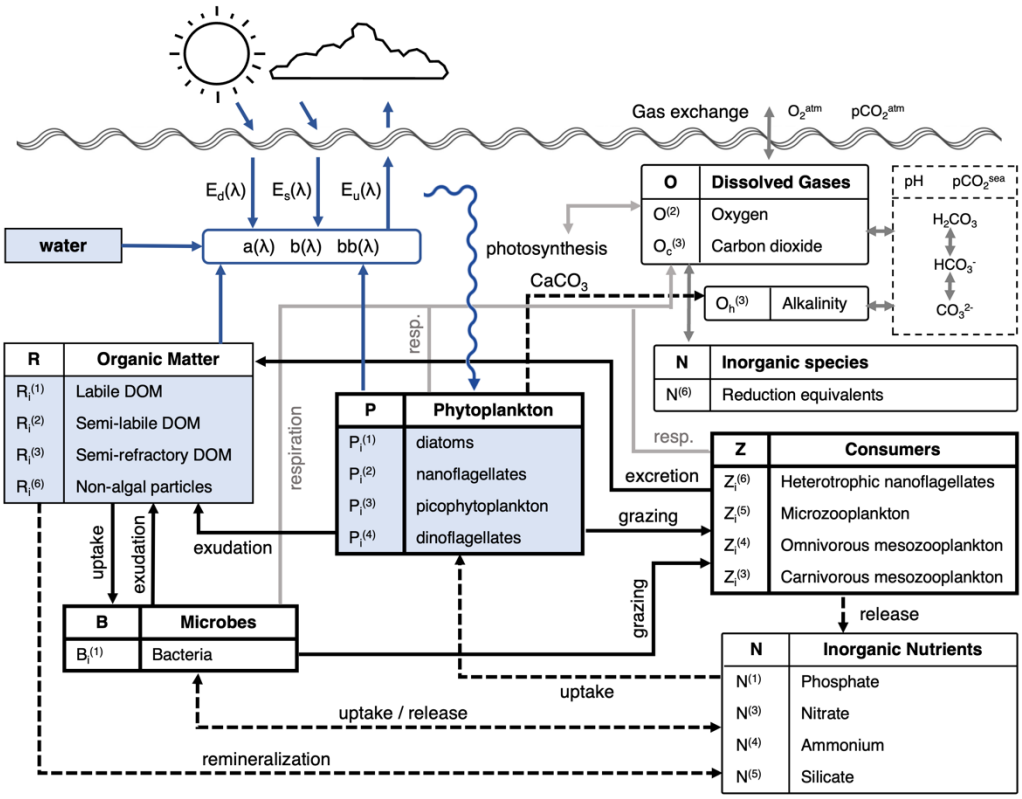

Figure II.3. *Scheme of the state variables and significant processes of the upgraded Biogeochemical Flux Model (BFM) version 5.2 including the new optical component.*

II.3. Description of the Data Assimilation scheme

The data assimilation of the surface chlorophyll concentration and of the vertical in situ profiles of chlorophyll and nitrate is performed through a variational scheme (3DVAR-BIOv3.3) during the 7 days of analysis of the Tuesday run of Fig. II.1 (for more details on 3DVarBio see Teruzzi et al., 2014, 2018, 2019,

2021 and Cossarini et al., 2019). The surface chlorophyll concentration is provided by satellite observations produced by the OCTAC; the in situ vertical profiles of chlorophyll, nitrate and oxygen are provided by BGC-Argo floats data made available by CORIOLIS DAC.

The data assimilation corrects the four phytoplankton functional groups (17 state variables including carbon, chlorophyll, nitrogen phosphorus and silicon internal quotas), two nutrients (i.e., phosphate and nitrate) and oxygen in the BFM.

The operational workflow of the analysis run (the Tuesday row in Fig. II.1) consists of a sequence of seven days of assimilation: the satellite surface chlorophyll map (i.e., a composite average in the range of ±3 days) is assimilated at 12:00 UTC of the previous Monday (i.e., day -8) and the in situ vertical profiles of chlorophyll and nitrate are assimilated from 12:00 UTC on day -8 to day -2. A pre-processing quality control is applied prior of the assimilation (Teruzzi et al., 2021; Amadio et al., 2023).

II.4. Upstream data and boundary conditions

The Med-MFC-Biogeochemistry system uses the following upstream data:

1. Initial conditions of biogeochemical variables are set as sub-basin (Fig. III.1) climatological profiles from a dataset (EMODnet2018_int) that integrates the in-situ aggregated EMODnet data collections (Buga et al., 2018) and the datasets listed in Lazzari et al. (2016) and Cossarini et al. (2015). A spin-up period (2 years) is carried out to reach the start date of the simulation (01/01/2019).
2. The physical ocean (current, temperature, salinity, vertical eddy diffusivity, SSH) and atmospheric (short wave radiation and wind stress) forcing daily fields are obtained from MEDSEA_ANALYSISFORECAST_PHY_006_013 produced by Med-PHY.
3. Surface chlorophyll and K_d are obtained from the satellite multi-sensor product OCEANCOLOUR_MED_CHL_L3_NRT_OBSERVATIONS_009_040 (i.e., a merged product of MODIS-AQUA, NOAA20-VIIRS, NPP-VIIRS and Sentinel3A-OLCI sensors).
4. The in situ vertical BGC-Argo profiles of chlorophyll, nitrate, oxygen, pH, biomass of phytoplankton are obtained from Coriolis Data Assembly Center (as described in Bittig et al., 2019) after QC procedures described before (II.3) and visual check.
5. The biogeochemical open boundary conditions in the Atlantic Ocean at the longitude of 9°W are provided through a Dirichlet-type scheme. Climatological profiles of phosphate, nitrate, silicate, dissolved oxygen are computed averaging the World Ocean Atlas 2018 data (Garcia et al., 2018; data from https://www.nodc.noaa.gov/OC5/woa18) for the area between 8°W-9°W and 34°N-37°N. Nitrate and phosphate profiles are revised to maintain an N:P ratio of 5 and 17 in the surface and subsurface layers, respectively. The oxygen profile unit was converted in mmol m^{-3} by using the seawater density profile computed from temperature and salinity data provided by the World Ocean Atlas 2018. Climatological profiles of DIC and Alkalinity are derived from the GLODAP v2 dataset (Olsen et al., 2016, 2019; data from https://www.nodc.noaa.gov/ocads/oceans/GLODAPv2_2019/) by averaging the available in situ observations in the area between 8°W-10°W and 34°N-37°N. A nudging scheme is applied between 9°W-7°W using the same profiles to avoid numerical instability
6. The biogeochemical open boundary conditions at the Dardanelles Strait are provided through a Dirichlet-type scheme. The values of nitrate, phosphate, silicate, DIC, alkalinity at the open boundary are set to constant values using literature information (Yalcin et al., 2017; Tugrul et al., 2002; Souvermezoglou et al., 2014; Copin, 1993; Schneider et al., 2007) after a tuning based on the consistency of modelled fluxes with published flux estimates (Perseus D4.6; Yalcin et al., 2017; Tugrul et al. 2002; Copin, 1993) and modelled tracer concentrations in the northern Aegean Sea

with published observations (Souvermezoglou et al., 2014; Krasakopoulou et al., 2017). A radiative condition at the open boundary is set for the other BFM tracers.

7. Atmospheric deposition rates of inorganic nitrogen and phosphorus were set according to the synthesis proposed by Ribera d'Alcalà et al. (2003) and based on measurements of field data (Loye-Pilot et al., 1990; Guerzoni et al., 1999; Herut and Krom, 1996; Cornell et al., 1995; Bergametti et al., 1992). Atmospheric deposition rates of nitrate and phosphate were assumed to be constant in time during the simulation year, but with different values for the western (580 Kt N yr^{-1} and 16 Kt P yr^{-1}) and eastern (558 Kt N yr^{-1} and 21 Kt P yr^{-1}) sub-basins. The rates were calculated by averaging the "low" and "high" estimates reported by Ribera d'Alcalà et al. (2003).
8. Terrestrial inputs of nutrient (N and P) and carbonate system variables (ALK and DIC) occur via 39 rivers (Fig. III.1), they include the Nile, Vjosë, Seman, Buna/Bojana, Piave, Tagliamento, Soca/Isonzo, Livenza, Brenta-Bacchiglione, Adige, Lika, Reno, Krka, Arno, Nerveta, Aude, Trebisjnica, Tevere/Tiber, Mati, Volturno, Shkumbini, Struma/Strymonas, Meric/Evros/Maritsa, Axios/Vadar, Arachtos, Pinios, Acheloos, Gediz, Buyuk Menderes, Kopru, Manavgat, Seyhan, Ceyhan, Gosku, Medjerda, Asi/Orontes. For all rivers except the Po River in Adriatic Sea, nitrogen and phosphorus climatological discharges (average of the 2000-2015 period) with a monthly modulation based on the monthly run-off are from the PERSEUS FP7-287600 project dataset (deliverable D4.6), while climatological monthly discharges of alkalinity and DIC are derived considering their typical concentrations per fresh water mass in macro coastal areas of the Mediterranean Sea (Copin, 1993; Meybeck and Ragu, 1995; Kempe et al., 1991) and the climatological monthly river water discharges from the PERSEUS dataset (Deliverable D4.6). For the Po River, daily discharges of nutrient (N and P) and carbonate system variables (ALK and DIC) are derived from daily run-off observations (data from ARPAE regional environmental protection agency; the same data is used by Med-PHY) multiplied by the typical concentrations of the biogeochemical tracers, derived from PERSEUS dataset and aforementioned references.
9. Atmospheric pCO2 concentration is set to the yearly average measured at Lampedusa station (Artuso et al., 2009) between 1992 and 2018 (http://cdiac.ess-dive.lbl.gov/ftp/trends/co2/lampedus.co2) with present-day values extrapolated via linear regression.
10. Surface evaporation-precipitation effects on dilution and concentration of tracers at surface are directly computed by OGSTM through the non-linear free-surface z*-coordinate configuration and using directly the sea surface anomaly evolution provided by the NEMO3.6 output.
11. The OASIM model requires ECMWF, ERA5 and MODIS derived data to resolve light propagation from the top of the atmosphere to sea surface level. Data are from operational analysis every 6 h and 0.10° horizontal-resolution and forecast fields from ECMWF distributed by the Italian National Meteo Service (USAM/CNMA). List of variables includes cloud cover, surface pressure, mean sea level atmospheric pressure, wind speed, and 2 m dew point temperature and 2m temperature to compute water vapour pressure and relative humidity. Precipitable water is derived from surface pressure, mean sea level atmospheric pressure and water vapour pressure. Total column cloud liquid water and total column ozone are derived as monthly climatology using 2011-2029 ERA5 reanalysis single levels data at 0.5 degree horizontal resolution. Aerosol optical thickness, asymmetry parameter, single scattering albedo, cloud droplet effective radius are derived as monthly climatology from 2011-2020 MODIS data at 1 degree horizontal resolution.

III. VALIDATION FRAMEWORK

The Med-MFC analysis and forecast system is validated using a 1-year qualification period from 1-Jan-2019 to 31-Dec-2019. Assessed products are total chlorophyll, total phytoplankton carbon biomass, chlorophyll of 4 PFTs (picoplankton, nanoflagellates, diatoms and dinoflagellates), zooplankton carbon biomass, net primary production, phosphate, nitrate, ammonium, silicate, oxygen, pH, pCO2, DIC, alkalinity and surface flux of CO2, and Kd490.
Data availability represents an important constrain in biogeochemical model validation (Salon et al., 2019): depending on the variables, different uncertainty levels can be provided on the basis of the availability of reference data. Thus, the validation analysis provides a "degree of confirmation" (Oreskes et al., 1994) with respect to the different scales of variability derived from the available observations.
Three different levels of validation are presented for the model variables:

(1) model capability to reproduce basin wide spatial gradients, mean annual values in sub-basin and average vertical profiles based on GODAE Class1 metrics (level-1);
(2) model capability to reproduce the variability due to mesoscale and daily dynamics based on GODAE Class4 metrics (level-2; Hernandez et al., 2018);
(3) model capability to reproduce key biogeochemical processes based on specific metrics (level-3; Salon et al., 2019).

Almost all variables are validated with GODAE class1 metrics using a reference climatology based on available in situ data (i.e., reference mean annual vertical profiles for the 16 sub-basins, Appendix A) or literature reviews (level-1). Only chlorophyll, nitrate and oxygen can be validated with NRT observations (satellite and BGC-Argo floats) available for the year 2019 (levels 2 and 3). Validation of phytoplankton carbon biomass, that uses BGC-Argo data, should be considered cautiously due to the uncertainty of the bbp700 – phytoplankton biomass relationship and the relatively low availability of BGC-Argo optical sensors.

Model chlorophyll data are compared with multi-sensor satellite chlorophyll from Copernicus Marine Service OCTAC OCEANCOLOUR_MED_CHL_L3_NRT_OBSERVATIONS_009_040 using metrics that refer to the "misfits" computed as the differences between satellite chlorophyll (7-day composite maps) and the model output before data assimilation (every 7 days). Thus, model skill after seven days of free simulation are reported as BIAS and RMSD time series for each sub-basin (Fig. III.1). Chlorophyll model outputs are also compared with BGC-Argo data (Fig. III.4) before data assimilation. BIAS, RMSD, correlation, and other metrics (e.g., DCM depth, total content in the 0-200 m layer and thickness of the layer of the winter bloom) of model output co-located with respect to BGC-Argo profiles are reported as time series for selected layers (Table III.1) and sub-basins (Fig. III.1) and as average statistics computed from all matching model-observation pairs.

Model net primary production data are compared with multi-annual simulations (Lazzari et al., 2012), satellite models (Bosc et al., 2004; Colella, 2006), and in-situ estimates (Siokou-Frangou et al., 2010).

Model phosphate, nitrate, ammonium, silicate, dissolved oxygen, DIC, alkalinity, pH in total scale and pCO2 data are compared with EMODnet_int climatology, i.e., aggregated EMODnet dataset (Buga et al., 2018) and datasets listed in Lazzari et al. (2016) and Cossarini et al. (2015) (see summary in Tables III.2 and 3). The validation of model variables considers consistency both with the vertical profiles for each sub-basin and with reference values at the layers listed in Table III.1. The product quality metric is the RMSD between the model and climatology. An additional qualitative comparison for nitrate and phosphate is performed using the World Ocean Atlas (WOA2013) climatological dataset. Regarding the carbonate system variables, the most observed variables are DIC and alkalinity (about 5300

observations), while pH was collected only in less than 30% of the samplings. Thus, pH and pCO2 have been reconstructed using CO2sys software (Lewis and Wallace, 1998) with available DIC, ALK and other regulatory information (i.e., temperature, salinity and concentration of phosphate and silicate).

Nitrate and dissolved oxygen model outputs are also compared with BGC-Argo floats data (Fig. III.4) to compute BIAS, RMSD, correlation and other metrics (vertically integrated values and depth of nutricline) between BGC-Argo profiles and the model output profiles before the data assimilation. The metrics are reported as time series for selected layers (Table III.1); and for sub-basins (Fig. III.1); and as average statistics computed from all the matching pairs of model and observation profiles for each sub-basin.

Phytoplankton biomass expressed as carbon is compared with BGC-Argo floats dataset of bbp700 from Coriolis DAC (Schmechtig et al., 2018). Data of bbp700 is converted to carbon biomass using the relationship proposed by Bellacicco et al. (2019). Given the scarce and sparse availability of such optical measurements and the uncertainty of the optical-biomass relationship only an indicative value can be provided by this level-2 validation framework.

Zooplankton biomass expressed as carbon is the total carbon content of all four zooplankton groups (heterotrophic nano flagellates, microzooplankton and 2 groups of mesozooplankton). As there are only very few estimations in the literature, this validation should be considered with caution. Most of observations are reported as integrated values over the top 200 m.

pCO2 has been validated with the SOCAT v6 Data Collection (Bakker et al., 2016). The dataset consists of 6500 observations of surface ocean fugacity (fCO2) in the Mediterranean Sea covering the period 1998-2016 (Fig. III.5). Fugacity measurements are converted to partial pressure measurements using the standard formula (Weiss, 1974; Wanninkhof, 2014). They do not equally cover all Mediterranean sub-basins and temporal coverage is limited up to 2016. Therefore, we calculated monthly climatologies for each sub-basin (although only 10 out of 16 sub-basins have reliable data) which are used to calculate RSMD.

Surface flux of CO2 has been validated through comparisons with published maps of mean annual values (von Schuckmann et al., 2018).

Diffuse attenuation coefficient for downwelling irradiance at the 490 nm wavelength (Kd490) is compared with multi-sensor satellite Kd490 from the Copernicus Marine Service OCTAC OCEANCOLOUR_MED_CHL_L3_NRT_OBSERVATIONS_009_040. Statistics are computed for each of the 16 sub-basins and reported in terms of RMSD and BIAS for the winter and summer periods.
Statistics are computed either on natural or logarithmic data to account for possible non-Gaussian distributions.

Model PFTs are compared quantitatively with in situ data and qualitatively (“class 1”) with the following PFT products derived from satellite multisensor data:

- The OCEANCOLOUR_MED_BGC_L3_MY_009_143 dataset for visual comparisons of PFT time series.
- An in situ HPLC climatology from the aggregated MAREDAT pigments dataset (Peloquin et al., 2013) and datasets listed in (Álvarez et al., 2022) and in the PERSEUS repository (Table III.4 and Figure III.6) are used to quantitatively validate the model. Model skill is assessed by comparing model average vertical profiles to in situ climatological profiles in two seasons (winter: 13 Nov-14 May and summer: 15 May-12 Nov) in all 16 sub-basins (Fig. III.1) and vertical layers in the upper 150 m (Tab. III. 1).

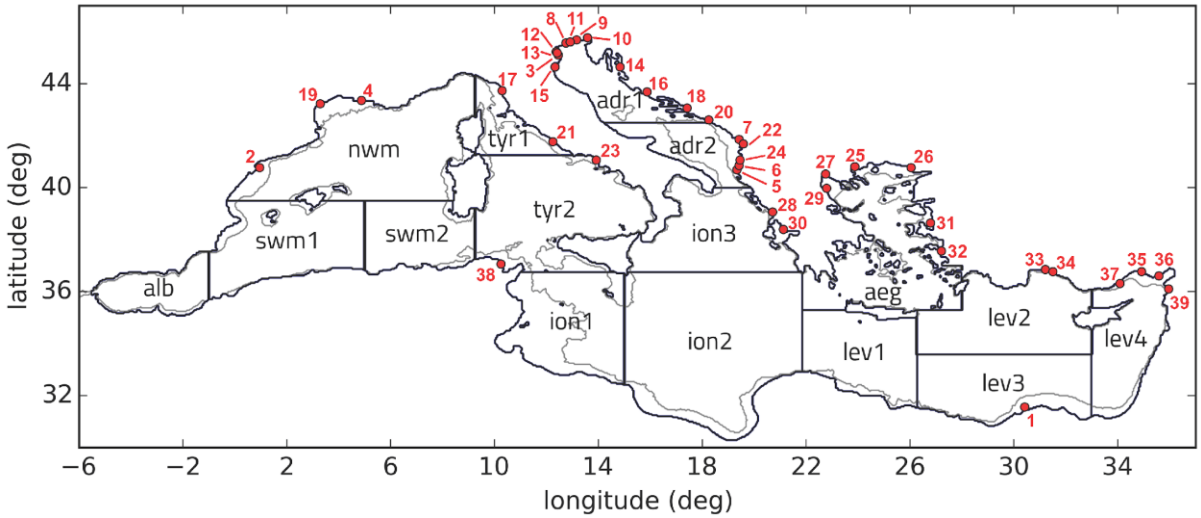

Figure III.1. *Subdivision of the model domain into sub-basins used for the regional model qualification. According to data availability and to ensure consistency and robustness of the metrics, different subsets of the sub-basins or some combinations among them can be used for the different metrics: lev = lev1+lev2+lev3+lev4; ion = ion1+ion2+ion3; tyr = tyr1+tyr2; adr = adr1+adr2; swm = swm1+swm2. The grey line shows the 200 m isobath. Red dots with numbers correspond to main river inflows: Nile (1), Ebro (2), Po (3), Rhone (4), Vjosë (5), Seman (6), Buna/Bojana (7), Piave (8), Tagliamento (9), Soca/Isonzo (10), Livenza (11), Brenta-Bacchiglione (12), Adige (13), Lika (14), Reno (15), Krka (16), Arno (17), Nerveta (18), Aude (19), Trebisjnica (20), Tevere (21), Mati (22), Volturno (23), Shkumbini (24), Struma/Strymonas (25), Meric/Evros/Maritsa (26), Axios/Vadar (27), Arachtos (28), Pinios (29), Acheloos (30), Gediz (31), Buyuk Menderes (32), Kopru (33), Manavgat (34), Seyhan (35), Ceyhan (36), Gosku (37), Medjerda (38), Asi/Orontes (39).*

Layer 1	Layer 2	Layer 3	Layer 4	Layer 5	Layer 6	Layer 7	Layer 8
0-10	10-30	30-60	60-100	100-150	150-300	300-600	600-1000

Table III.1. *Vertical layers (in m) considered for the model validation.*

Dataset name	Period	Area
EMODnet (2018)	**1997-2016**	**Mediterranean**
SINAPSI 3,4	2002-2003	Eastern Med.
JGOFS-FRANCE	1999	Western Med.
BIOPT 6	2006	Eastern Med.
DYFAMED	1998-2007	North-Western Med.
RHOFI 3,2,1	2001-2003	Ligurian Sea
NORBAL 1, 2, 3, 4	2000-2003	Algerian Sea
CIESM SP1,SP2,SP3	1998-2006	Mediterranean
MELISSA	2004, 2007	Western Med.
MEDGOOS 2, 3, 4, 5	2001-2002	Mediterranean
METEOR 51	2001	Western Med.
REGINA MARIS, GARCIA DEL CID	Apr, Sep 2008	Alboran Sea
SESAME ADRIATIC SEA	Apr, Sep 2008	Adriatic Sea
CARBOGIB 01,02,03,04,05,06	2005-2006	Alboran Sea, Gibraltar Strait
METEOR 84/3	2011	Mediterranean

Table III.2. *Nutrient and oxygen dataset EMODnet2018_int: combining the aggregated EMODnet data collections (Buga et al., 2018) and the datasets listed in Lazzari et al. (2016).*

Name	Variables	Period	Location	# data	Reference
METEOR51	DIC, ALK, anc. vars	Oct-Nov 2001	TransMed	253	Schneider et al., 2007
BUOM2008	DIC, ALK, anc. vars	June-July 2008	TransMed	567	Touratier et al., 2011
PROSOPE	DIC, pH@25, anc. vars	Sep-Oct 1999	West Med	188	Begovic and Copin, 2013
METEOR 84/3	DIC, ALK, pH@25, anc. vars	Apr 2011	TransMed	845	Tanhua, et al., 2012.
SESAME-EGEO	DIC, ALK, T,S	Apr and Sep 2008	Aegean Sea	265	http://isramar.ocean.org.il/PERSEUS_Data/
SESAME regina_maris	ALK, pH@25, anc. vars	Apr 2008	Alboran Sea	254	http://isramar.ocean.org.il/PERSEUS_Data/
SESAME Garcia del Cid	ALK, pH@25, anc. vars	Sep 2008	Alboran Sea	331	http://isramar.ocean.org.il/PERSEUS_Data/
SESAME Adriatic	ALK, pH@25, anc. vars	Apr and Sep 2008	Adriatic Sea	333	http://isramar.ocean.org.il/PERSEUS_Data/
CARBOGIB	ALK, DIC, pH@25, anc. vars	May, Sept, Dec 2005; Mar, May, Dec 2006	Alboran Sea	229	Huertas, 2007a
GIFT	ALK, DIC, pH@25, anc. vars	Jun, Nov 2005	Alboran Sea	30	Huertas, 2007b
DYFAMED Station	ALK, DIC	Almost monthly from 1999 to 2004	North West Med	707	Copin-Montegut and Begovic, 2002
MEDSEA 2013	DIC, ALK, T,S	May 2013	TransMed	462	Goyet et al., 2015
MOOSE dyfamed MOOSE-GE 2013-2016	DIC, ALK, T,S	2013-2016	North West Med	700	EMODnet, 2018

Table III.3. *Dissolved inorganic carbon, alkalinity, pH and pCO2 dataset EMODnet2018_int: combining the aggregated EMODnet data collections (Buga et al., 2018) and the datasets listed in Cossarini et al. (2015). "TransMed" refers to the scientific cruise of the same name; "anc. vars" refers to ancillary variables (T, S); "pH@25" refers to pH reported at 25°C.*

Dataset name	Period	Repository	Reference
MAREDAT pigments	1991-2005	PANGAEA	(Peloquin et al., 2013)
TARA Oceans	2009	SeaBASS	(Boss & Claustre, 2012)
TARA Mediterranean	2014	SeaBASS	(Boss & Claustre, 2014)
BOUM2008	2008	SeaBASS	(Behrenfeld & Dall´Olmo, 2020)
BOUSSOLE Station	2001-2020	obs-vlfr.fr	(Antoine & Vellucci, 2021)
SESAME project	2008	PERSEUS	http://isramar.ocean.org.il/PERSEUS_Data/

Table III.4. *HPLC dataset containing pigment measurements and total Chl-a concentrations. The chlorophyll concentration of the 4 PFTs have been calculated using the algorithm in DiCicco et al. (2017).*

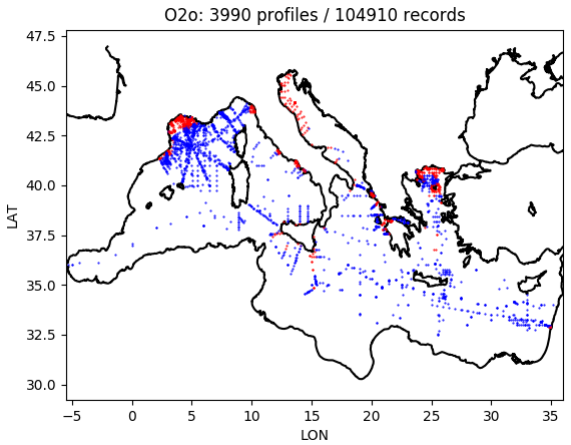

Figure III.2. *Map of oxygen sampling locations in EMODnet2018_int dataset. Nutrients (with the exception of ammonium) have similar maps. Blue dots represent the open sea data used to build climatologies.*

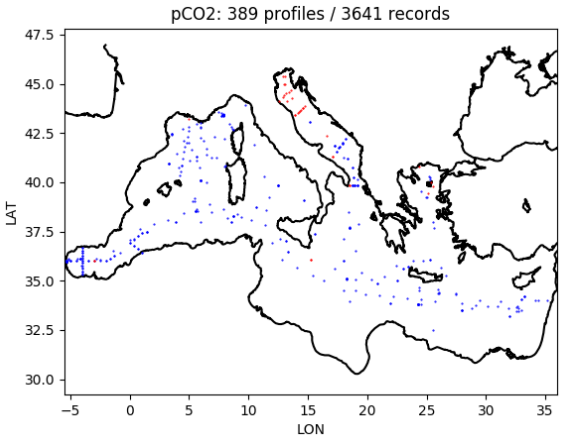

Figure III.3. *Map of alkalinity observations in the EMODnet2018_int dataset. DIC, pH, and pCO2 have similar maps. Blue dots represent the open sea data used to build climatologies.*

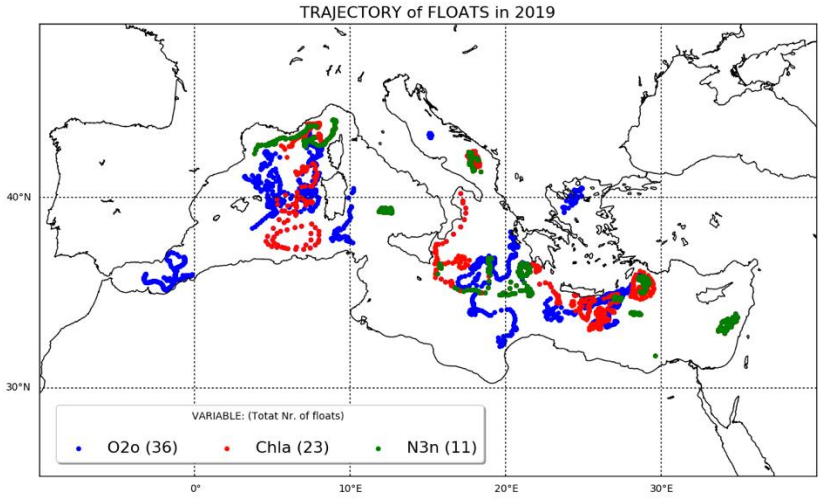

Figure III.4. *Trajectories of 47 BGC-Argo floats in 2019 (i.e., 36 oxygen, 23 chlorophyll and 11 nitrate sensors). Data quality described in Section II.3.*

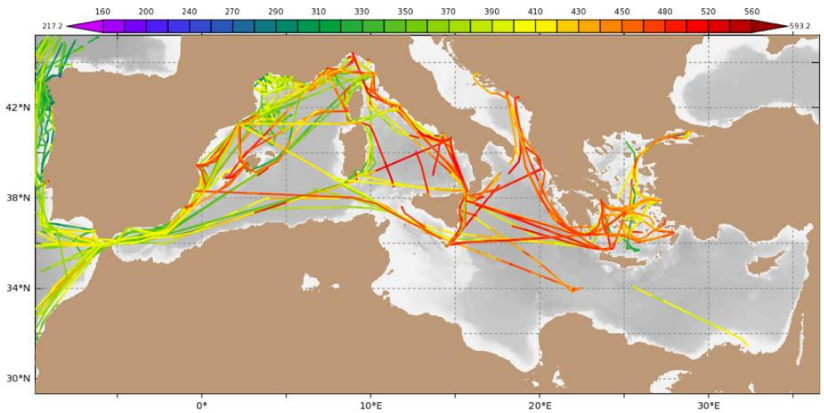

Figure III.5. Map of surface fCO2 observations from the SOCAT dataset for the period 1998-2016.

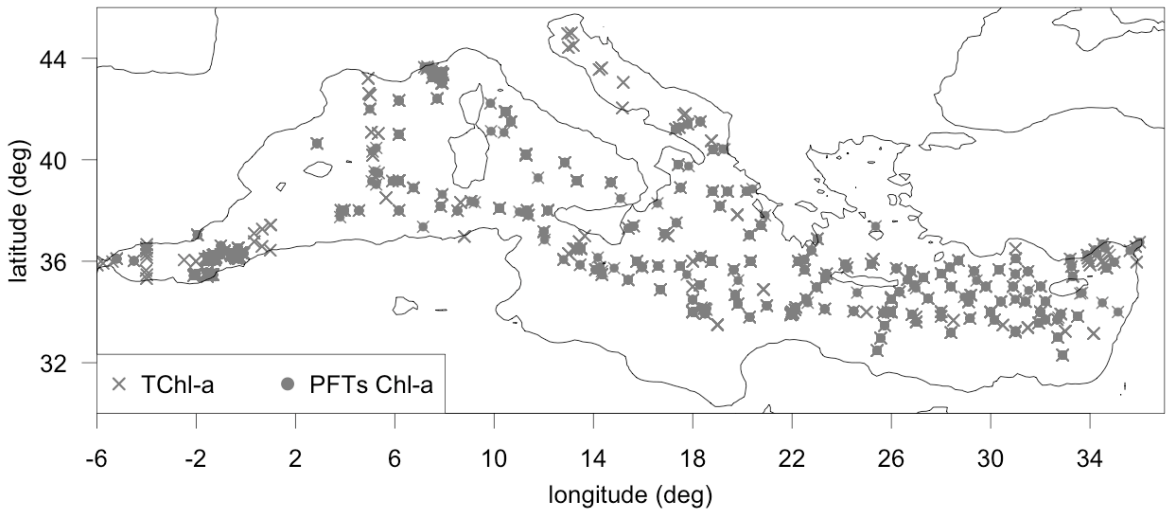

Figure III.6. Map of total chlorophyll data and chlorophyll for the 4 PFTs in the HPLC dataset (see Table III.4).

IV. VALIDATION RESULTS

IV.1. Chlorophyll

The comparison between annual average of modelled surface chlorophyll (Fig IV.1.1 top) with satellite data (Fig. IV.1.1 middle) shows that the model correctly reproduces the basin-wide zonal gradient, the spatial heterogeneity at the subbasin scale and the coastal-off shore pattern in ROFIs (Po, Rhone, Ebro and the Nile), the external inflow into the straits (Gibiltar and Dardanelles) and shallow eutrophic areas (Gulf of Gabes). However these areas and the Western Mediterranea in general show higher RMSD (Fig IV.1.1 bottom). Also the temporal evolution of the blooms is quite well captured in the different regions (Fig IV.1.2). Time series of BIAS and RMS of the differences are plotted in Fig. IV.1.3 for selected sub-basins. Their seasonal averages, which are computed for both log-transformed and natural values, are reported in Tables IV.1.1 and IV.1.2 for open sea and coastal areas, respectively. The coastal areas limit is defined by the model grid isobath at 200 m. It is well known that The western Mediterranean sub-basins are typically characterized by higher Chl concentrations and more pronounced seasonal cycles than the eastern ones (Colella et al., 2016). These regional differences are well reprocured in the model runs and are consistent with satellite observations (Tab. IV.1.1 and IV.1.2).

RMSD is higher in the open sea areas of the western sub-basins (Fig. IV.1.3) with values exceeding 10 mg/m^3, particularly in regions with a high natural variability (ALB, NWM, SWM2) (Tab. IV.1). In general, uncertainties are slightly higher during winter (Fig. IV.3 and Table IV.1) because the variability of the chlorophyll is also higher in winter. RMSD for the entire Mediterranean is 0.06 and 0.01 mg/m^3 for winter and summer, respectively, while BIAS is 0.03 mg/m^3 in winter and below 0.005 mg/m^3 in summer (Tab. IV.1).

Since the version Q2/2018, the MedBFM system assimilates chlorophyll data on both coastal and open-sea areas. Thus, MedBFM provides a good model performance also in the coastal areas (see Tab. IV.1.2). In these areas, the mean RMSD is about 0.30 mg/m^3 for winter and 0.27 mg/m^3 for summer. The coastal areas with the highest RMSD are the Adriatic Sea (ADR1; climatological land nutrient input – except from Po – might fail to reproduce high temporal dynamics of local blooms), the southern Ionian (ION1; high uncertainty in the areas of the Gabes Gulf in summer), and the southern and eastern Levantine (LEV3 and LEV4, possible underestimation of the local fertilization effect of the Nile input along the south-eastern levantine coastal zone indicates a possible underestimation of the nutrient input from the PERSEUS project dataset).

Fig. IV.1.1 (bottom) shows that the grid cells with the highest RMSD are located in coastal (see above) and transitional areas (i.e., Alboran Sea, western Sicily channel), and in areas characterized by surface winter blooms (e.g., Gulf of Lion, Rhodes gyre).

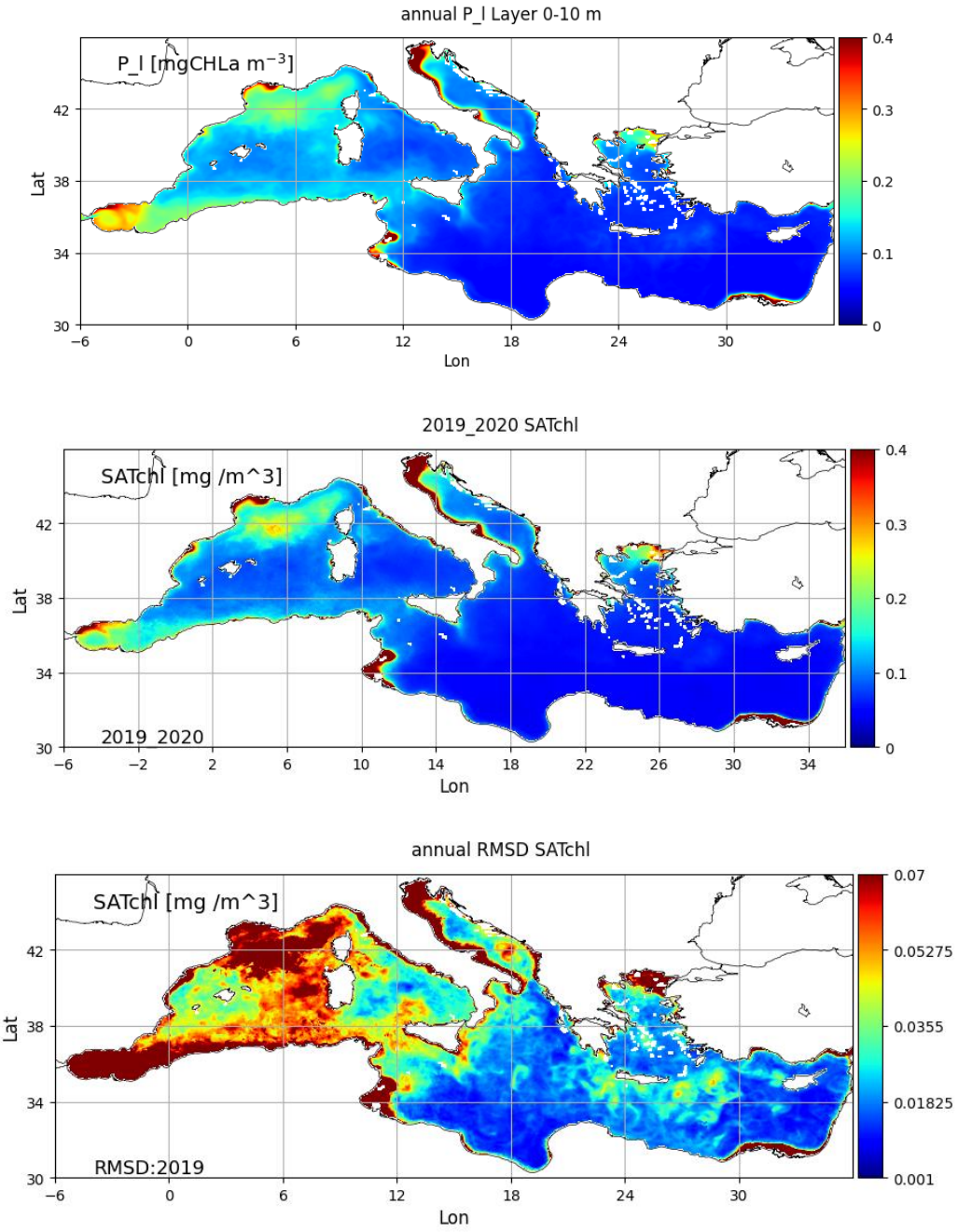

Figure IV.1.1 *Maps of 2019 annually averaged surface chlorophyll from model (top) and NRT multi-sensor satellite data (middle) with corresponding RMSD (bottom). The model average is computed for the 0-10 m layer.*

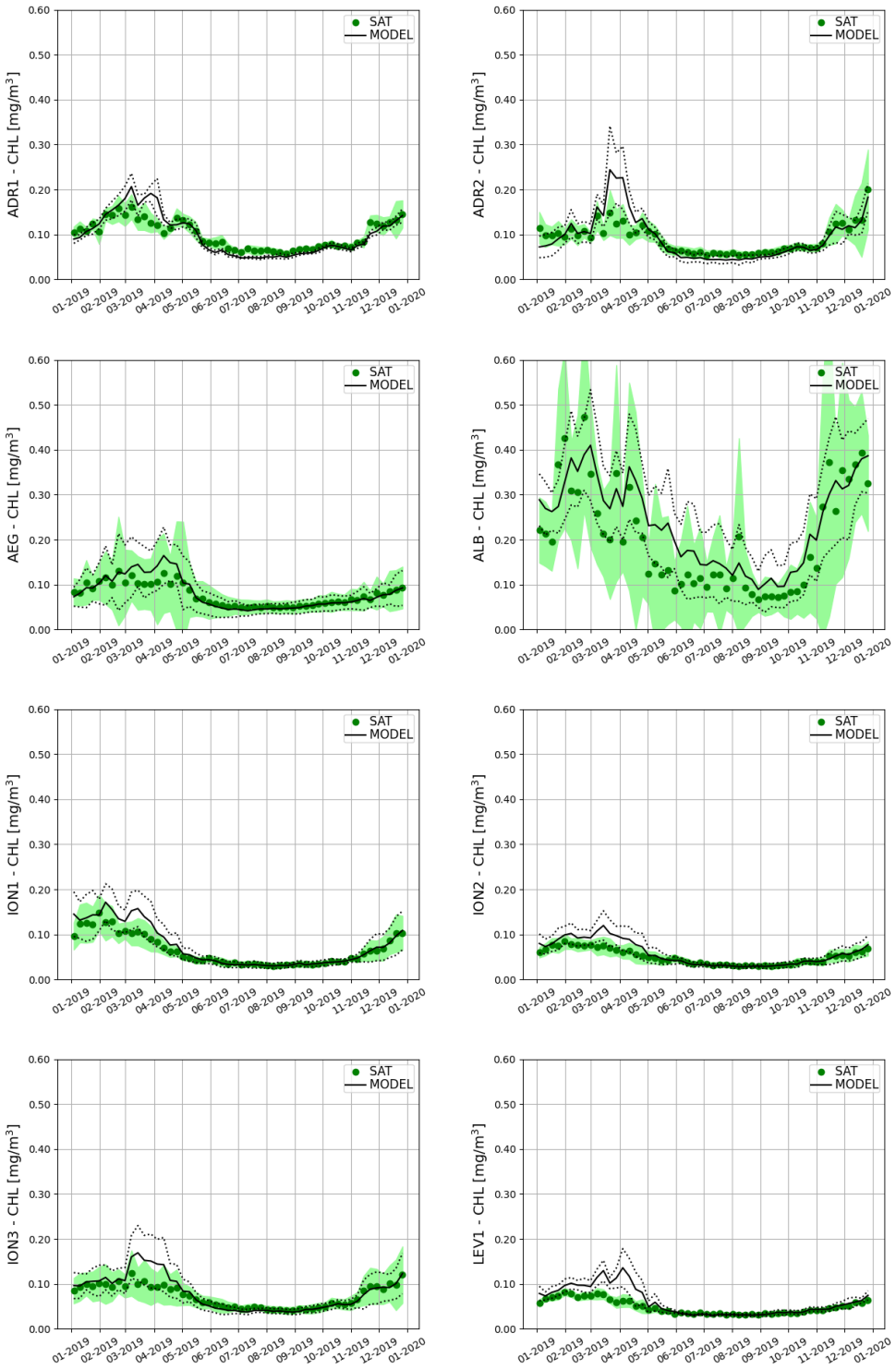

Figure IV.1.2. *Time series of weekly mean surface chlorophyll concentration in open sea areas (black solid line, model) with the spatial standard deviation (STD, dotted black line) and the NRT multi-sensor satellite data (green dots, SAT) with corresponding STD (shaded green area) for the 16 sub-basins from Fig. III.1. Model data (sub-surface 0-10 m layer) and satellite data are reported only for open sea areas (continues on next page).*

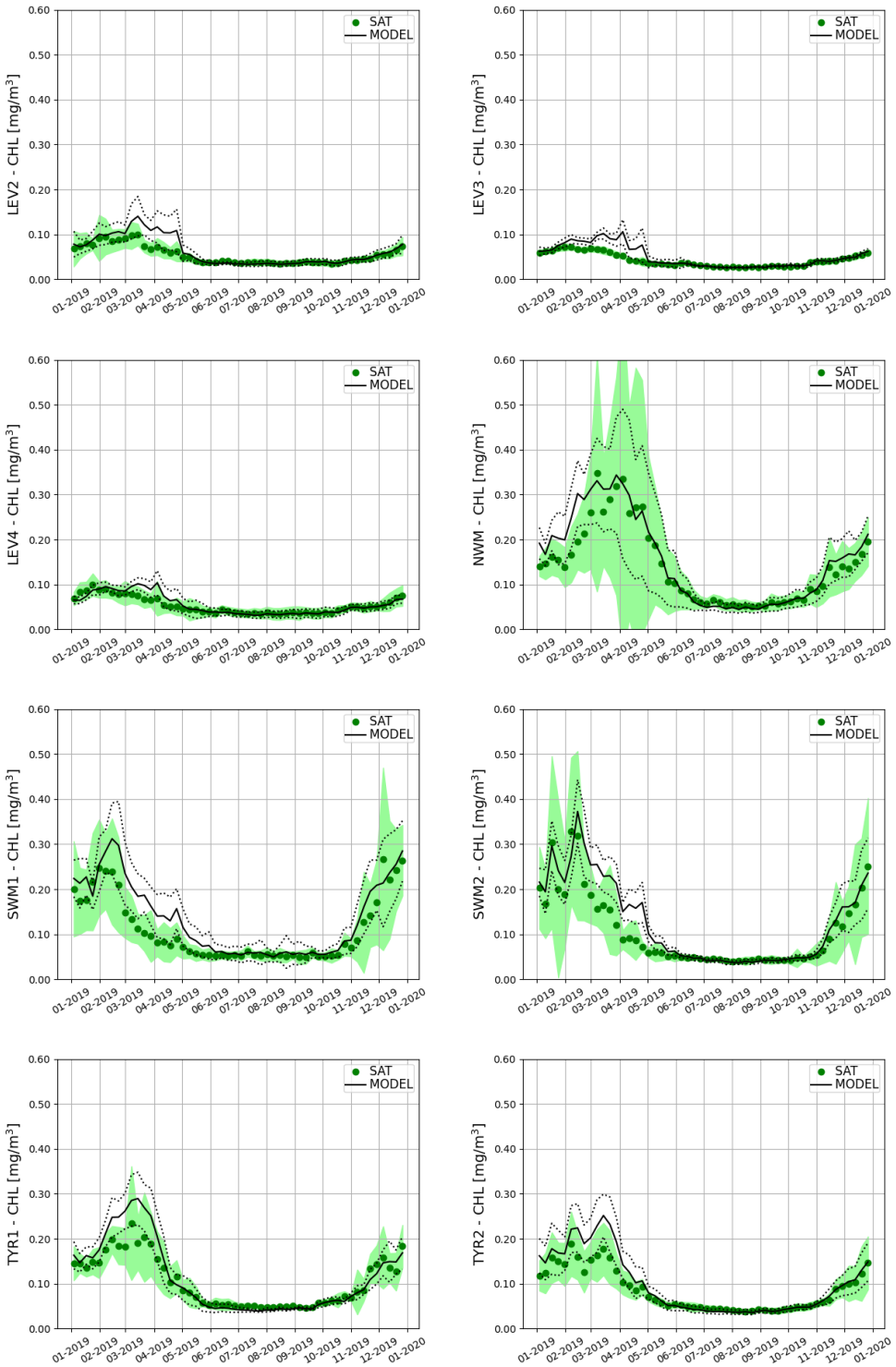

Figure IV.1.2 (cont.). *See above.*

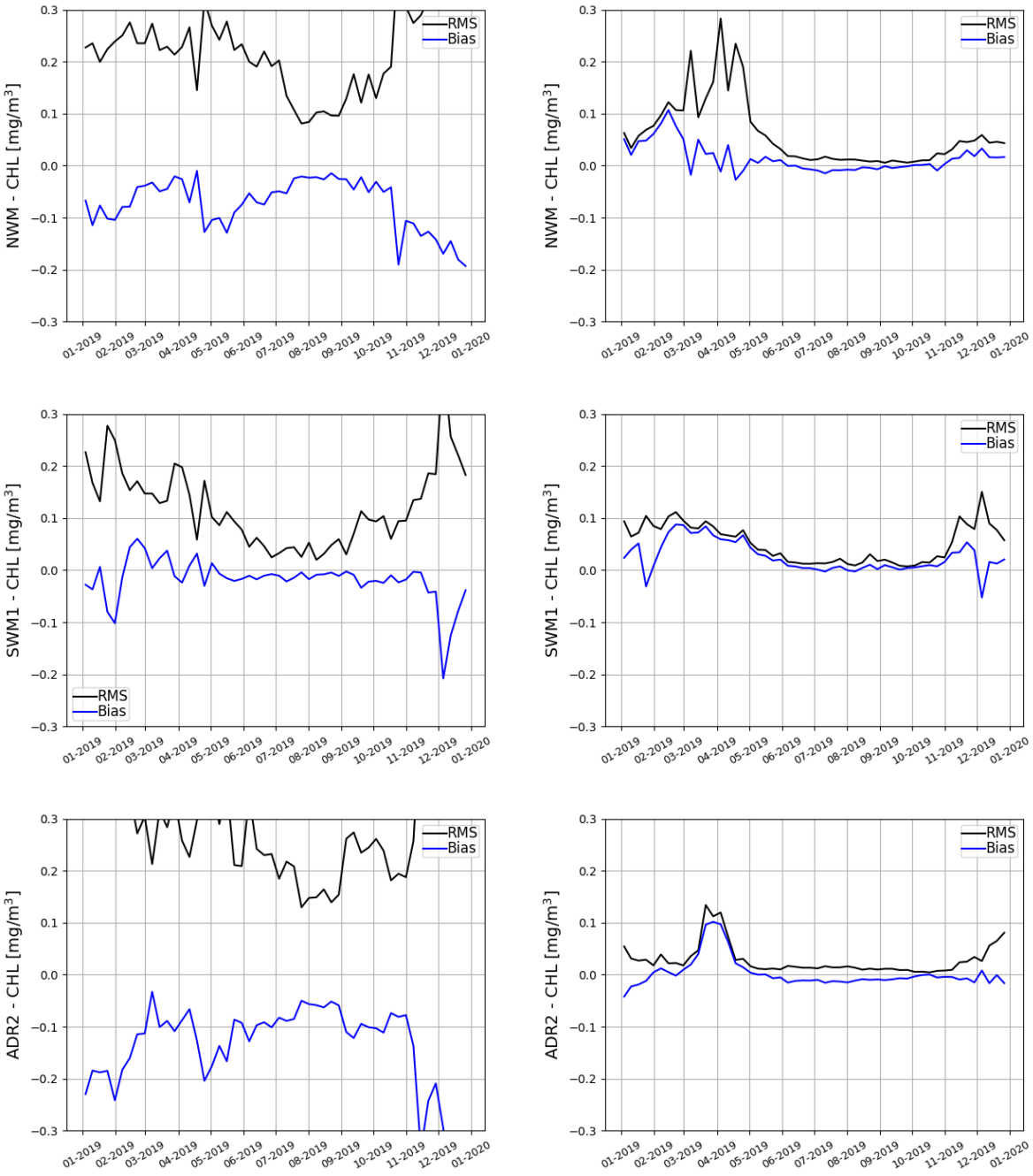

Figure IV.1.3. *Weekly time series of BIAS (model-reference; blue) and RMSD (black) computed for 5 of the 16 sub-basins (cf. Fig. III.1). BIAS and RMSD are based on weekly mean surface chlorophyll concentrations in coastal (left) and open sea (deeper than 200 m, right) areas (cf. Fig. III.1).*

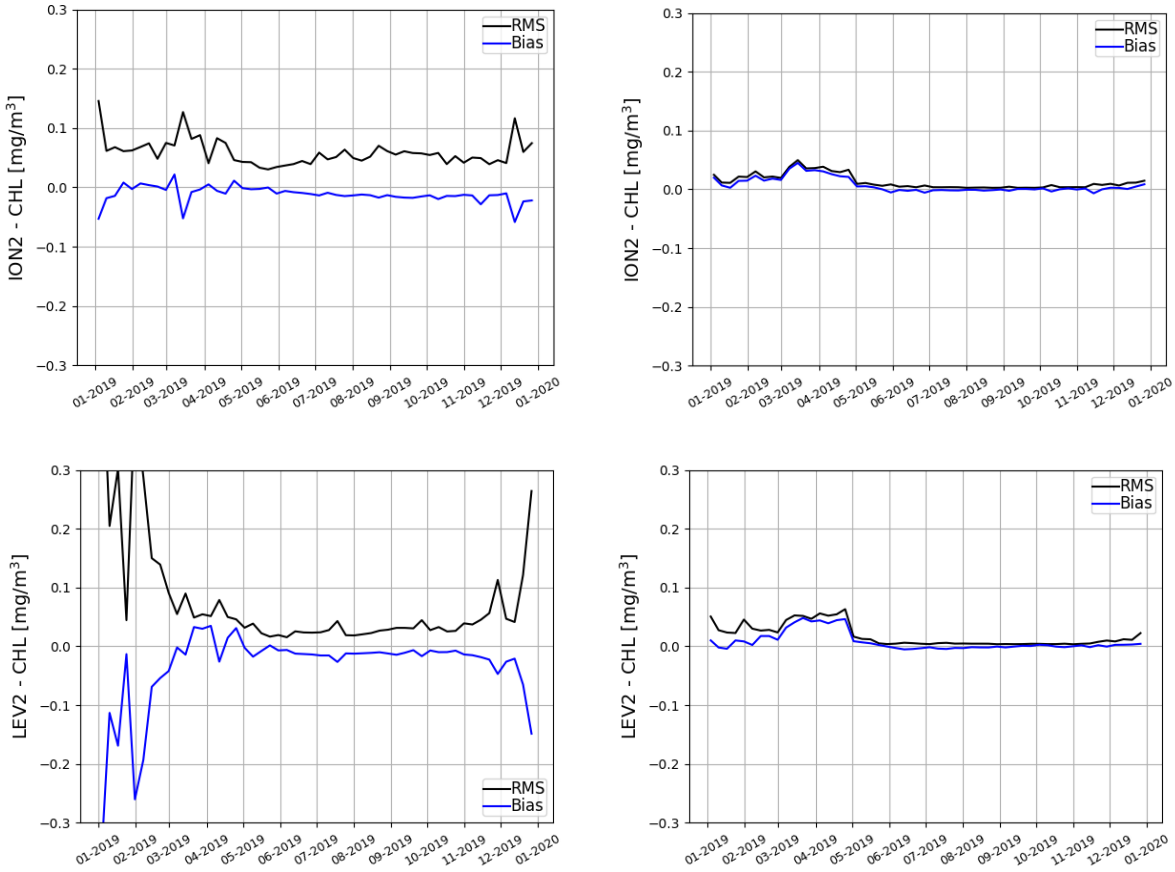

Figure IV.1.3 (cont.). *See above.*

OPEN SEA	Surface (0-10 m) chlorophyll Mod-Sat [mg/m^3]				Surface (0-10 m) chlorophyll log_{10}(Mod)-log_{10}(Sat)			
	RMSD		BIAS		RMSD		BIAS	
	win	sum	win	sum	win	sum	win	sum
alb	0.15	0.08	0.04	0.04	0.21	0.22	0.10	0.15
swm1	0.08	0.02	0.05	0.01	0.21	0.09	0.17	0.03
swm2	0.11	0.01	0.05	0.00	0.22	0.05	0.16	-0.01
nwm	0.13	0.01	0.04	0.00	0.19	0.08	0.11	-0.04
tyr1	0.06	0.01	0.04	-0.01	0.14	0.07	0.08	-0.06
tyr2	0.06	0.01	0.04	0.00	0.15	0.06	0.11	-0.04
adr1	0.03	0.01	0.02	-0.01	0.10	0.10	0.04	-0.09
adr2	0.05	0.01	0.02	-0.01	0.15	0.10	0.05	-0.09
aeg	0.05	0.01	0.02	0.00	0.13	0.06	0.07	-0.03
ion1	0.04	0.00	0.03	0.00	0.13	0.04	0.10	-0.01
ion2	0.03	0.00	0.02	0.00	0.13	0.05	0.11	-0.02
ion3	0.04	0.01	0.02	-0.01	0.14	0.06	0.09	-0.04
lev1	0.04	0.00	0.03	0.00	0.17	0.05	0.15	-0.01
lev2	0.04	0.00	0.02	0.00	0.16	0.05	0.11	-0.02
lev3	0.03	0.00	0.02	0.00	0.15	0.04	0.12	0.00
lev4	0.03	0.01	0.01	0.00	0.12	0.07	0.06	-0.02
Med ave	**0.06**	**0.01**	**0.03**	**0.00**	**0.16**	**0.07**	**0.10**	**-0.02**

Table IV.1.1. *Mean RMSD [mg/m^3] and BIAS [mg/m^3] for surface chlorophyll with respect to satellite maps of open sea areas (deeper than 200 m) for the period January – December 2019. On the right side, the skill indices are computed using log-transformed values. Winter (win) corresponds to January to April, summer (sum) corresponds to June to September.*

COAST	Surface (0-10 m) chlorophyll Mod-Sat [mg/m^3]				Surface (0-10 m) chlorophyll log_{10}(Mod)-log_{10}(Sat)			
	RMSD		BIAS		RMSD		BIAS	
	win	sum	win	sum	win	sum	win	sum
alb	0.32	0.12	-0.09	0.00	0.22	0.20	-0.01	0.06
swm1	0.17	0.05	0.00	-0.01	0.21	0.15	0.08	-0.05
swm2	0.32	0.08	-0.05	-0.01	0.24	0.15	0.06	-0.04
nwm	0.24	0.15	-0.07	-0.04	0.20	0.18	0.00	-0.08
tyr1	0.31	0.16	-0.10	-0.05	0.25	0.22	-0.05	-0.12
tyr2	0.27	0.13	-0.05	-0.03	0.23	0.17	0.03	-0.06
adr1	0.45	0.84	-0.14	-0.27	0.17	0.28	-0.05	-0.19
adr2	0.32	0.21	-0.14	-0.09	0.26	0.26	-0.10	-0.17
aeg	0.29	0.12	-0.05	-0.02	0.19	0.12	0.02	-0.06
ion1	0.44	1.23	-0.10	-0.30	0.22	0.36	-0.01	-0.16
ion2	0.07	0.05	-0.01	-0.01	0.16	0.18	0.02	-0.09
ion3	0.14	0.03	-0.03	-0.02	0.19	0.14	-0.03	-0.10
lev1	0.03	0.03	0.03	0.00	0.18	0.14	0.15	-0.02
lev2	0.15	0.03	-0.07	-0.01	0.26	0.14	-0.08	-0.08
lev3	0.84	0.72	-0.42	-0.34	0.32	0.41	-0.13	-0.28
lev4	0.52	0.44	-0.25	-0.19	0.34	0.40	-0.18	-0.27
Med ave	**0.30**	**0.27**	**-0.10**	**-0.09**	**0.23**	**0.22**	**-0.02**	**-0.11**

Table IV.1.2. *Same as Table IV.1.1 but for coastal areas (shallower than 200 m, cf. Fig. III.1).*

Comparing co-located modelled chlorophyll and BGC-Argo data provides information on model skill for reproducing temporal and spatial (vertical) dynamics of phytoplankton (details in Salon et al., 2019) (Figure IV.1.4).

Chlorophyll BIAS and RMSD time series for selected layers and aggregated sub-basins (Figure IV.1.5) and as annual averages (Table IV.1.3) (reported weekly at https://medeaf.inogs.it/nrt-validation), show that the model has a stable performance as long as the number of available BGC-Argo floats remains constant. RMSD is of the order of 0.04-0.09 mg/m^3 at the surface and 0.04-0.07 mg/m^3 between 60-100 m (Table IV.1.3). Generally, the modelled surface chlorophyll slightly overestimates the satellite data (Table IV.1.1 and Fig IV.1.1) and underestimates the BGC-Argo float data at surface (0-10 m, Tab. IV.1.3). While this might point toward a consistency issue between satellite and BGC-Argo data, it illustrates the very good performance of the MedBFM model as its values lie between the two observing systems.
The Hovmöller diagrams (Fig. IV.1.4) show the model's ability to reproduce the temporal succession of winter vertically mixed blooms, the depth and temporal dynamics of the DCM. The 4th-7th panels of Fig. IV.1.4 show the time series of the quantitative metrics computed on the vertical profiles. The agreement between model (lines) and float (dots) chlorophyll values at the surface, at the DCM and for the 0-200 m vertical average is pretty good (4th and 5th panels of Fig. IV.1.4). The depth of the DCM (blue line and dots in the lower panel of Fig. IV.1.4) is very well reproduced both in terms of vertical displacement and temporal evolution. The thickness of the winter bloom layer (WBL, red lines and dots in the lower panel of Fig. IV.1.4) is fairly good reproduced, although it is not always computable from BGC-Argo float data or model results.
Table IV.1.4 reports the average of the new metrics considering 6 aggregated sub-basins. Statistics for the alb sub-basin are not available for lack of float data in that area while those for swm sub-basin may not be fully reliable considering the low number of BGC-Argo float profiles. Due to the limited number of Argo floats (23 in year 2019), these comparisons should be considered with caution.
Overall, the MedBFM model appears to have a very high skill in reproducing the vertical dynamics of the phytoplankton chlorophyll, including the high spatial heterogeneity and seasonal cycle. In particular, the correlation between model vertical profiles and observations is above of 0.8 in all sub-basins (Tab. IV.1.4). DCM depth and the WBL thickness are characterized by a mean RMSD of 8 m and 27 m, respectively. The RMSD for the top 200 m vertical averages is always below 0.04 mg/m^3 (Table IV.1.4).

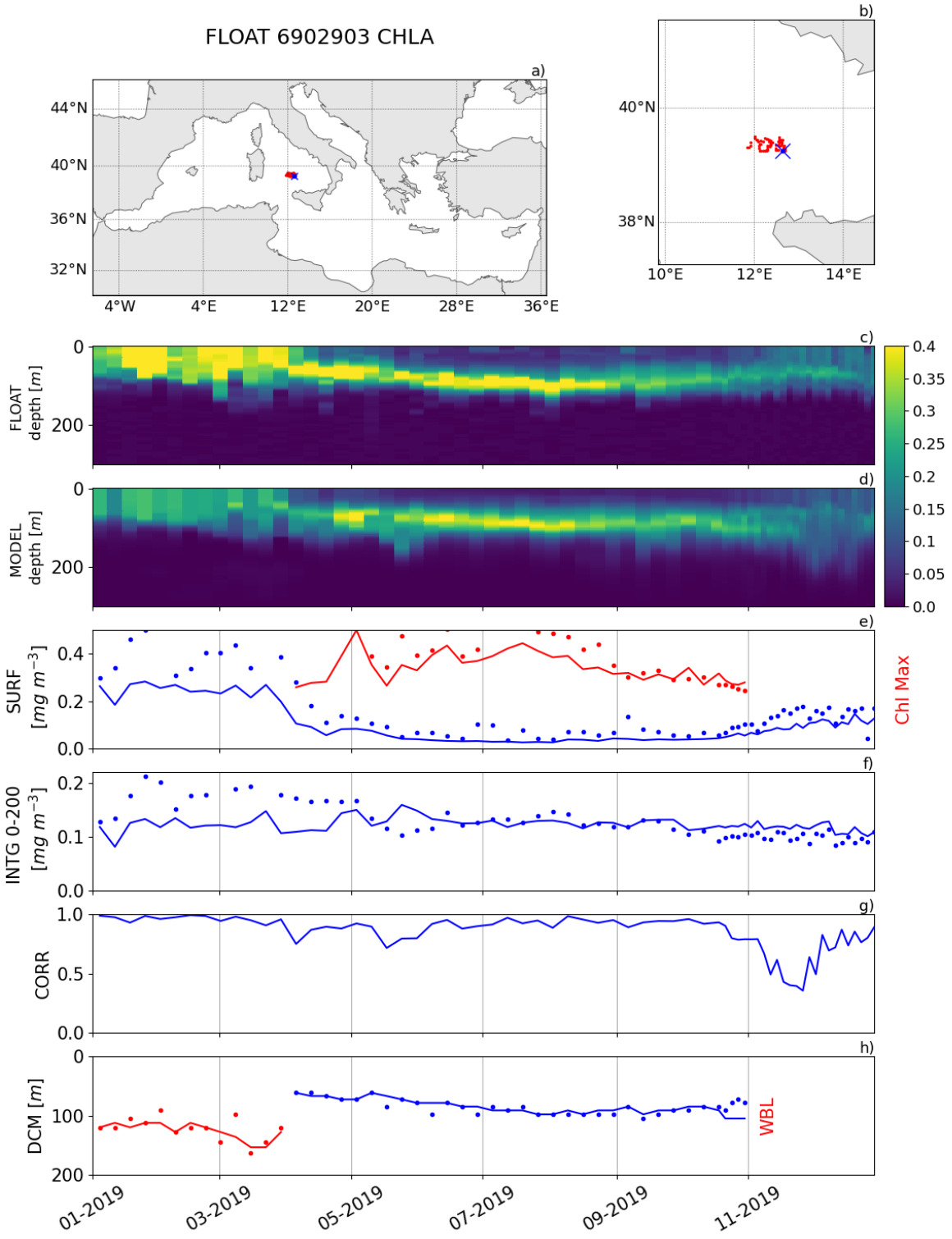

Figure IV.1.4. *Trajectory of BGC-Argo float 6902903 (a) and b)) with the first record in the time window shown as a blue cross. Hovmöller diagrams showing the chlorophyll concentration [mg/m^3] (c) and the corresponding (co-located) model output (d). The skill metrics are: chlorophyll at surface and at DCM (SURF and Chl Max, panel e), 0-200 m vertically averaged chlorophyll (INTG, panel f), correlation (CORR, panel g), DCM depth (blue) and vertical extent of the winter bloom layer (WBL, red, panel h). Model output are represented by a solid line, float data by dots. (continues on next page).*

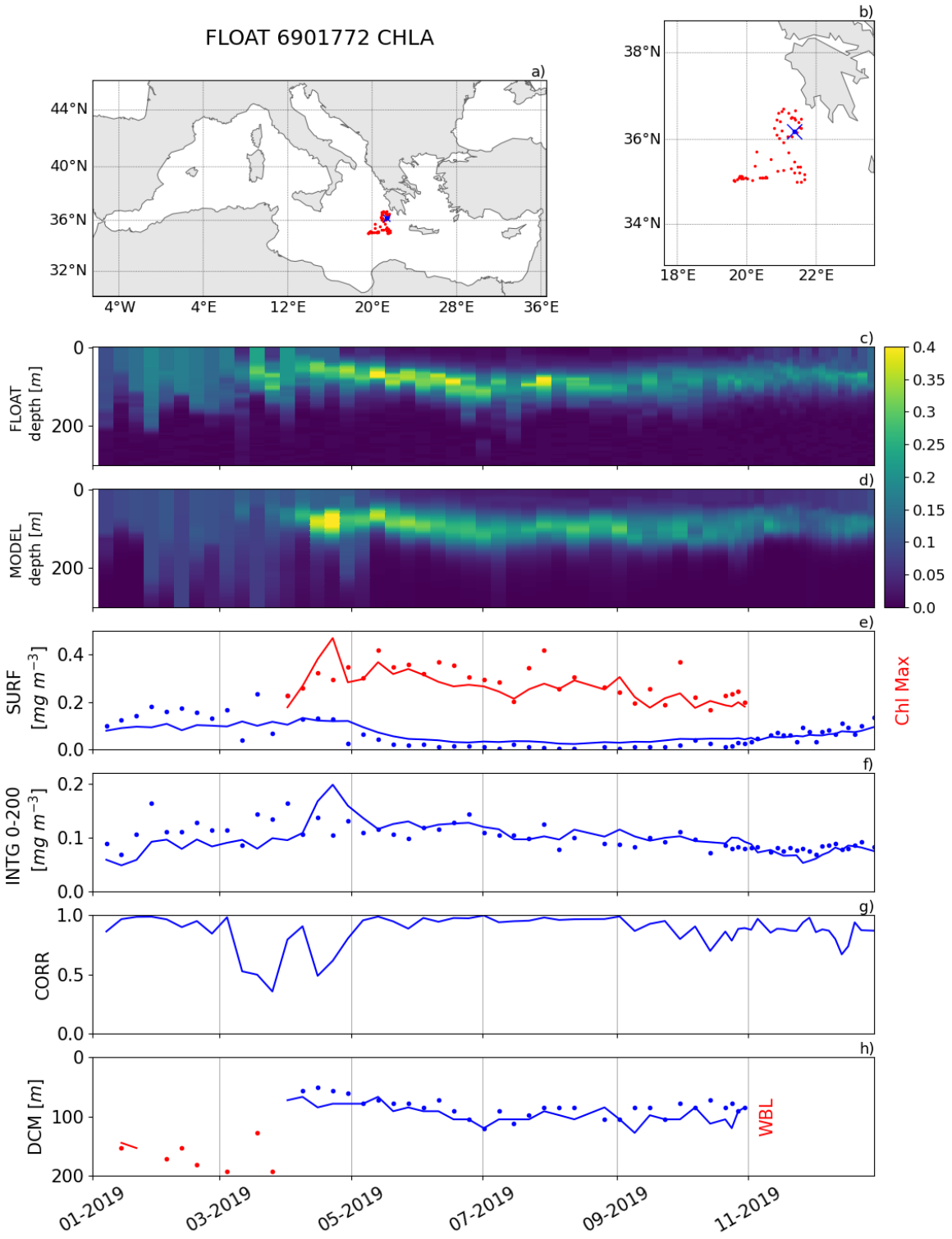

Figure IV.1.4 (cont.). *As above but for Argo float 6901772.*

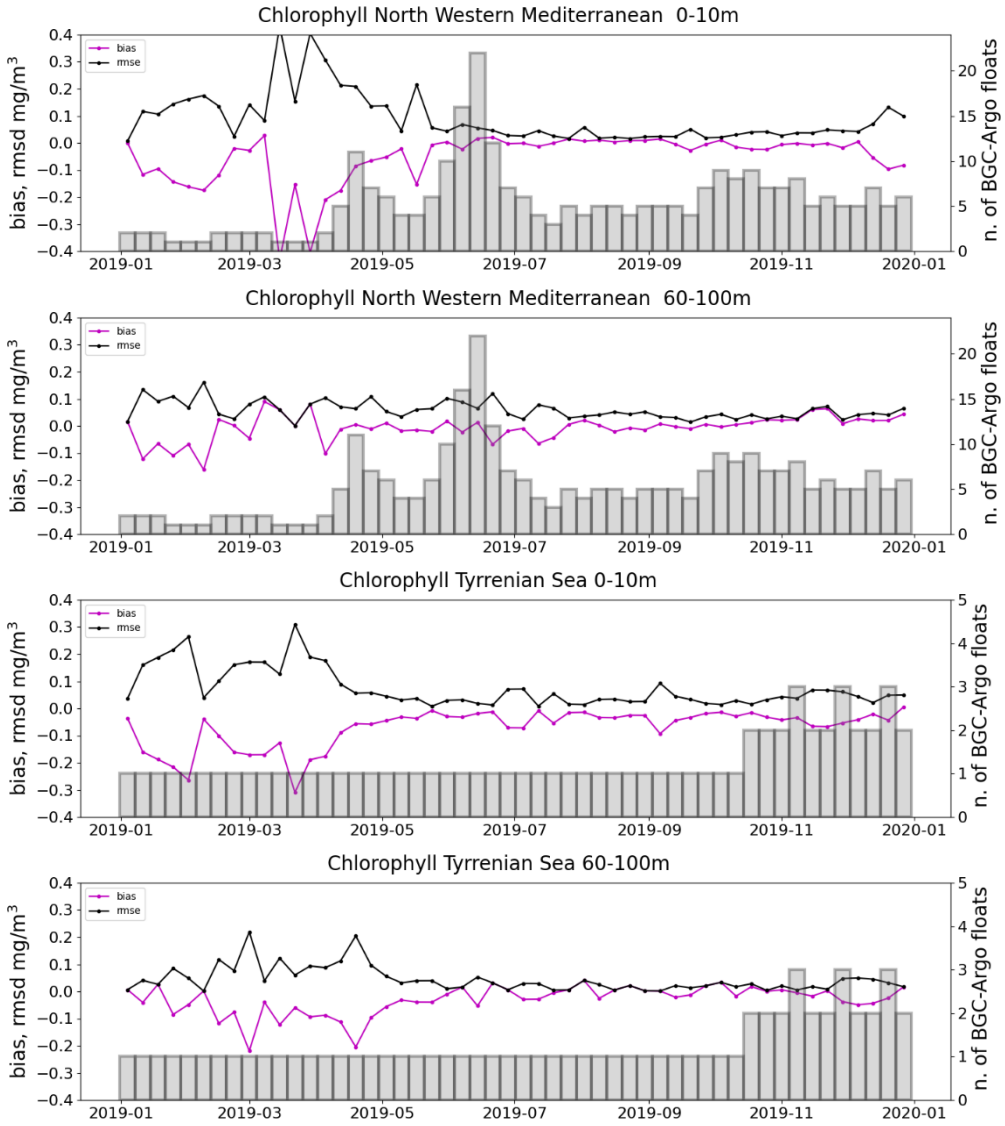

Figure IV.1.5. *Time series of model chlorophyll BIAS and RMSD [mmol/m^3] with respect to BGC-Argo float data for model layers 0-1 0 m and 60-100 m, aggregated for each sub-basin (cf. Fig. III.1) (except swm). Number of data profiles used is shown as grey vertical bars (right axes).*

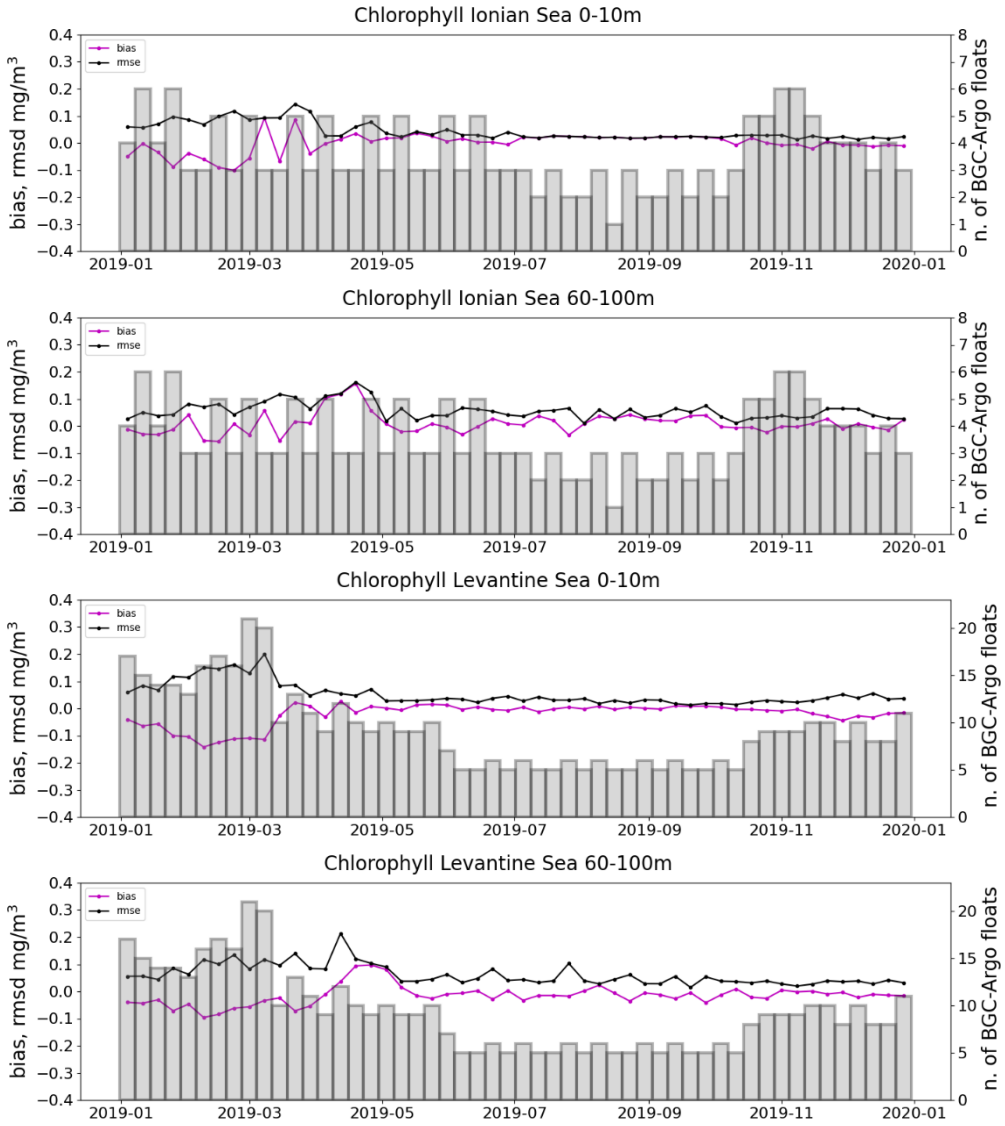

Figure IV.1.5 (cont.). *See above.*

	BIAS [mg/m^3]					RMSD [mg/m^3]				
	0-10 m	10-30 m	30-60 m	60-100 m	100-150 m	0-10 m	10-30 m	30-60 m	60-100 m	100-150 m
alb	-	-	-	-	-	-	-	-	-	-
swm	-0.02	-0.03	-0.02	0.01	-0.01	0.07	0.07	0.07	0.07	0.03
nwm	-0.06	-0.06	-0.06	-0.01	0.00	0.09	0.09	0.12	0.06	0.02
tyr	-0.07	-0.07	-0.05	-0.03	0.02	0.07	0.07	0.07	0.04	0.05
adr	-0.02	-0.02	-0.02	0.02	0.00	0.05	0.05	0.05	0.06	0.03
ion	0.00	0.00	-0.01	0.01	0.02	0.04	0.04	0.05	0.06	0.05
lev	-0.02	-0.02	-0.02	-0.02	0.01	0.05	0.05	0.08	0.06	0.05

Table IV.1.3. *Time averaged model BIAS and RMSD for chlorophyll (mg/m^3) with respected to ARGO data in selected layers, aggregated over sub-basins for the period January – December 2019.*

		Average 0-200 m [mg/m^3]		DCM depth [m]		WBL depth [m]		average number of available profiles per month
	CORR	BIAS	RMSD	BIAS	RMSD	BIAS	RMSD	
alb	-	-	-	-	-	-	-	0
swm	0.86	-0.01	0.03	-1	7	6	39	3
nwm	0.93	-0.01	0.02	0	3	19	25	23
tyr	0.87	-0.01	0.04	2	11	15	23	6
adr	0.91	0	0.03	3	6	5	48	6
ion	0.86	0.01	0.02	9	14	-4	10	16
lev	0.8	0	0.02	5	7	14	15	40

Table IV.1.4. *Time averages of the chlorophyll ecosystem indicators based on the BGC-Argo floats and model comparison for the period January – December 2019.*

IV.2. Net primary production

Due to the lack of sufficient observations, no quantitative comparison can be conducted and we perform a qualitative assessment with regard to literature values instead (Fig. IV.2.1 and Tab. IV.2.1). While modelled NPP slightly overestimates literature values (Tab. IV.2.1), the general east-to-west increase in NPP as well as other regional differences are well reproduced: this is evaluated comparing Fig. IV.2.1. with reference multi-annual simulation in Fig 8c in Lazzari et al. (2012), and with climatological satellite estimates based on the period September 1997 – December 2001 (Fig. 13 in Bosc et al., 2004).

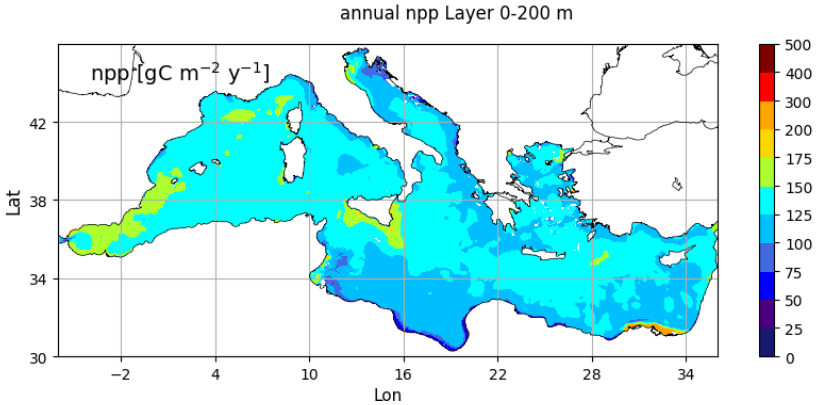

Figure IV.2.1*. 2019 yearly averaged vertically integrated primary production (gC m^{-2} yr^{-1}) from the qualification run.*

	MODEL Lazzari et al. (2012)	SATELLITE Colella (2006)	IN-SITU ESTIMATES Siokou-Frangou et al., 2010 (reported in their Table 1, only in-situ estimates)		MedBFM for year 2019
	Annual mean [gC/m²/y]	Annual mean [gC/m²/y]	Annual mean [gC/m²/y]	Short term estimates [mgC/m³/d]	Annual mean [gC/m²/y]
Mediterranean Sea (MED)	98±82	90±48			129
Alboran Sea (ALB)	274±155	179±116		353–996; May-Jun1996 142; Nov2003	150
South West Med – West (SWM1)	160±89	113±43		186–636 (avg. 440) Oct1996	143
South West Med –East (SWM2)	118±70	102±38			137
North West Med (NWM)	116±79	115±67	105.8-119.6 86-232 (only DYFAMED station) 140-170 (South Gulf of Lion)	353–996; May–Jun1996 401; Mar-Apr1998 (G. Lion) 166; Jan-Feb1999 (G. Lion) 160–760; May-Jul (Cat-Bal) 150–900; Apr1991 (Cat-Bal) 450, 700; Jun1993 (Cat-Bal) 210, 250; Oct1992 (Cat-Bal) 1000±71 Mar1999 (Cat-Bal) 404±248 Jan-Feb00 (Cat-Bal)	140
Levantine (LEV1+LEV2+LEV3+LEV 4)	76±61	72±21	59 (Cretan Sea)		127
Ionian Sea (ION1+ION2+ION3)	77±58	79±23	61.8	119–419; May-June 1996 208–324; April-May 1999 186±65; August 1997-98	122
Tyrrhenian Sea (TYR1 + TYR2)	92±5	90±35		398; May–Jun1996 273; Jul2005 429; Dec2005	127

Table IV.2.1. *Annual averages and short-term estimates of the vertically integrated net primary production for selected sub-regions. Estimates are from a multi-year simulation (Lazzari et al., 2012), a satellite model (Colella, 2006), in-situ estimates (Siokou-Frangou et al., 2010), and from MedBFM.*

IV.3. Phytoplankton biomass

Phytoplankton biomass (mgC/m^3) is simulated using 4 phytoplankton functional groups and a variable chlorophyll to carbon ratio (based on photoacclimatation and the balance between synthesis and loss terms) (Lazzari et al., 2012).

Accuracy is assessed using Class4 metrics on BGC-Argo particulate backscattering data (bbp700) that is converted into biomass using the relations ship from Bellacicco et al. (2019). Statistics (Table IV.3.1) show that the profile shapes are reproduced with a correlation above 0.65 except in the ADR and LEV regions. The 0-200 m depth-averaged values are reproduced with an RMSD around 1.3 mgC/m^3 for absolute (depth-averaged) model values ranging from 2.9-5.0 mgC/m^3. The uneven distribution of BGC-Argo data (mostly confined to open sea areas and certain sub-basins) limits the reliability of this comparison.

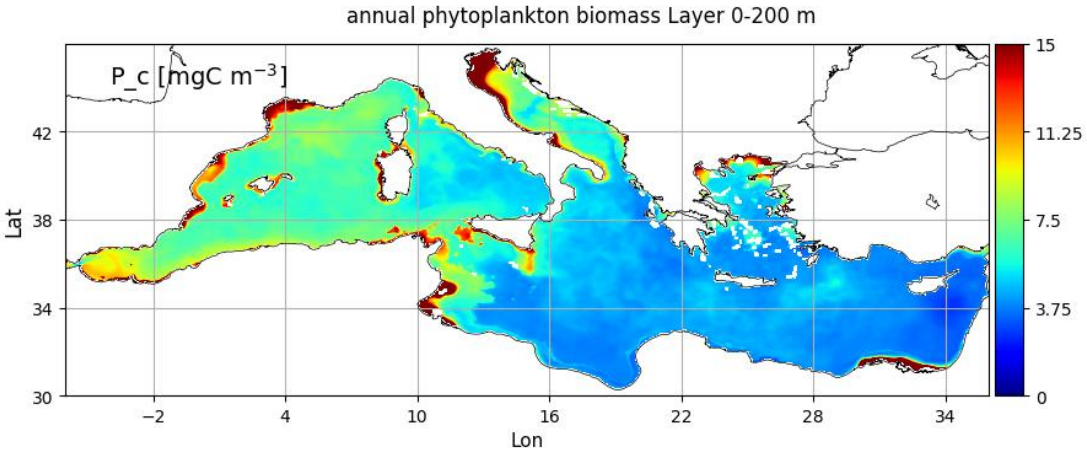

Fig. IV.3.1. *Depth-averaged (0-200 m) annual mean (2019) phytoplankton carbon biomass (mg/m^3).*

	Model	Model at BGC-Argo locations *	Skill metrics		Correlation	Average number of available profiles per month
			BIAS	RMSD		
alb	10.13±4.91	-	-	-	-	0
swm	7.26±1.92	3.98	0.89	0.90	0.92	3
nwm	7.96±3.27	6.95	1.69	3.00	0.72	23
tyr	6.43±2.63	5.03	0.98	1.12	0.82	5
adr	11.08±11.13	2.91	-0.44	0.76	0.50	6
ion	5.23± 3.77	3.97	0.38	0.75	0.65	15
lev	4.73±5.53	3.78	0.94	1.42	0.51	40

Table IV.3.1. *Phytoplankton carbon biomass and skill metrics based on BGC-Argo data aggregated for sub-basins. Values and statistics correspond to depth-averaged (0-200 m) annual means (2019) in units [mgC/m3]. *Model output co-located with Argo data (open sea area only).*

IV.4. Zooplankton biomass

Zooplankton biomass (mgC/m^3) represents the sum of the four zooplankton functional groups. Due to the lack of sufficient observations, no quantitative comparison can be conducted and we perform a qualitative assessment of the consistency of the modelled zooplankton biomass with regards to measurements published in scientific literature (Tab. IV.4.1). Measurements of zooplankton are often reported as biomass (or abundancy) over square meter of a portion of the water column (often considering the layer 0-200 m) given the usual sampling methodologies for this ecosystem component. Scientific studies generally address one of the three components (i.e., HNF, micro and mesozooplankton), seldom all three zooplankton components are simultaneously sampled, and studies refer to a few very sparse locations for non-synoptic and non-repeated temporal samplings (e.g., a single month in a single year). Thus, only literature reporting at least data from large samplings (i.e., extended in some of the Mediterranean sub-basins at least) or addressing all zooplankton components are considered. The scarcity and the lack of homogeneity of the data prevents the direct comparison between the total carbon biomass of zooplankton simulated by the model and the sum of the measurements for the different zooplankton compartments from different sources.
Notwithstanding these limitations, the qualitative comparison between the map of Fig IV.4.1 and the values of Table IV.4.1 shows that the model satisfactory simulated the order of magnitude of the variable

(i.e., in the range of 0.5-2 gC/m^2 for the layer 0-200 m) and the basin-wide gradient with higher values in the western sub-basins and lower values in the eastern ones.

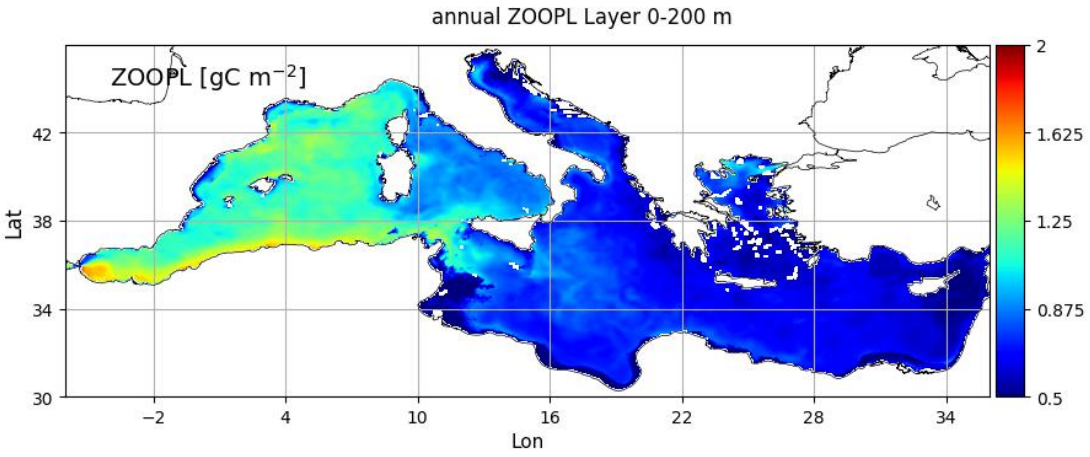

Fig. IV.4.1. *2019 yearly averaged vertically (in layer 0-200 m) integrated biomass of total zooplankton [gC/m^2]. The total zooplankton biomass is the sum of the carbon content of the four zooplankton function groups of the BFM model (i.e., heterotrophic nano flagellates, microzooplankton and 2 groups of mesozooplankton).*

Model subbasin	Heterotrophic Nanoflagelates [gC/m²] in layer 0-20 0 m		Microzooplankton [gC/m²] in layer 0-20 0 m		Mesozooplankton [gC/m²] in layer 0-20 0 m		Model Total carbon biomass of Zooplankton [gC/m²] in layer 0-20 0 m
ALB					0.26	Apr [e]	1.25 ± 0.21
					0.72;0.5****	Winter/spring [c]	
SWM1					1.45***	Jun [f]	1.17 ± 0.17
SWM2	0.5	Jun/Jul [a]					1.17 ± 0.15
NWM	0.88	Jun/Jul [a]	0.1-0.2*	May/Jun [d]	0.82±0.15	Apr [e]	1.12 ± 0.16
	0.46-1.3** (NW Med current) 0.17-1.7** (NW offshore transect)	May/Jun [c]			0.9***	Jun [f]	
					0.58; 1.16; 1.6	different studies [c]	
					0.3;0.4;0.45****	Mar/Spring[c]	
TYR							0.91 ± 0.16
ADR					0.30±00.05 0.15±00.02	Feb/Oct [e]	0.68 ± 0.16
AEG	0.2* 0.8*	Mar/Sep [b]	0.16±0.04* 0.12±0.05*	Mar/Sep [b]	0.19±0.04* 0.16±0.04*	Mar/Sep [b]	0.64 ± 0.14
					0.2 – 0.4****	Mar/Spring[c]	
ION	0.25 (western) 0.45 (southern) 0.40 (northern)	Jun/Jul [a]	0.02-0.28*	May/Jun [d]	Sicily channel 0.24±0.04 0.19±0.02	Mar/Sep [e]	0.72 ± 0.16
					0.4****	Mar [c]	
					0.24±0.03 0.22±0.02	Mar/Aug [e]	
					0.95*** (eastern) 1.05*** (central) 0.85*** (central)	Jun [f]	
					0.4	Spring [c]	
LEV	0.25 (western) 0.26 (southern) 0.30 (Cyprus) 0.31 (Rhode gyre)	Jun/Jul [a]	0.08-0.12*	May/Jun [d]	0.44±0.26 (Rhode gyre) 0.20±0.02	Mar/Sep/Oct [e]	0.63± 0.09
	0.23-0.52**	Sep [c]			0.7*** (rhode gyre) 0.4*** (south Cyprus) 0.65*** (MersaMatruh gyre)	Jun [f]	

Table IV.4.1. *Measurements of the vertically integrated zooplankton biomass for the three components for some selected sub-regions. Model total carbon biomass of zooplankton [gC/m²] in the 0-200 m layer (last column). [a] Data from Christaki et al. (2001); [b] Southern Aegeran for layer 0-100 m, data from Siokou-Frangou et al. (2002); [c] data for from Siokou-Frangou et al. (2010); [d] Data for from Dolan et al., (1999); [e] data from Mazzocchi et al., (2014); [f] data from Siokou et al., 2019. *data for 0-100 m; **data converted from abundance to biomass using 2.9 pg/ind (estimation retrieved using data from Christaki et al., 2001); ***data converted from 0-100 0 m to 0-200 m using the conversion factor of 0.75; ****dry weigh converted to biomass using the factor 4 grDW: 1grC.*

IV.5. Phosphate

The quality of phosphate concentration is assessed by Class 1 metrics: a quantitative comparison between model average vertical profiles and the reference climatological profiles (Figures IV.16.1; Appendix A) with skill performance statistics computed for each sub-basin based on climatological values and the corresponding model annual means (Table IV.5.1).
MedBFM has a good accuracy in reproducing the average values and shape of the profiles along the Mediterranean sub-basins. In particular, the modelled profiles are within the range of variability of the EMODnet2018_int climatological profiles (Fig. IV.16.1, Appendix A). On average, phosphate RMSD is 0.03 mmol/m^3 in the upper layers and ranges between 0.03 and 0.05 mmol/m^3 in the layers below 60 m (Table IV.5.1). The results illustrate the good performance of the MedBFM model in reproducing the negative gradient from the western to the eastern sub-basins of the subsurface layers (correlation values higher than 0.7 below 30 m). Low phosphate values in the surface layers (i.e., 0-10 m and 10-30 m) affect the model capability to clearly reproduce the west-to-east gradient, thus the correlation value is low.

	Phosphate		
Layer depth	**BIAS [mmol/m^3]**	**RMSD [mmol/m^3]**	**CORR**
0-10 m	-0.01	0.03	0.32
10-30 m	0.00	0.03	0.27
30-60 m	0.00	0.03	0.72
60-100 m	0.00	0.03	0.92
100-150 m	0.03	0.05	0.89
150-300 m	0.03	0.03	0.97
300-600 m	-0.03	0.04	0.99
600-1000 m	-0.02	0.03	0.98

Table IV.5.1 *Skill metrics (BIAS, RMSD and correlation) for the comparison of phosphate (model outputs averaged over the sub-basins and the period January – December 2019) with respect to climatology in open sea (EMODnet2018_int dataset). The metric is calculated for the selected layers of Table III.1.*

IV.6. Nitrate

The quality of nitrate is assessed by two validation analyses:

(i) a quantitative comparison with EMODnet2018_int vertical climatological profiles to assess the skill in reproducing the vertical characteristics along the 16 Mediterranean sub-basins (Fig. IV.16.1, appendix A) and Table. IV.6.1;

(ii) a quantitative comparison with BGC-Argo float data to assess the quality of the model in reproducing the nitrate dynamics at the mesoscale and at weekly temporal scale (Figs. IV.6.1,2, and 3 and Tabs. IV.6.2 and 3).

MedBFM has a good accuracy in reproducing the average values and shape of the profiles along the Mediterranean sub-basins. In particular, the modelled profiles are within the range of variability of the EMODnet2018_int climatological profiles (Fig. IV.16.1, appendix A. On average, the RMSD of nitrate is 0.6 mmol/m^3 in the upper layers and less than 0.9 mmol/m^3 in the layers below 60 m; absolute BIAS never exceeds 0.6 mmol/m^3 in the upper layers. Both nitrate and phosphate results corroborates the good performance of the MedBFM model in reproducing the deepening of the nutricline and the decreasing concentration values in the deep layers from the western to the eastern sub-basins. Low nitrate values in the surface layer affect the model capability to clearly reproduce the west-to-east gradient, thus the correlation value is low.

	Nitrate		
Layer depth	**BIAS [mmol/m^3]**	**RMSD [mmol/m^3]**	**CORR**
0-10 m	0.26	0.51	0.21
10-30 m	0.38	0.59	0.12
30-60 m	0.31	0.66	0.52
60-100 m	0.26	0.73	0.83
100-150 m	0.58	0.97	0.88
150-300 m	0.22	0.69	0.94
300-600 m	-0.58	0.89	0.94
600-1000 m	-0.49	0.68	0.96

Table IV.6.1 *Skill metrics for the comparison of nitrate with respect to climatology in open sea.*

Validation of nitrate can benefit from the availability of BGC-Argo floats data. Even if the number of BGC-Argo floats mounting a nitrate sensor is smaller than that for chlorophyll (i.e., 11 BGC-Argo floats during year 2019), the float data undoubtedly represent a fundamental source of information to validate the MedBFM model results at the mesoscale and weekly temporal scale.
Since MedBFM version at Q2/2020, the system assimilates nitrate BGC-Argo profiles, and the comparison is performed using misfits (i.e., model-observation differences just before the observations are assimilated). Given the frequency of BGC-Argo data is generally weekly, the misfit can be influenced by the assimilation of the same BGC-Argo float occurred in a location 50-150 km from the present position one week before (i.e., BGC-Argo float should be considered as semi-independent data). Nevertheless, the comparison of modelled nitrate with the BGC-Argo float data evaluates not just the *accuracy* of nitrate product (i.e., BIAS and RMSD for selected layers and sub-basins), but also the *consistency* of the MedBFM to simulate key coupled physical-biogeochemical processes (i.e., water column nutrient content, shape of nitrate profile, and depth and intensity of the nitracline; Figs. IV.6.1 and 2 and Table IV.6.2). This validation framework is based on matching a BGC-Argo float profile with the corresponding (in time and space) modelled profile (e.g., Hovmöller diagrams in the 2th and 3th panels of Fig. IV.6.1). Based on the model-float vertical match-up, specifically developed metrics are:

- surface concentration and 0-200 m vertically averaged values (4th and 5th panels of Fig. IV.6.1);
- correlation between model and BGC-Argo float profiles (6th panel of Fig. IV.16.1);
- depth of the nitracline (NITRACL1 defined as the depth at which the nitrate concentration is 2 mmol/m^3; and NITRACL2 defined as the depth at which the depth derivative of the nitrate profile is maximum; 7th panel of Fig. IV.6.1).

The two Hovmöller plots of Fig. IV.6.1 exemplify the high level of potentiality of the BGC-Argo float data for validating the model results. From a qualitative point of view the nitrate signatures of the two floats are pretty well reproduced by the MedBFM model simulation (2nd and 3rd panels of Fig. IV.6.1). From a quantitative point of view we observe a good model performance in reproducing the temporal evolution of the 0-200 m averaged values, the shape of the profile (i.e. correlation values) and of the nitracline depth (4th – 7th panel of Fig. IV.6.1).
The nitrate metrics of the 11 floats are averaged over the aggregated sub-basins (Table IV.6.2). Even if the scarcity of the available floats possibly limits the generalization of the results, our validation framework highlights that the MedBFM model system shows a good performance in simulating the shape of profiles and the seasonal evolution of the mesoscale dynamics. In particular, the mean value of nitrate on the 0-200 m layer is simulated, with an accuracy of about 0.22 mmol/m^3 (Tab. IV.6.2), the correlation is always higher than 0.75 and the depth of the nitracline (NITRACL1) is simulated with a mean uncertainty of 13 m in all aggregated sub-basins (Tab. IV.6.2).

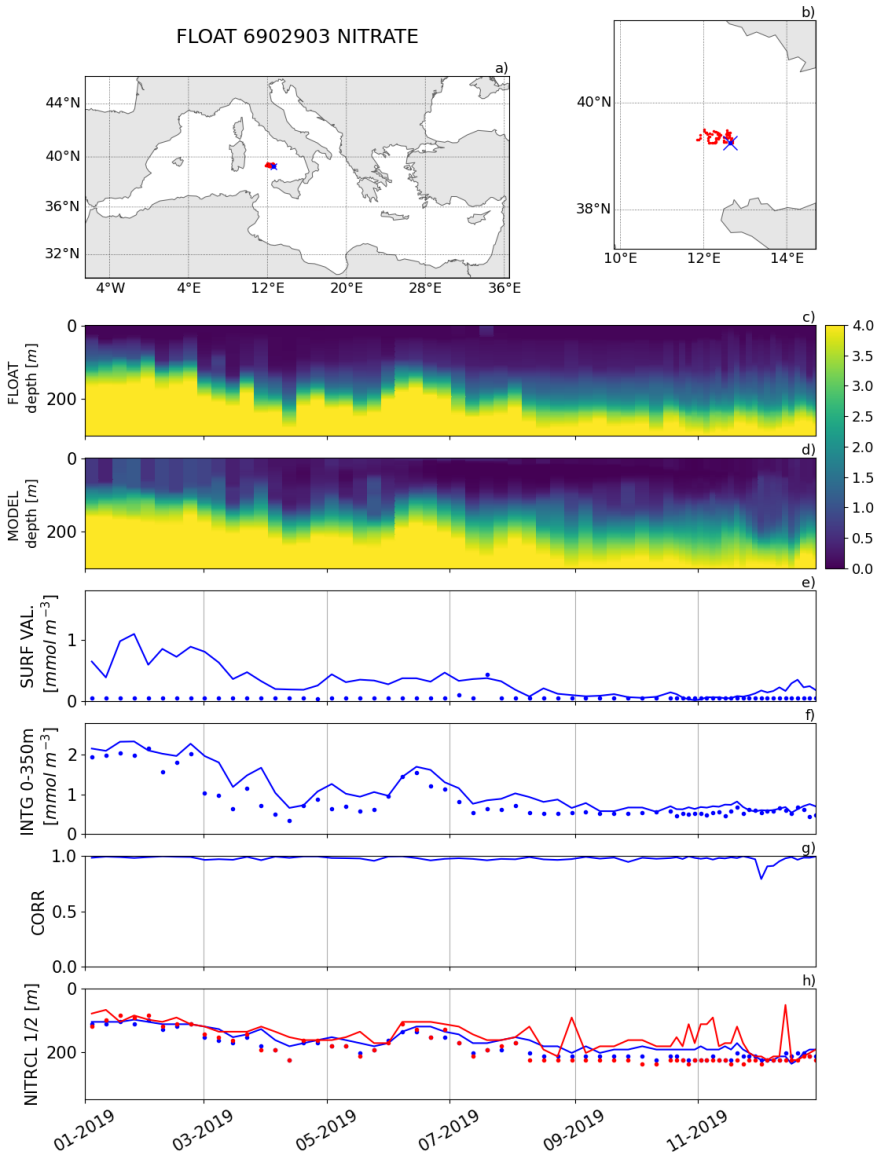

Figure IV.6.1. *Trajectory of BGC-Argo float 6902903 (a) and b)) with the first record in the time window shown as a blue cross. Hovmöller diagrams showing nitrate concentration [mmol/m^3] (c) and the corresponding (co-located) model output (d). The skill metrics are: nitrate at surface (SURF, panel e), 0-350 m vertically averaged concentration (INTG, panel f), correlation (CORR, panel g), nitracline depth (in blue NITRACL1 defined as the depth at which the nitrate concentration is 2 mmol/m^3; and in red NITRACL2 defined as the depth at which the depth derivative of the nitrate profile is maximum). Model output are represented by a solid line, float data by dots. (continues on next page).*

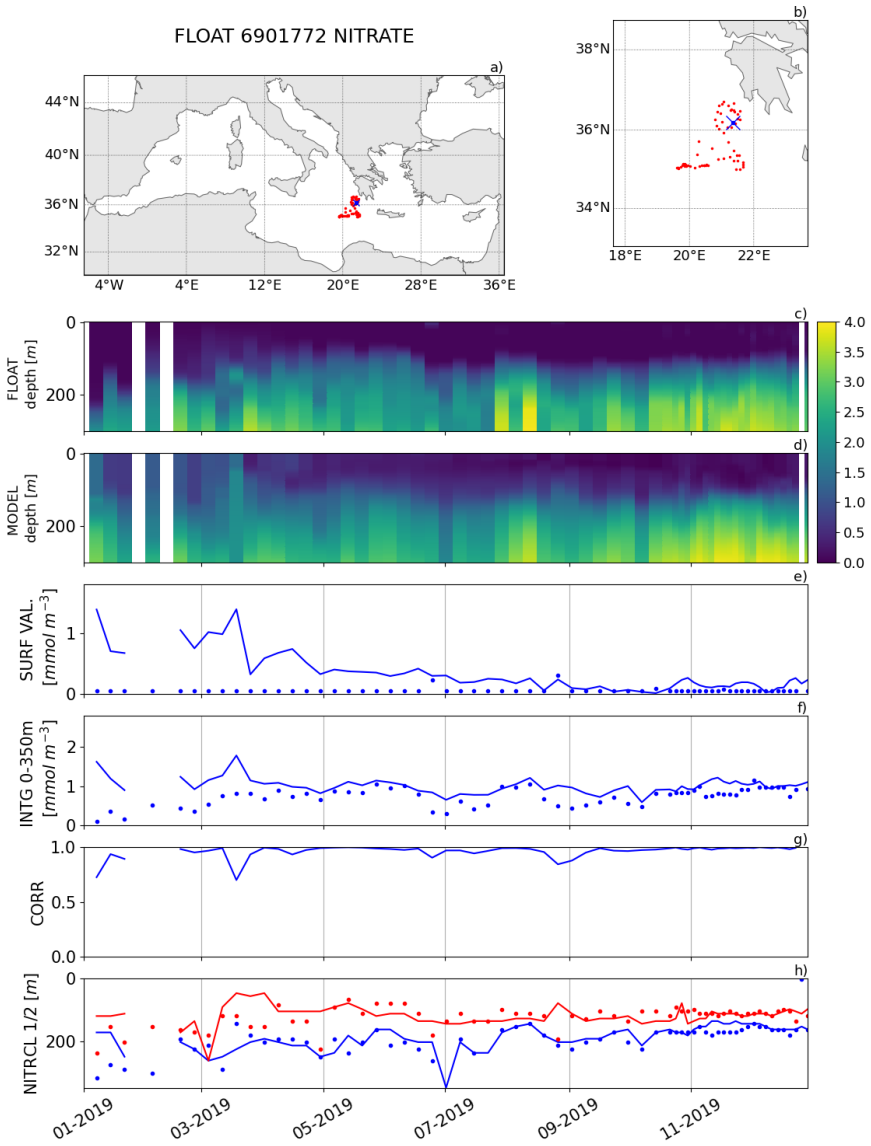

Figure IV.6.1. *As above but for Argo float 6901772.*

	CORR	mean nitrate concentration 0-200 m [mmol/m³]		Depth of the nitracline [m]		Average number of profiles per month
		BIAS	RMSD	BIAS	RMSD	
alb	-	-	-	-	-	0
swm	-	-	-	-	-	0
nwm	0.99	-0.13	0.2	2	4	11
tyr	0.98	0.25	0.3	-13	16	6
adr	0.96	-0.2	0.26	12	16	6
ion	0.96	0.07	0.14	-1	13	12
lev	0.75	0.03	0.19	-2	16	16

Table IV.6.2. *Averages of the monthly nitrate indicators plotted in Figure IV.6.2 during the period January – December 2019. The indicators are the correlation between model and BGC-Argo float data, the BIAS and RMSD of the vertically 0-200 m averaged nitrate concentration, the BIAS and RMSD of the depth of the nitracline (depth of nitrate concentration reaching 2 mmol/m³). Statistics are computed for selected aggregated sub-basins.*

Finally, BIAS and RMS of nitrate concentration between model and BGC-Argo floats are computed for selected layers (listed in Table III.1) and aggregated sub-basins and they are reported as time series in Fig. IV.6.2 and averaged in Tab. IV.6.3. These metrics, which are reported and operationally updated weekly in the thematic regional validation webpage medeaf.inogs.it/nrt-validation, show that the model has stable performance as long as the number of available BGC-Argo floats remains constant (Fig. IV.6.2).

The availability of a sufficient number of floats equipped with the nitrate sensor might pose some issue on the reliability and sustainability of these metrics. In fact, as an example, there are no floats available in the South Western Mediterranean (swm) and Alboran (alb) sub-basins in 2019 and the statistics in Ionian and North Western Mediterranean sub-basins might be biased by the sparse and uneven distribution of the floats (Fig. III.4). In spite of these limitations, the metrics show that the mean RMSD is less than 0.6 mmol/m^3 in the upper 60 m (with a few exceptions) and less than 0.7 mmol/m^3 in layers between 60 and 600 m.

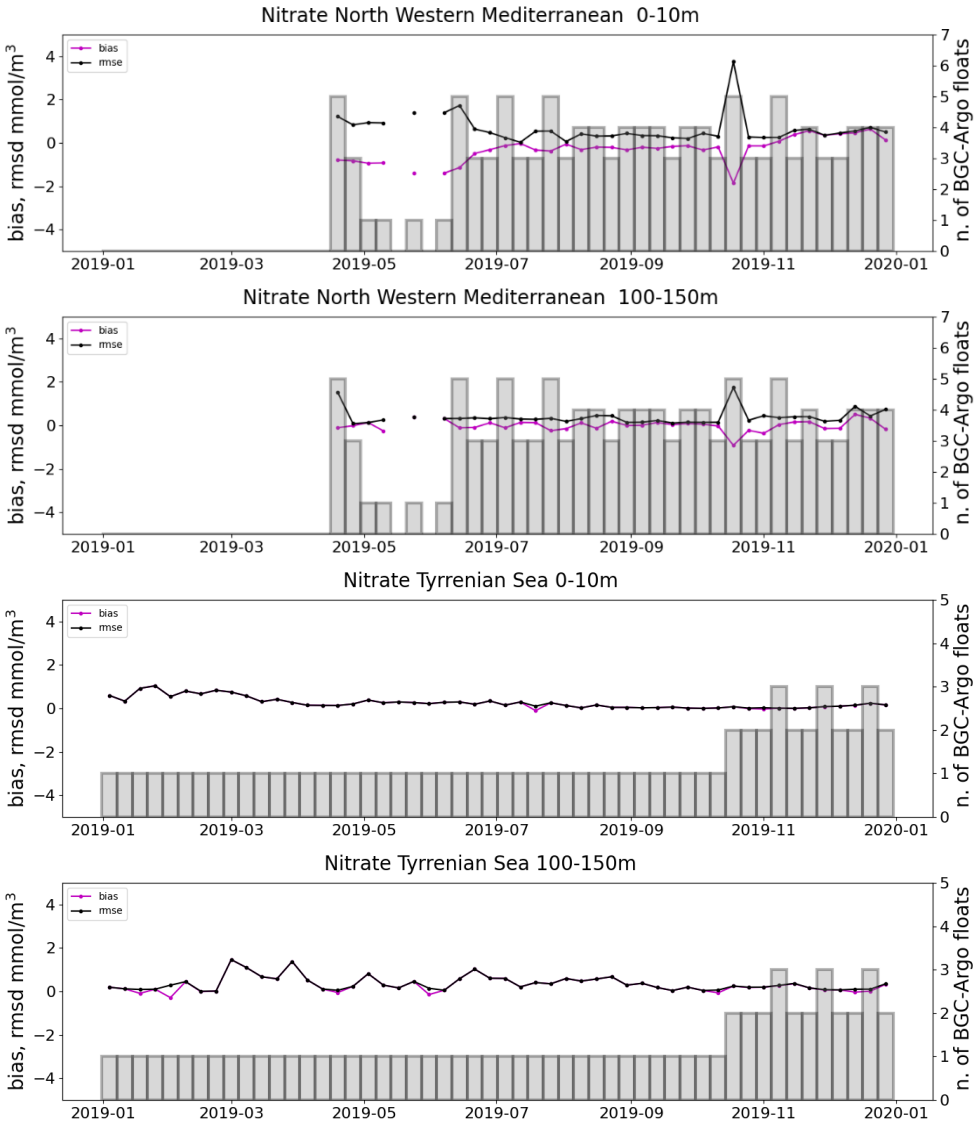

Figure IV.6.2. *Time series of BIAS (purple) and RMSD (black) of nitrate concentration [mmol/m^3] between BGC-Argo float data and model for the 0-10 m and 100-150 m layers and 4 aggregated sub-basins of Fig. III.1 (except swm). Number of data profiles used is shown by the grey vertical bars.*

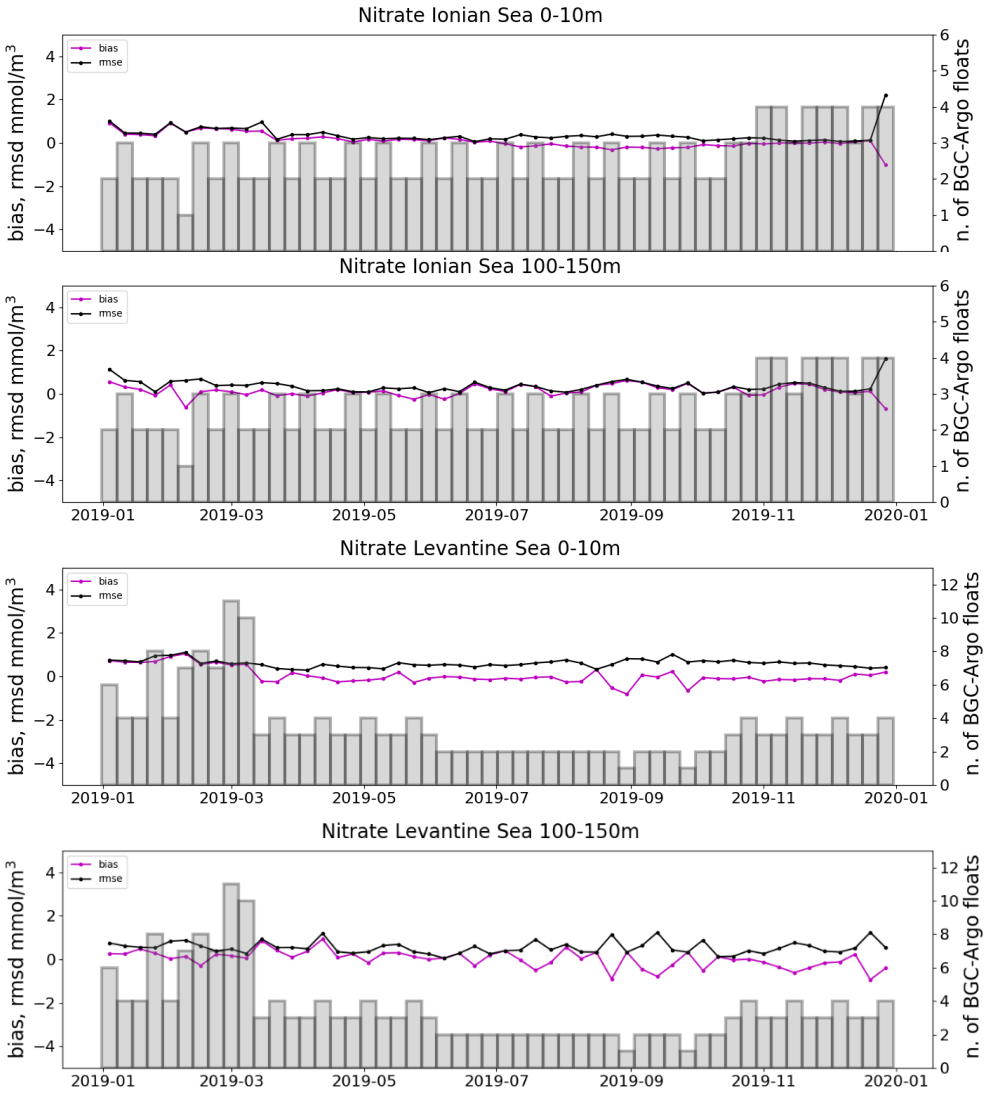

Figure IV.6.2. *(continue) Same as above.*

Layer Depth (m)	BIAS [mmol/m³]								RMSD [mmol/m³]							
	0-10	10-30	30-60	60-100	100-150	150-300	300-600	600-1000	0-10	10-30	30-60	60-100	100-150	150-300	300-600	600-1000
alb	-	-	-	-	-	-	-	-	-	-	-	-	-	-	-	-
swm	-	-	-	-	-	-	-	-	-	-	-	-	-	-	-	-
nwm	-0.30	-0.33	-0.42	0.04	0.00	-0.01	-0.04	-0.83	0.65	0.67	0.69	0.58	0.38	0.23	0.16	0.89
tyr	0.25	0.20	0.11	0.16	0.33	0.22	0.00	-0.11	0.26	0.22	0.20	0.21	0.36	0.31	0.09	0.25
adr	-0.25	-0.19	-0.38	-0.22	0.06	-0.14	-0.03	-0.29	0.32	0.28	0.41	0.31	0.32	0.20	0.18	0.30
ion	0.10	0.06	0.03	0.03	0.14	0.02	-0.23	-1.18	0.37	0.36	0.37	0.42	0.37	0.29	0.38	1.21
lev	0.05	0.04	0.07	-0.03	0.02	0.10	-0.35	-1.09	0.60	0.58	0.62	0.66	0.54	0.48	0.52	1.26

Table IV.6.3. *Averaged BIAS and RMSD of nitrate w.r.t. BGC-Argo floats for the layers of Tab. III.1, aggregated sub-basins for the period January – December 2019.*

IV.7. Dissolved Oxygen

The quality of dissolved oxygen is assessed by two validation analyses:

(i) the quantitative comparison with EMODnet2018_int vertical climatological profiles to assess the skill in reproducing the vertical characteristics along the 16 Mediterranean sub-basins (Fig. IV.16.1, Appendix A, and Table IV.7.1);

(ii) the quantitative comparison with BGC-Argo float to illustrate the quality of the model in reproducing the oxygen dynamics at the spatial mesoscale and weekly temporal scales (Figs. IV.7.1, 2 and 3 and Tabs. IV.7.2 and 3).

Modelled oxygen profiles are well simulated within the range of variability of the climatology (Fig. IV.16.1, Appendix A), with absolute BIAS and RMSD lower than 6 and 7 mmol/m^3 in all selected layers, respectively (Tab. IV.7.1).

	Oxygen		
Layer depth	**BIAS [mmol/m^3]**	**RMSD [mmol/m^3]**	**CORR**
0-10 m	2.54	5.53	0.77
10-30 m	0.77	5.15	0.79
30-60 m	-3.26	5.63	0.78
60-100 m	0.79	3.76	0.86
100-150 m	1.02	6.11	0.72
150-300 m	-1.27	5.68	0.88
300-600 m	5.69	6.88	0.96
600-1000 m	1.84	5.98	0.85

Table IV.7.1 *Skill metrics for the comparison of oxygen with respect to climatology in open sea.*

The validation of dissolved oxygen can benefit from the availability of BGC-Argo floats data.

Since MedBFM version at Q4/2022, the system assimilates oxygen BGC-Argo profiles, and the comparison is performed using misfits (i.e., model-observation differences just before the observations are assimilated). Given the frequency of BGC-Argo data is generally weekly, the misfit can be influenced by the assimilation of the same BGC-Argo float occurred at a location 50-150 km from the present position one week before (i.e., BGC-Argo float should be considered as semi-independent data).

Figure IV.7.1 shows the Hovmoller diagram of one selected BGC-Argo float and the corresponding model profiles along the trajectory covered by the floats. The MedBFM simulates, consistently with the BGC-Argo float data, the seasonal evolution of the oxygen, reproducing the mixed water column in winter and the formation of a maximum oxygen layer in correspondence of the DCM during summer and the depletion of the oxygen content at surface during summer.

Figure IV.7.2 reports the time series of the BIAS and RMSD metrics computed in the layers and aggregated sub-basins, and Table IV.7.2 reports their averages showing an absolute BIAS between 0 and 2 mmol/m^3 and an RMSD lower than 4 mmol/m^3 (except for LEV) in the surface layer. Higher uncertainty is computed for the layers below 100 m with RMSD values between 2 and 9 mmol/m^3. The time series of Fig. IV.7.2 displaying BIAS and RMSD are reported and operationally updated weekly in the thematic regional validation webpage https://medeaf.inogs.it/nrt-validation.

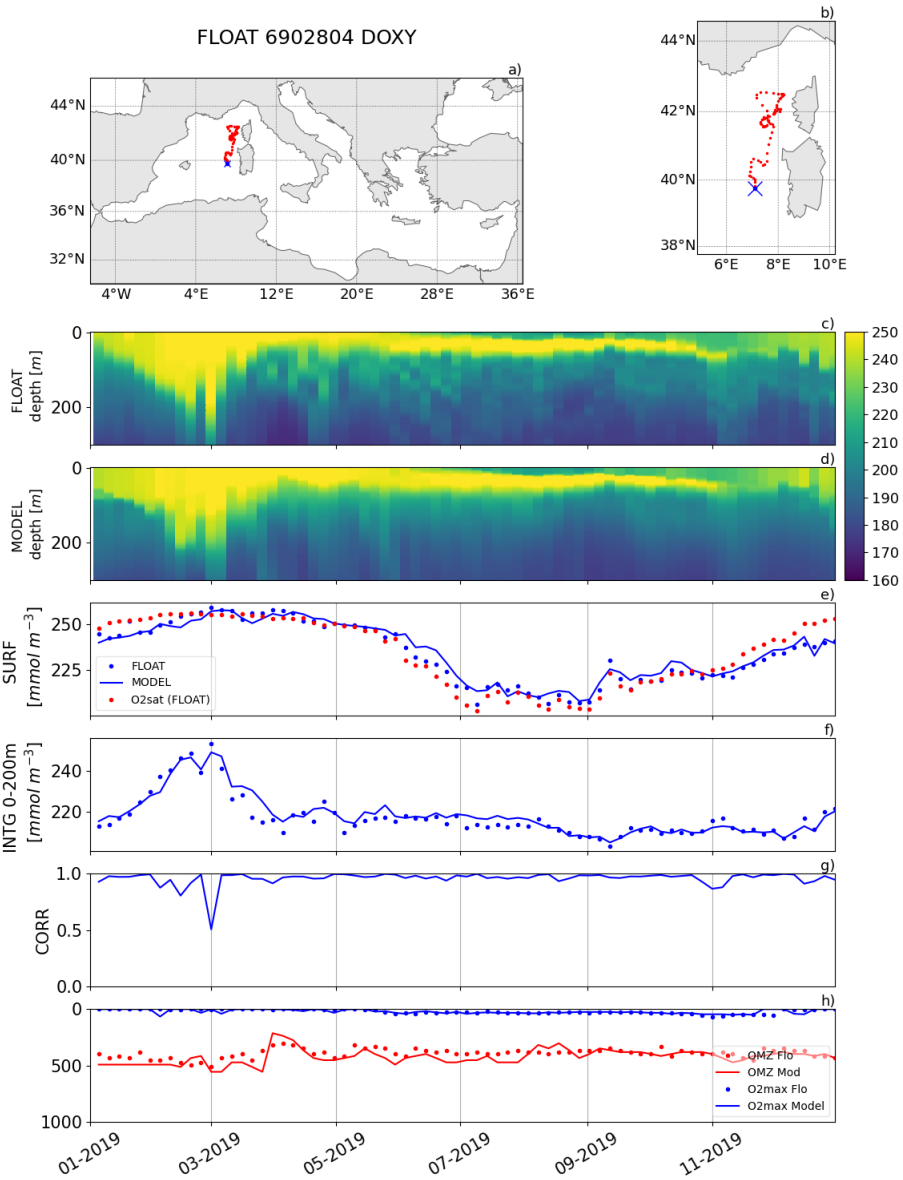

Figure IV.7.1 *Trajectory of BGC-Argo float 6902804 (a) and (b) with the first record in the time window shown as a blue cross.* ***Hovmöller*** *diagrams of dissolved oxygen [mmol/m^3] of float data (c) and the corresponding (co-located) model output (d). The skill metrics are: oxygen concentration at surface compared with Oxygen at saturation (SURF, c) 0-200 m vertically averaged chlorophyll (INTG, panel f), correlation (CORR, panel g), the oxygen maximum depth and the oxygen minimum zone depth (panel h).*

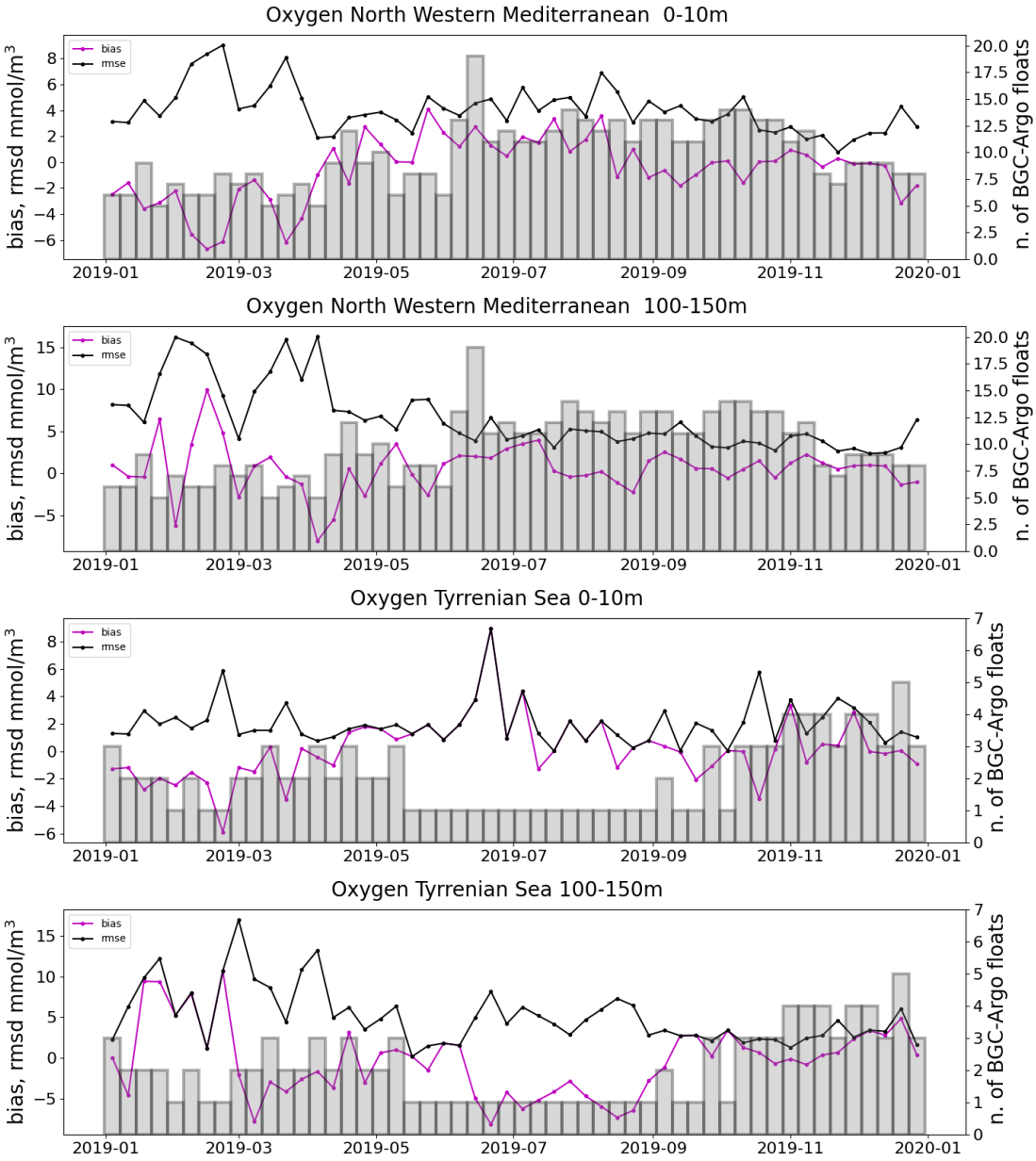

Figure IV.7.2. *Time series of dissolved oxygen BIAS and RMSD [mmol/m^3] between BGC-Argo float data and model for 0-1 0 m and 60-10 0 m layers and the aggregated sub-basins of Fig. III.1. Number of data profiles used is shown by the grey vertical bars.*

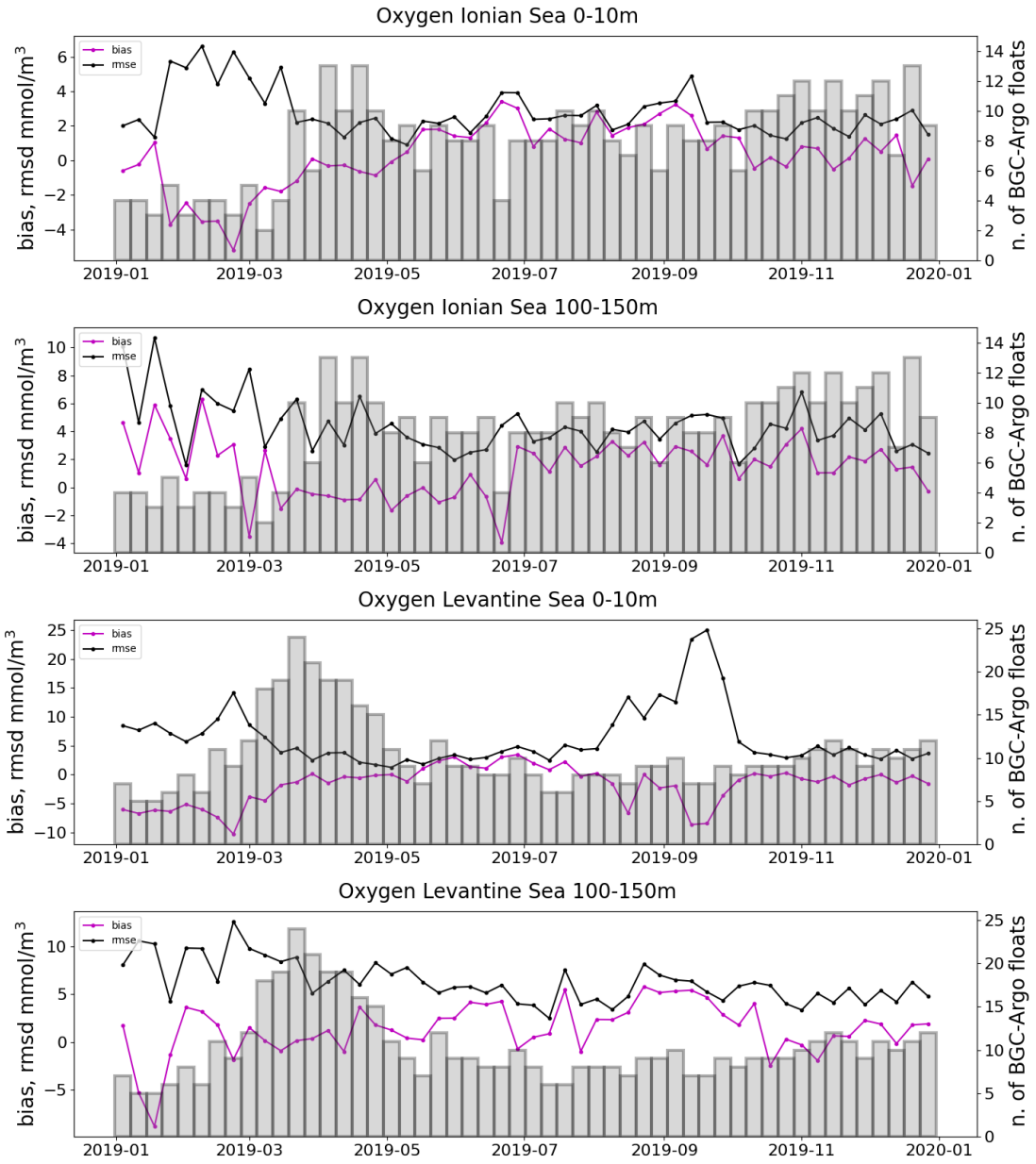

Figure IV.7.2. *(continue) Same as above.*

Layer Depth (m)	BIAS [mmol/m³]								RMSD [mmol/m³]							
	0-10	10-30	30-60	60-100	100-150	150-300	300-600	600-1000	0-10	10-30	30-60	60-100	100-150	150-300	300-600	600-1000
alb	-1.0	-3.0	-3.2	1.7	0.3	-4.6	5.0	2.4	4.5	4.3	7.1	6.5	5.8	5.5	5.1	3.3
swm	1.6	-0.6	-2.0	0.9	0.3	-0.2	5.3	7.3	3.2	3.7	5.4	5.5	6.1	3.4	6.1	7.6
nwm	-0.6	-0.9	0.5	1.3	0.6	1.1	2.7	5.6	4.0	3.9	6.1	6.3	6.5	4.6	4.4	6.9
tyr	0.1	-1.5	-3.8	0.8	-0.4	-1.2	3.0	2.5	2.0	2.8	5.6	3.3	5.0	3.2	3.3	2.8
adr	-0.6	-1.7	1.8	4.9	2.5	5.0	0.8	-3.2	3.9	5.5	5.1	6.3	4.6	7.2	1.3	3.2
ion	0.3	-0.7	-2.6	0.6	1.4	0.8	1.2	3.5	2.8	3.2	5.5	4.5	4.4	3.4	3.2	5.3
lev	-1.8	-4.1	-4.7	-0.1	1.4	-0.1	2.3	7.4	6.2	8.3	9.2	7.4	6.3	5.0	4.4	8.3

Table IV.7.2. *Averaged dissolved oxygen BIAS and RMSD of the comparison between BGC-Argo float and model values for the layers of Tab. III.1 and aggregated sub-basins of Fig. III.1.*

IV.8. Ammonium

Ammonium accuracy is assessed with Class 1 metrics: it consists of the comparison between model average vertical profiles and the EMODnet2018_int reference climatological profiles (Figures IV.16.1; appendix A) and the statistics computed using the 16 sub-basins climatological values and the corresponding model annual means (Table IV.8.1). As reported in Table IV.8.1, ammonium concentrations are simulated by the MedBFM model with an error of less than 0.4 mmol/m^3 in the upper layers and of 0.3-0.6 mmol/m^3 in the deeper layers (i.e., below 100 m). The low and negative correlation values indicate that the model has some deficiencies in reproducing typical vertical profiles and spatial gradient of ammonium, however the low data availability (only 7 sub-basins covered) might have affected the accuracy evaluation.

	Ammonium		
Layer depth	BIAS [mmol/m³]	RMSD [mmol/m³]	CORR
0-10 m	-0.33	0.38	-0.14
10-30 m	-0.14	0.19	-0.16
30-60 m	-0.06	0.15	-0.08
60-100 m	-0.03	0.24	-0.44
100-150 m	-0.10	0.31	-0.41
150-300 m	-0.22	0.32	-0.26
300-600 m	-0.37	0.43	0.77
600-1000 m	-0.40	0.55	0.84

Table IV.8.1 *Skill metrics for the comparison of ammonium with respect to climatology in open sea.*

IV.9. Silicate

Silicate validation is performed with Class 1 metrics assessment: it consists in the comparison between model average vertical profiles and the EMODnet2018_int reference climatological profiles (Figures IV.16.1; appendix A) and the statistics computed using the 16 sub-basins climatological values and the corresponding model annual means (Table IV.9.1). As shown in figures IV.16.1 (appendix A), the profiles are well simulated within the range of variability of the climatology except in the western basins where the model overestimates concentration at the surface. As reported in Table IV.9.1, silicate concentrations are simulated by the MedBFM model with an uncertainty below of 0.7 mmol/m^3 in the upper layers and of about 0.5-0.8 mmol/m^3 in the deeper layers (i.e., below 60 m). Low correlation value in the surface layer indicates that the model has some deficiencies in reproducing the typical surface

spatial gradient of silicate concentration, that occurs especially in the western basin. The correlation values of the deep layers are pretty high (around 0.8) highlighting that subsurface modelled gradients are consistent with observations.

	Silicate		
Layer depth	**BIAS [mmol/m^3]**	**RMSD [mmol/m^3]**	**CORR**
0-10 m	0.59	0.65	0.77
10-30 m	0.63	0.69	0.71
30-60 m	0.49	0.55	0.78
60-100 m	0.35	0.51	0.74
100-150 m	0.57	0.81	0.62
150-300 m	0.56	0.83	0.73
300-600 m	-0.48	0.72	0.89
600-1000 m	-0.43	0.65	0.93

Table IV.9.1 *Skill metrics for the comparison of silicate with respect to climatology in open sea.*

IV.10. pH

pH validation is performed with Class 1 metrics assessment: it consists in the comparison between model average vertical profiles and the EMODnet2018_int reference climatological profiles (Figure IV.16.2 appendix A). The comparison between model vertical profiles and the reference climatological profiles (Class1 metric validation of Figures IV.16.2 in appendix A) shows the good skill of the model in representing the basin-wide gradient and sub-basin vertical pH profiles. The statistics computed using the 16 sub-basins climatological values and the corresponding model annual means (Table IV.10.1) highlights that uncertainty, which never exceeds 0.04, is lower at deeper layers than at surface.

	pH in total scale		
Layer depth	**BIAS [-]**	**RMSD [-]**	**CORR**
0-1 0 m	-0.012	0.032	0.78
10-3 0 m	-0.011	0.023	0.68
30-6 0 m	-0.016	0.028	0.43
60-10 0 m	-0.001	0.025	0.66
100-15 0 m	0.008	0.017	0.78
150-30 0 m	0.006	0.014	0.92
300-60 0 m	0.012	0.014	0.97
600-100 0 m	0.004	0.007	0.97

Table IV.10.1 *Skill metrics for the comparison of pH with respect to sub-basin profiles climatology in open sea.*

IV.11. Alkalinity

The validation of the Alkalinity (ALK) is performed with Class 1 metrics assessment: it consists in the comparison between model average vertical profiles and the EMODnet2018_int reference climatological profiles (Figure IV.16.2 appendix A). It is worth to note that alkalinity is typically reported as μmol/kg whereas the product in the Copernicus Marine Service catalogue is reported as mol/m^3. The density of seawater is needed for the conversion. As shown in figures IV.16.2 (appendix A), the profiles are well simulated within the range of variability of the climatology except in the western basins where the model overestimates concentration of alkalinity at the surface. As reported in Table IV.11.1, alkalinity concentrations are simulated by the MedBFM model with an error of around 40 μmol/kg in

the upper layers and of about 10-20 μmol/kg in the deeper layers (i.e., below 60 m). High correlation values in all layers indicate that the model reproduces the typical spatial gradient of alkalinity.

	Alkalinity		
Layer depth	**BIAS** [μmol kg^{-1}]	**RMSD** [μmol kg^{-1}]	**CORR**
0-10 m	22.61	39.25	0.93
10-30 m	21.69	29.88	0.97
30-60 m	16.48	22.70	0.98
60-100 m	6.24	18.93	0.94
100-150 m	8.73	10.22	0.99
150-300 m	1.55	13.49	0.93
300-600 m	0.50	9.89	0.89
600-1000 m	-0.09	8.27	0.93

Table IV.11.1 *Skill metrics for the comparison of alkalinity with respect to sub-basin profiles climatology in open sea.*

IV.12. Dissolved Inorganic Carbon (DIC)

The validation of dissolved inorganic carbon (DIC) is performed with Class 1 metrics assessment: it consists in the comparison between model average vertical profiles and the EMODnet2018_int reference climatological profiles (Figure IV.16.2, appendix A). It is worth to note that DIC is typically reported as [μmol/kg] whereas the Copernicus Marine Service product is reported as [mol/m^3]. The density of seawater is needed for the conversion. As shown in figures IV.16.2 (appendix A), the profiles are well simulated within the range of variability of the climatology except in the western and ION1 sub-basins where the model slightly overestimates concentration of DIC at the surface. As reported in Table IV.12.1, DIC concentrations are simulated by the MedBFM model with a mean error of around 30 μmol/kg in the upper layers and of about 4-16 μmol/kg in the deeper layers (i.e., below 60 m). High correlation values in all layers indicate that the model reproduces the typical spatial gradient of DIC.

It is worth to note that, for both DIC and alkalinity, higher uncertainty is associated with high variability. In fact, DIC and alkalinity profiles are characterized by high variability in the upper layers (down to 60 m) whereas deeper values remain almost constant during the year. This high variability at the surface of DIC and ALK dynamics is determined by three major factors: the input in the eastern marginal seas (the terrestrial input from the Po and other Italian rivers and the input from the Dardanelles), the effect of evaporation in the eastern basin (which has a seasonal component), and the influx of the low-ALK and low-DIC Atlantic waters in the western basin. The thermohaline basin-wide circulation modulates the intensity and the patterns of the spatial gradients. Intermediate and deep layers show weaker dynamics and less variability (see figures IV.16.2, appendix A).

	Dissolved inorganic carbon		
Layer depth	**BIAS** [µmol kg^{-1}]	**RMSD** [µmol kg^{-1}]	**CORR**
0-10 m	22.2	34.0	0.93
10-30 m	24.3	30.6	0.95
30-60 m	17.0	24.1	0.93
60-100 m	4.5	16.4	0.88
100-150 m	0.8	14.3	0.87
150-300 m	-2.8	8.2	0.82
300-600 m	-7.4	11.0	0.79
600-1000 m	-1.6	4.1	0.93

Table IV.12.1 *Skill metrics for the comparison of dissolved inorganic carbon with respect to sub-basin profiles climatology in open sea.*

IV.13. Surface partial pressure of CO2

Two reference datasets are used for the validation of surface pCO2: one of in situ or recalculated pCO2 values derived from the EMODnet 2018 dataset (Fig. III.3) and the dedicated global dataset SOCAT v2 (Fig. III.5). Climatological reference values at sub-basin scale are derived from the two datasets and compared with the modelled 2019 average.

Class 1 comparison between surface pCO2 model and the reference climatological surface values from Emodnet2018_int (Class1 metric validation) are shown in Figure IV.16.2 in appendix A. Metrics of comparison between sub-basin values from model and climatology are reported in the first row of Table IV.13.1.

The mean monthly evolutions of SOCAT and model for selected subbasins (class 1 comparison) are shown in Figure IV.13.1. Metrics of comparison between monthly values from model and climatology are computed for the 16 sub-basins, then averaged and reported in the second row of Table IV.13.1.

As shown in the comparison between model and the two reference climatologies the spatial gradients and seasonal cycle are well reproduced (high correlation values in Tab. IV.13.1 and values in Fig IV.13.2). The model overestimation, mostly in summer months (Fig. IV.13.1). Model uncertainty can be partly due to the fact that the two climatologies refer to a past condition (observations from the 2000-2015 period). Thus, the current trend of surface pCO2 is not fully accounted in the reference datasets but simulated by the model. The lack of NRT observations represents a limit for an accurate validation of this variable.

Dataset	**Surface pCO2 [µatm]**		
	BIAS	**RMSD**	**CORR**
EMODnet2018; pCO2 at 0-10 m	16.6	36.0	0.69
SOCAT v2; surface pCO2	35.7	42.4	0.91

Table IV.13.1 *Skill metrics for the comparison of surface pCO2 with respect to sub-basin climatology in open sea.*

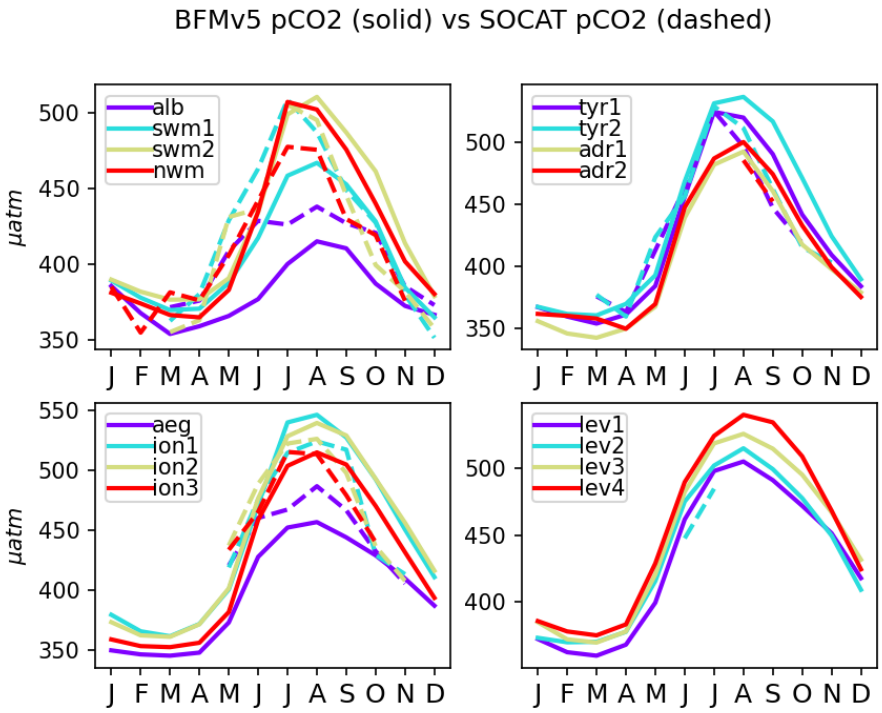

Figure IV.13.1 *Monthly evolution of surface pCO2 [µatm] of model (solid lines) and climatology derived from SOCAT dataset (dashed lines when present) for the Mediterranean sub-basins.*

IV.14. Surface flux of CO2

The modelled mean annual surface flux of CO2 (Fig. IV.14.1) can be qualitatively compared with previous published estimations (section 1.7 of the Ocean State Report in von Schuckmann et al., 2018; d'Ortenzio et al., 2008; Melaku Canu et al., 2015). The mean annual patterns, i.e. western-to-eastern and the northern-to-southern decreasing gradients and the almost neutral condition are consistently in agreement with the previous estimations. The west to east gradient of the surface flux of CO2 simulated by the operational product is consistent with the reanalysis product presented in the Ocean State Report, even if values tend to be mostly positive in this specific year (sink flux from the atmosphere to the sea), however reasonable.

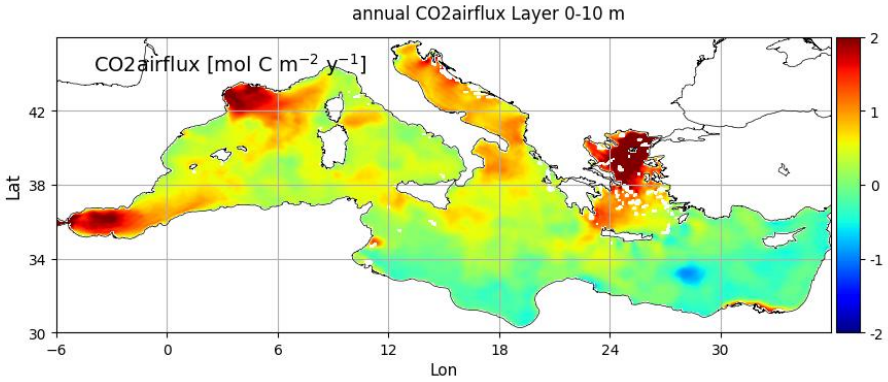

Figure IV.14.1. *Mean annual map of surface flux of CO2.*

IV.15. Light attenuation coefficient at 490 nm (Kd490)

Modelled diffuse attenuation coefficient for downwelling irradiance at the 490 nm wavelength is compared with the Copernicus Marine Service Ocean Color MED_CHL_L3_REP_OBSERVATIONS_009_078 products. Statistics are computed for each of the 16 sub-basins (open sea) and reported in table IV.15.1.

The highest uncertainty values (i.e., RMSD computed for each grid cell) are in the western sub-basins in winter. Model slightly overestimates the Kd490 in eastern sub-basins in summer.

OFF SHORE	Light attenuation coefficient (Kd490) Mod-Sat [m^{-1}]				Light attenuation coefficient (Kd490) log_{10}(Mod)-log_{10}(Sat)			
	RMSD		BIAS		RMSD		BIAS	
	win	Sum	win	sum	win	sum	win	sum
alb	0.016	0.011	-0.002	0.006	0.107	0.111	-0.005	0.076
swm1	0.01	0.007	0.002	0.006	0.093	0.095	0.026	0.089
swm2	0.013	0.007	-0.002	0.006	0.105	0.101	0.002	0.099
nwm	0.014	0.005	-0.007	0.004	0.101	0.07	-0.053	0.057
tyr1	0.009	0.005	-0.007	0.004	0.083	0.07	-0.064	0.063
tyr2	0.007	0.006	-0.004	0.006	0.069	0.094	-0.036	0.092
adr1	0.006	0.003	-0.004	0.001	0.059	0.034	-0.046	0.014
adr2	0.005	0.003	-0.002	0.002	0.054	0.043	-0.019	0.032
aeg	0.007	0.005	-0.001	0.004	0.06	0.073	-0.008	0.063
ion1	0.005	0.006	-0.001	0.006	0.06	0.101	-0.003	0.099
ion2	0.004	0.006	0.002	0.006	0.055	0.102	0.035	0.1
ion3	0.005	0.006	-0.001	0.005	0.051	0.088	-0.009	0.083
lev1	0.005	0.006	0.004	0.006	0.067	0.096	0.052	0.095
lev2	0.005	0.006	0.002	0.006	0.065	0.096	0.026	0.094
lev3	0.005	0.006	0.004	0.006	0.071	0.1	0.064	0.098
lev4	0.005	0.006	0.002	0.006	0.061	0.102	0.026	0.097
Med ave	0.0075	0.006	-0.001	0.005	0.073	0.086	-0.001	0.078

Table IV.15.1. *Mean RMSD and BIAS of light attenuation coefficient [m^{-1}] between model and satellite for the period January – December 2019. On the right side, the skill indexes are computed on the log-transformed model and satellite chlorophyll. Winter (win) corresponds to January to April, summer (sum) corresponds to June to September.*

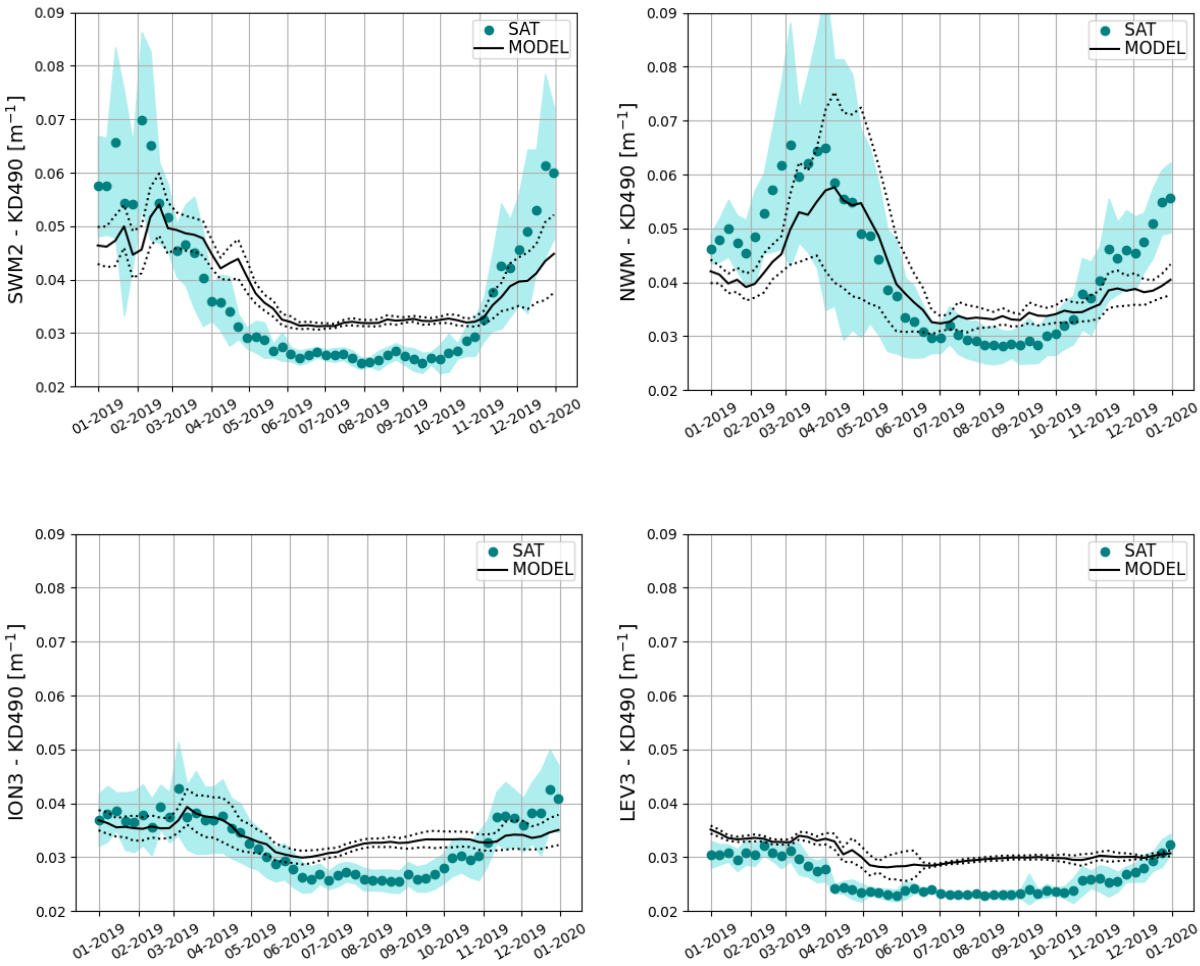

Figure IV.15.2. *Time series of the weekly qualification run mean surface kd490 in open sea (black solid line, RAN) with the spatial standard deviation (STD, dotted black line) and the DT multi-sensor satellite data (dark turquoise dots, SAT) with its STD (shaded turquoise area) for four of the Mediterranean basins of Fig. III.1.*

IV.16. Phytoplankton Functional Types (PFTs)

Modelled chlorophyll of the phytoplankton functional types (Diatoms, Nanoflagellates, Picophytoplankton and Dinoflagellates) are compared with chlorophyll values derived from the pigment HPLC measurements using the Di Cicco et al. (2017) equations. Figure IV.16.1 reports the winter and summer chlorophyll profiles of model and HPLC data averaged over the Mediterranean Sea, while Tables IV.16.1-4 report the statistics (BIAS, RMSD, CORR and n. of data) for selected layers. The model reproduces quite well diatoms, picophytoplankton and dinoflagellates profiles and seasonal cycle, while the nanoflagellates group shows the highest RMSD and a general model underestimation.

A visual comparison of the model results with the satellite-derived PFTs from ocean colour data is reported in Figures IV.16.2-3 showing the timeseries of surface chlorophyll in the 16 sub-basins. The comparison shows that both PFTs estimates (model and satellite-derived) have the same seasonal cycles (i.e., surface winter bloom and summer low values), the same spatial gradients (i.e., higher values in the western sub-basins with respects to eastern sub-basins) and the same dominance of the

picophytoplankton in summer period. With regards the winter surface bloom, the two estimates (model and satellite-derived) shows some different behaviours depending on the specific sub-basin.

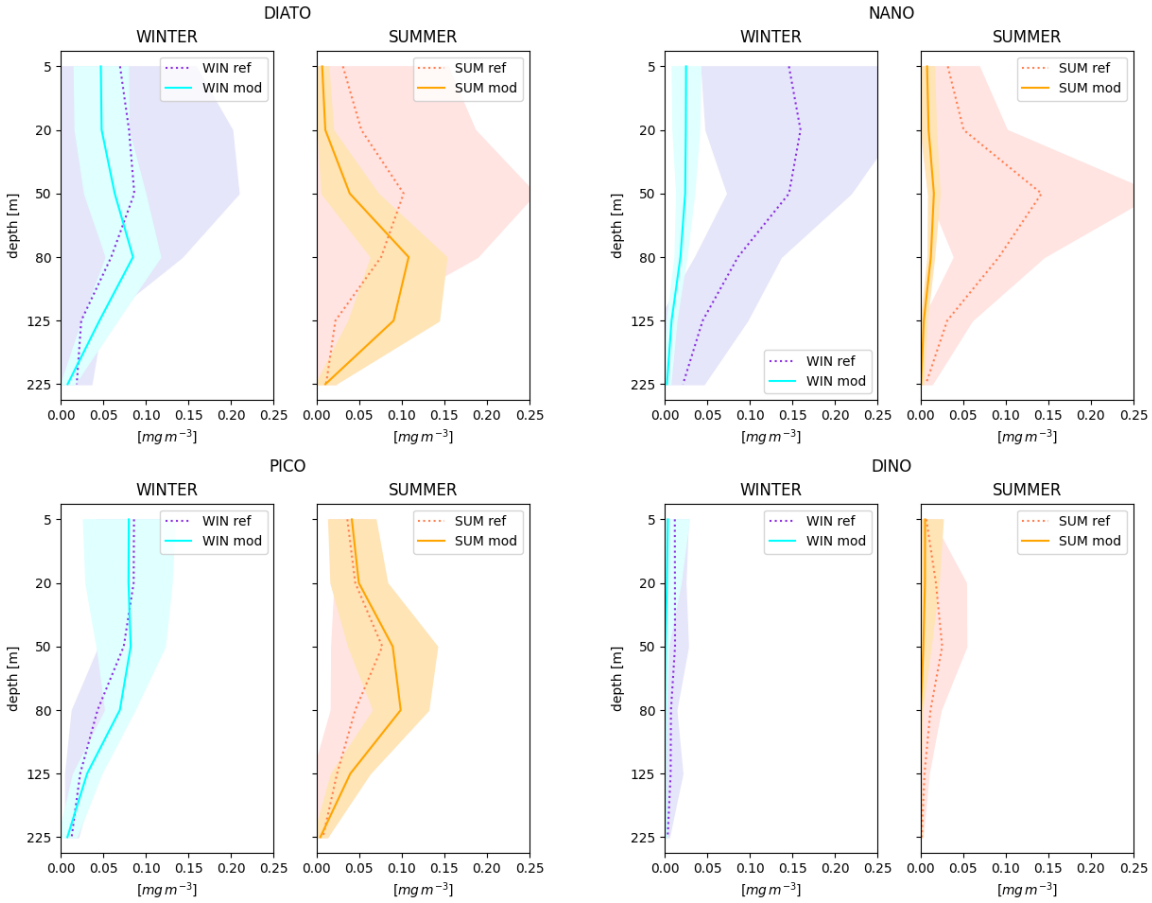

Figure IV.16.1. *climatological winter and summer profiles of the 4 PFTs for model (solid line) and HPLC data (dashed line). The four PFTs are diatoms (DIATO), nanoflagellates (NANO), picophytoplankton (PICO) and dinoflagellates (DINO).*

	BIAS [mg/m^3]							
Layer depth	DIATO		NANO		PICO		DINO	
	win	sum	Win	sum	win	sum	win	sum
0-1 0 m	-0.03	-0.01	-0.11	-0.02	0.00	0.00	-0.01	0.00
10-3 0 m	-0.04	-0.01	-0.12	-0.02	0.00	0.00	-0.01	-0.01
30-6 0 m	-0.03	-0.03	-0.12	-0.10	0.01	0.02	-0.01	-0.02
60-10 0 m	0.02	0.06	-0.06	-0.09	0.03	0.05	-0.01	-0.01
100-15 0 m	0.02	0.06	-0.03	-0.03	0.01	0.01	-0.01	0.00
150-30 0 m	0.00	0.00	-0.01	-0.01	0.00	-0.01	0.00	0.00

Table IV.16.1. *Winter and summer mean BIAS [mg/m^3] calculated on the aggregated sub-basins for the 4 PFTs with respect to HPLC data for selected layers in the euphotic zone.*

	RMSD [mg/m^3]							
Layer depth	DIATO		NANO		PICO		DINO	
	win	sum	Win	sum	win	sum	win	sum
0-1 0 m	0.06	0.03	0.12	0.02	0.05	0.01	0.01	0.01
10-3 0 m	0.08	0.04	0.14	0.03	0.05	0.02	0.01	0.03
30-6 0 m	0.09	0.06	0.13	0.13	0.04	0.03	0.01	0.03
60-10 0 m	0.08	0.08	0.07	0.11	0.03	0.06	0.01	0.01
100-15 0 m	0.04	0.08	0.04	0.03	0.02	0.02	0.01	0.01
150-30 0 m	0.01	0.01	0.02	0.01	0.01	0.01	0.00	0.00

Table IV.16.2. *Winter and summer mean RMSD [mg/m^3] calculated on the aggregated sub-basins for the 4 PFTs with respect to HPLC data for selected layers in the euphotic zone.*

	CORR [mg/m^3]							
Layer depth	DIATO		NANO		PICO		DINO	
	win	sum	win	sum	win	sum	win	sum
0-1 0 m	0.58	0.07	0.67	0.89	0.40	0.64	0.09	0.84
10-3 0 m	0.73	0.50	0.51	0.56	0.40	0.41	0.14	0.29
30-6 0 m	0.58	0.73	0.56	0.71	0.36	0.87	0.21	0.56
60-10 0 m	-0.33	0.00	0.05	0.36	0.07	0.13	0.36	0.53
100-15 0 m	-0.40	-0.37	0.31	0.55	0.52	0.70	-0.14	-0.45
150-30 0 m	0.67	0.33	0.80	0.17	0.68	0.56	0.70	0.67

Table IV.16.3. *Winter and summer mean correlation calculated on the aggregated sub-basins for the 4 PFTs with respect to HPLC data for selected layers in the euphotic zone.*

	Size (n)							
Layer depth	DIATO		NANO		PICO		DINO	
	win	sum	win	sum	win	sum	win	sum
0-1 0 m	11	14	11	14	11	14	11	13
10-3 0 m	11	13	11	13	11	13	11	11
30-6 0 m	11	13	11	13	11	13	10	12
60-10 0 m	11	13	11	13	11	13	11	11
100-15 0 m	10	11	10	11	10	11	9	9
150-30 0 m	10	12	8	11	8	11	5	6

Table IV.16.4. *Winter and summer number of basin HPLC data used for the statistics calculated in Tables IV.16.1-3 for the 4 PFTs in both season for the selected layers in the euphotic zone.*

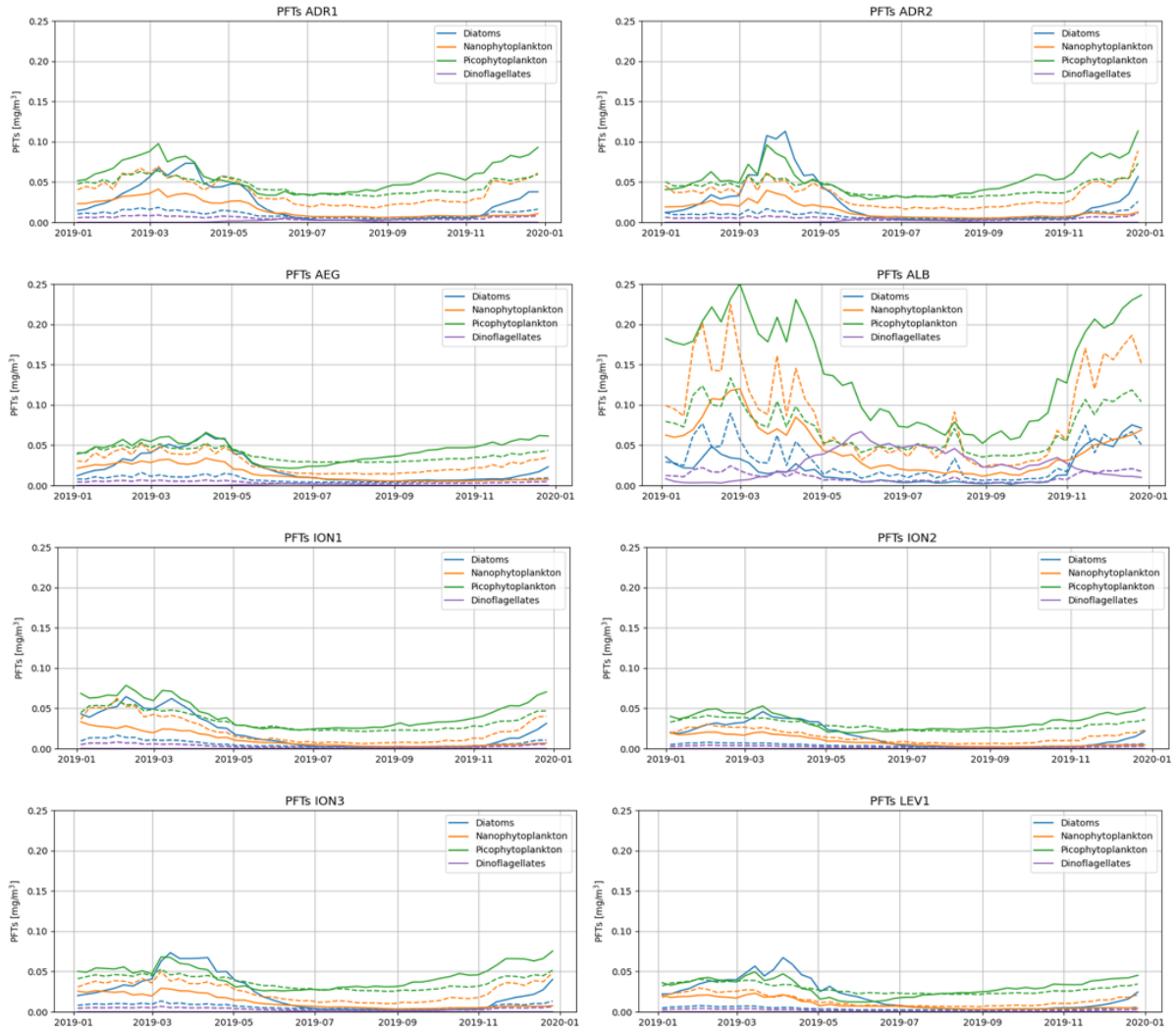

Figure IV.16.2. *Time series of the 4 PFTs from model (solid lines) and from satellite-derived ocean colour (dashed lines) in the 16 sub-basins of Fig. III.1.*

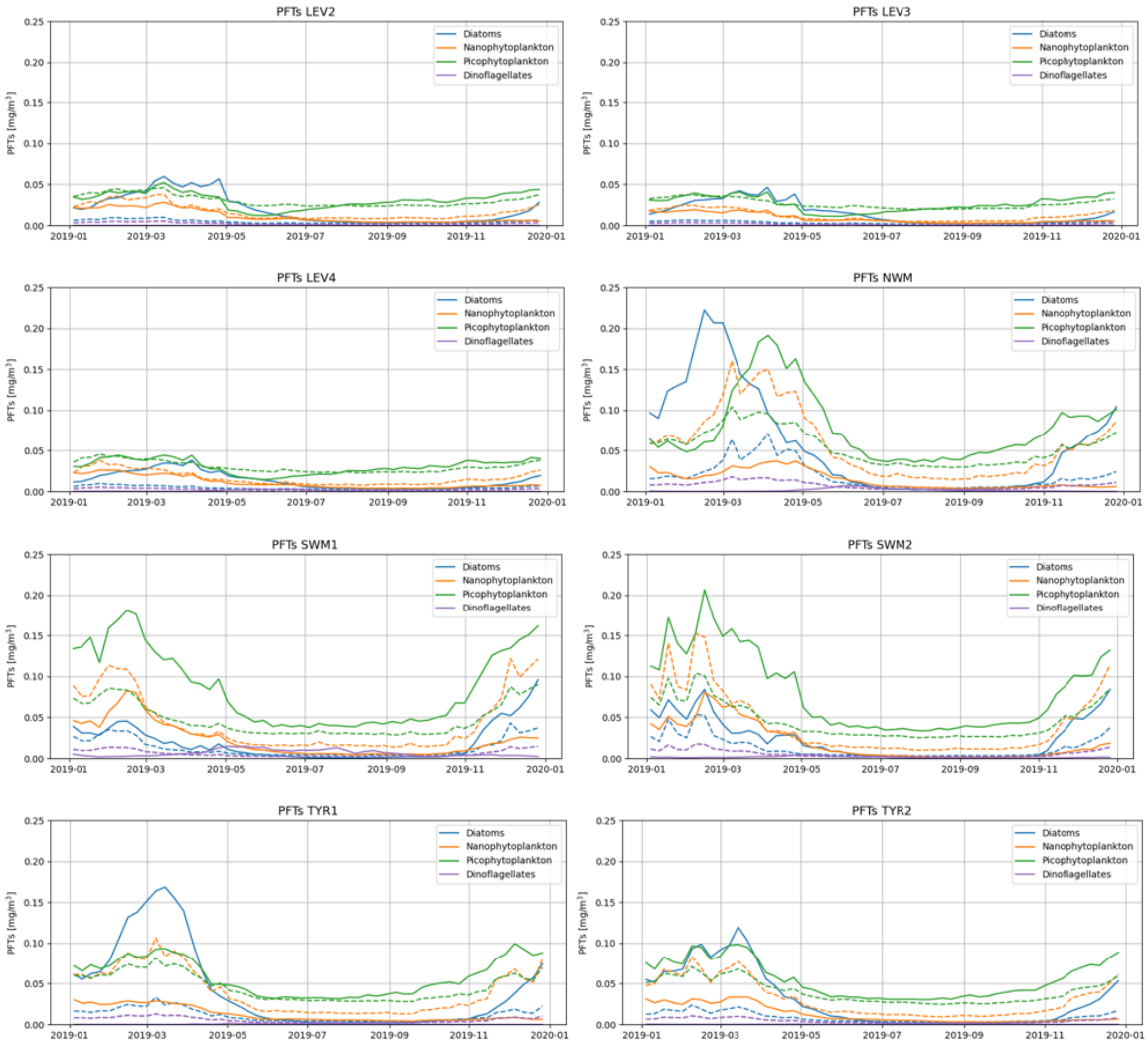

Figure IV.16.3. *(continue) Same as above.*

IV.17. Appendix A: class 1 climatological comparison

This section reports the class 1 visual comparison for all the model variables. Weekly (grey lines) and overall average (black lines) profiles for the model run 2019 are compared with climatological vertical profiles (red dots for means and dashed lines for standard deviations) for the 16 sub-basins of Fig. III.1. Two sets of figures are presents: one for oxygen and nutrient variables (Figure IV.16.1), and one for carbonate system variables (Figures IV.16.2).

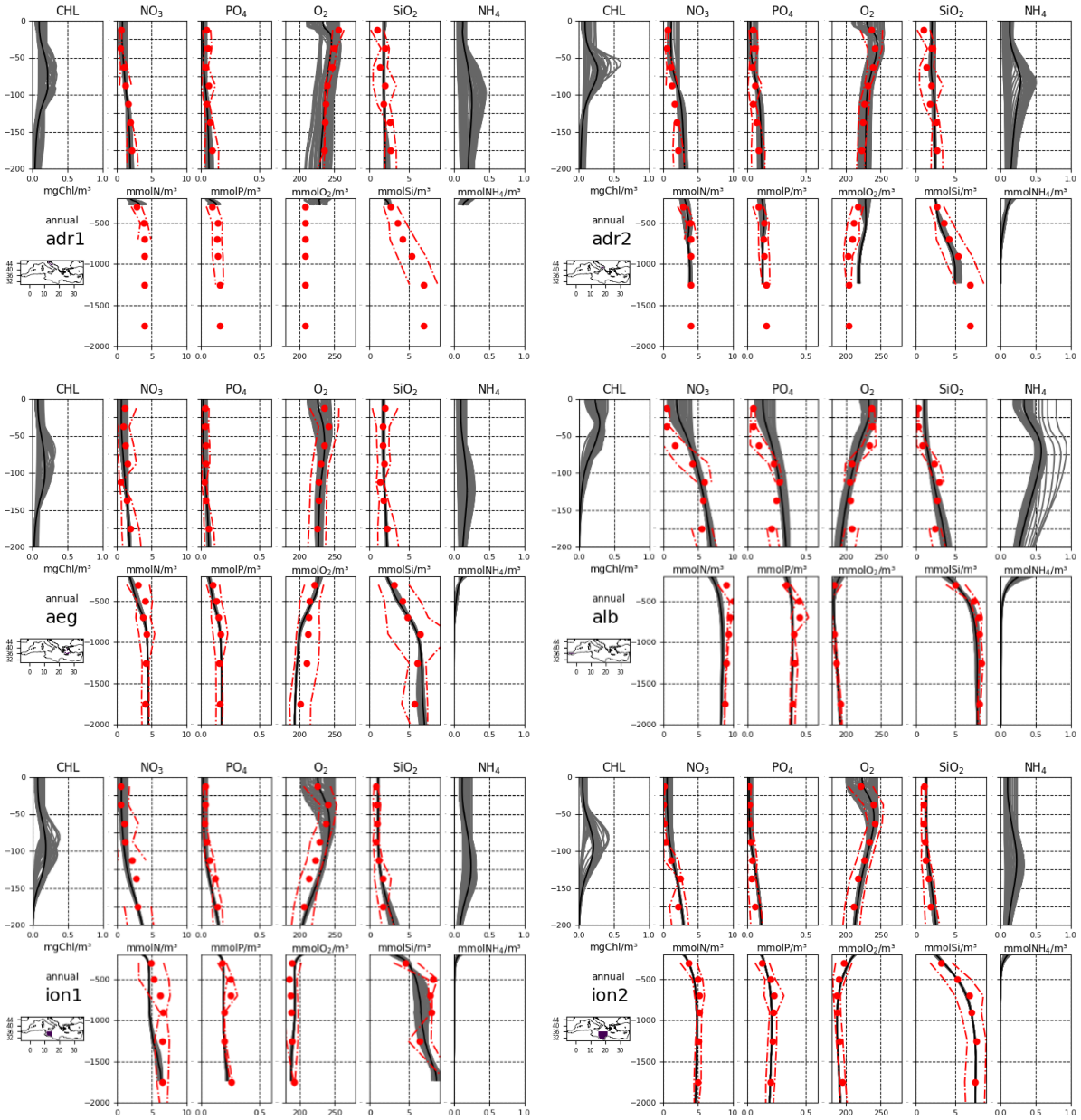

Fig. IV.16.1 *Comparison between weekly (grey lines) and annual (black lines) vertical profiles from the Copernicus Marine model run for the Mediterranean sub-basins (except ADR1 due to lack of reference data) and climatological profiles of nitrate, phosphate and dissolved oxygen, Silicate and Ammonium retrieved from EmodeNET dataset (red dots).*

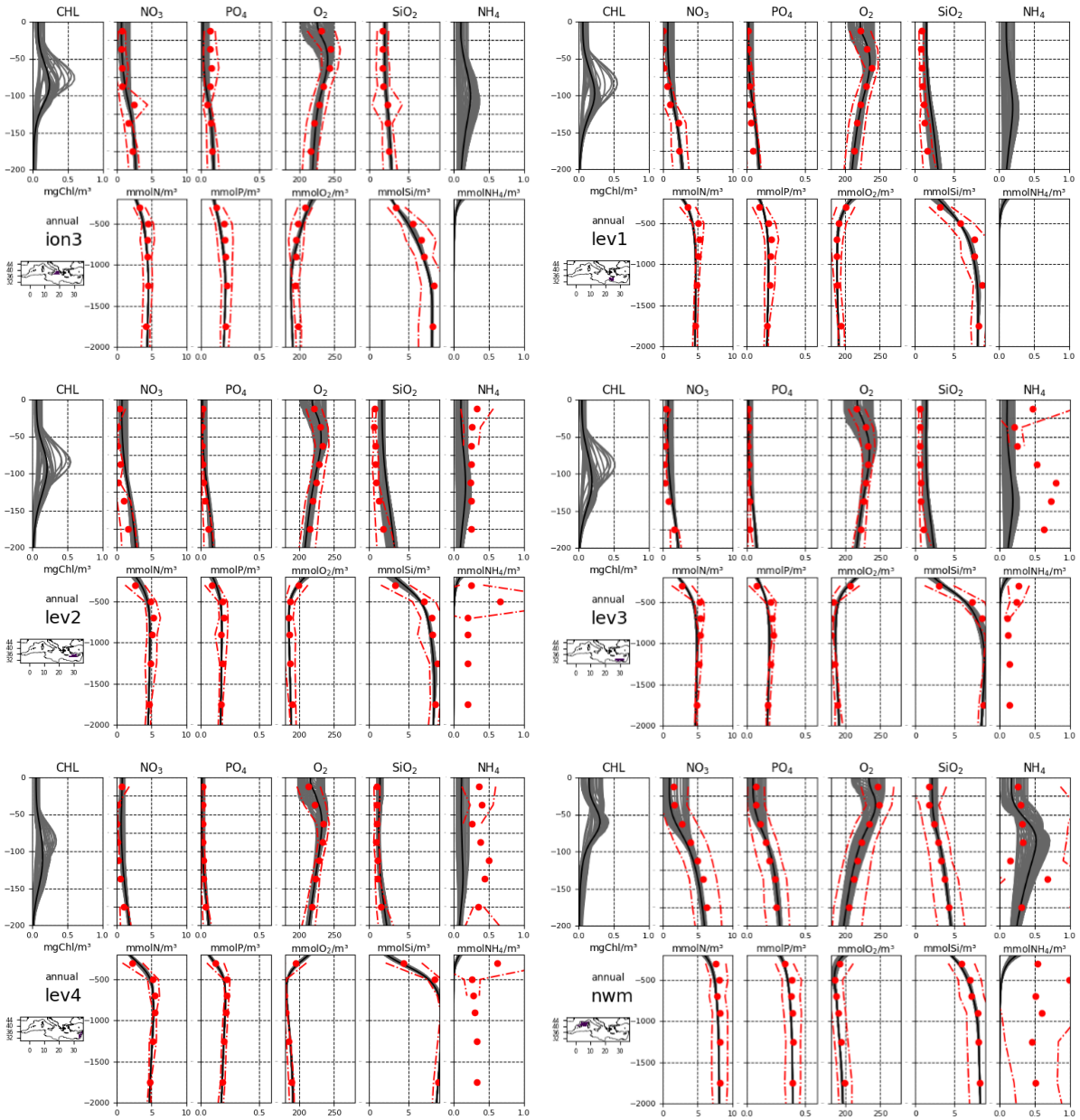

Fig. IV.16.1 *(cont). See above.*

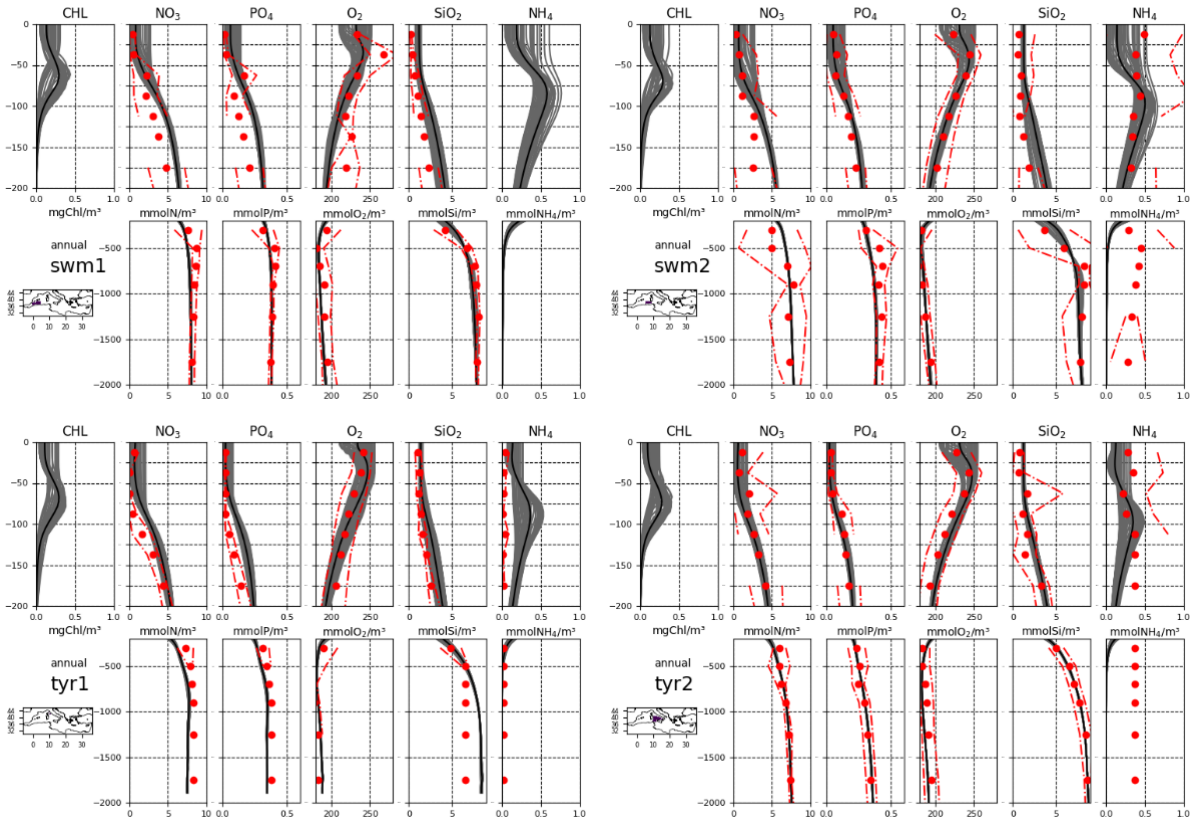

Fig. IV.16.1 *(cont.). See above.*

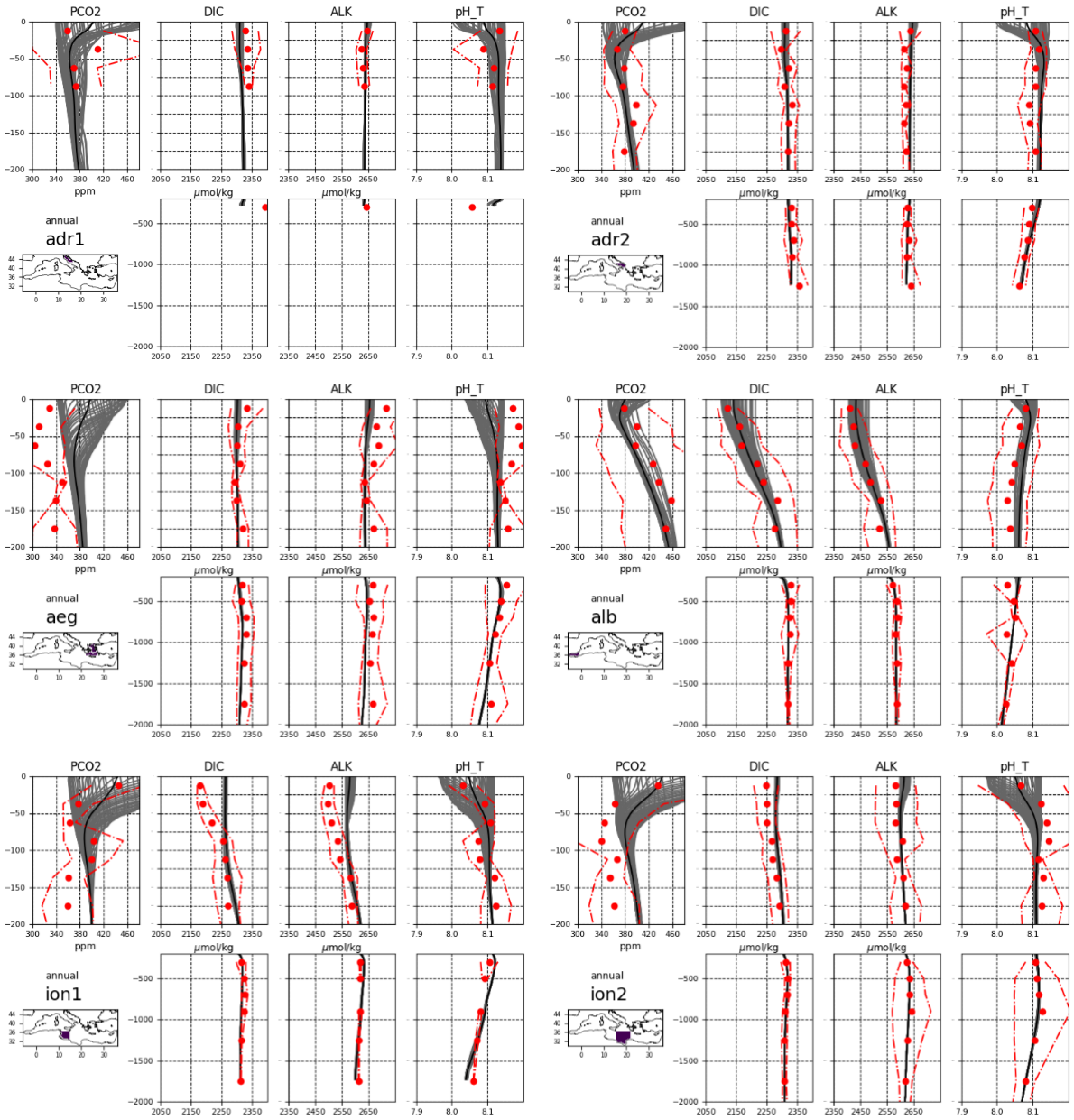

Figure IV.16.2 *Profiles of pCO2, DIC, ALK and pH in total scale: mean weekly model profiles (grey color lines; from January to December 2019), mean annual model profiles (black lines) and CarbSys derived climatological (±standard deviation) profiles (red dots and dashed lines) for the sub-basins of Fig. III.1.*

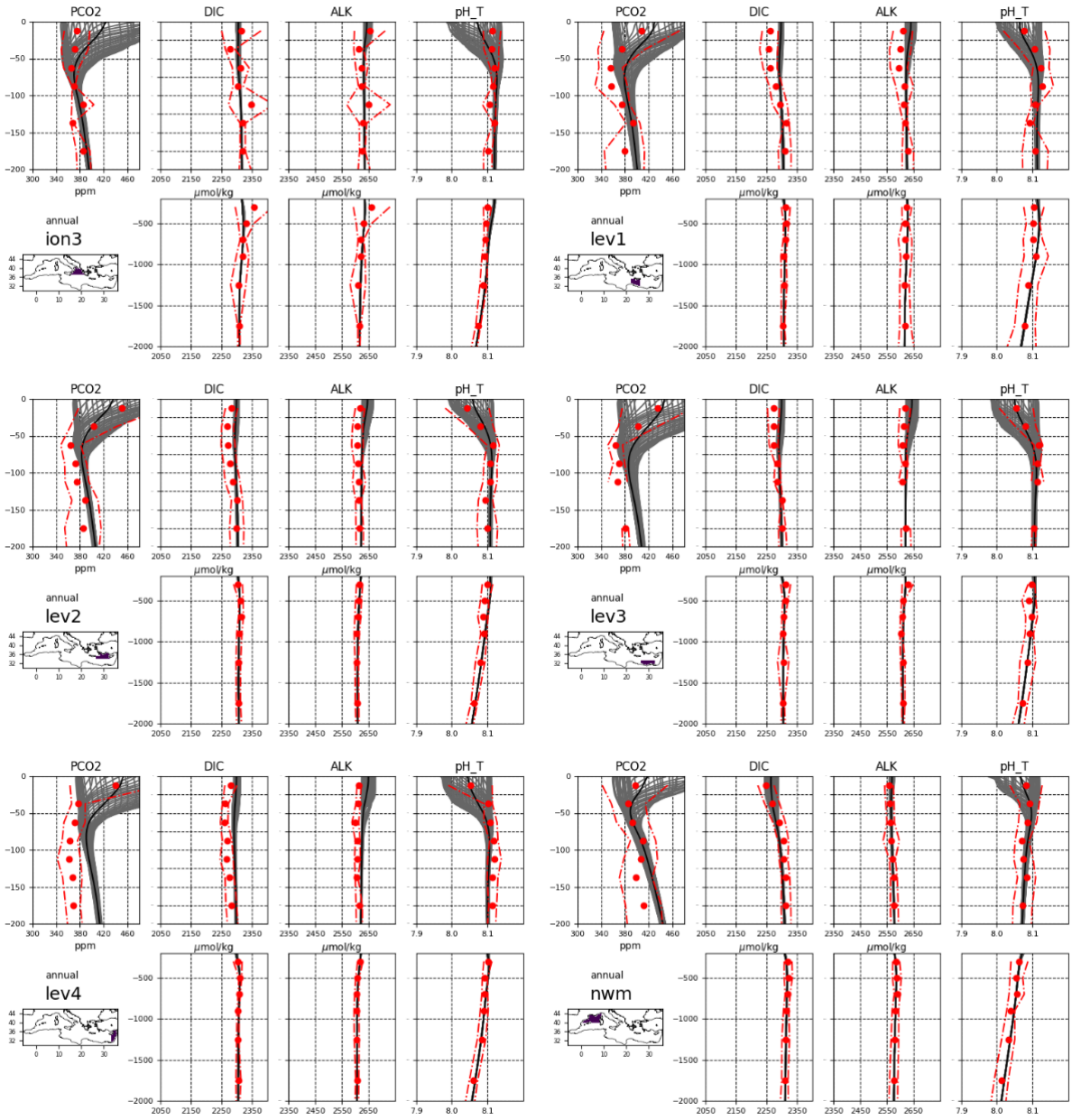

Figure IV.16.2 *(cont.) See above.*

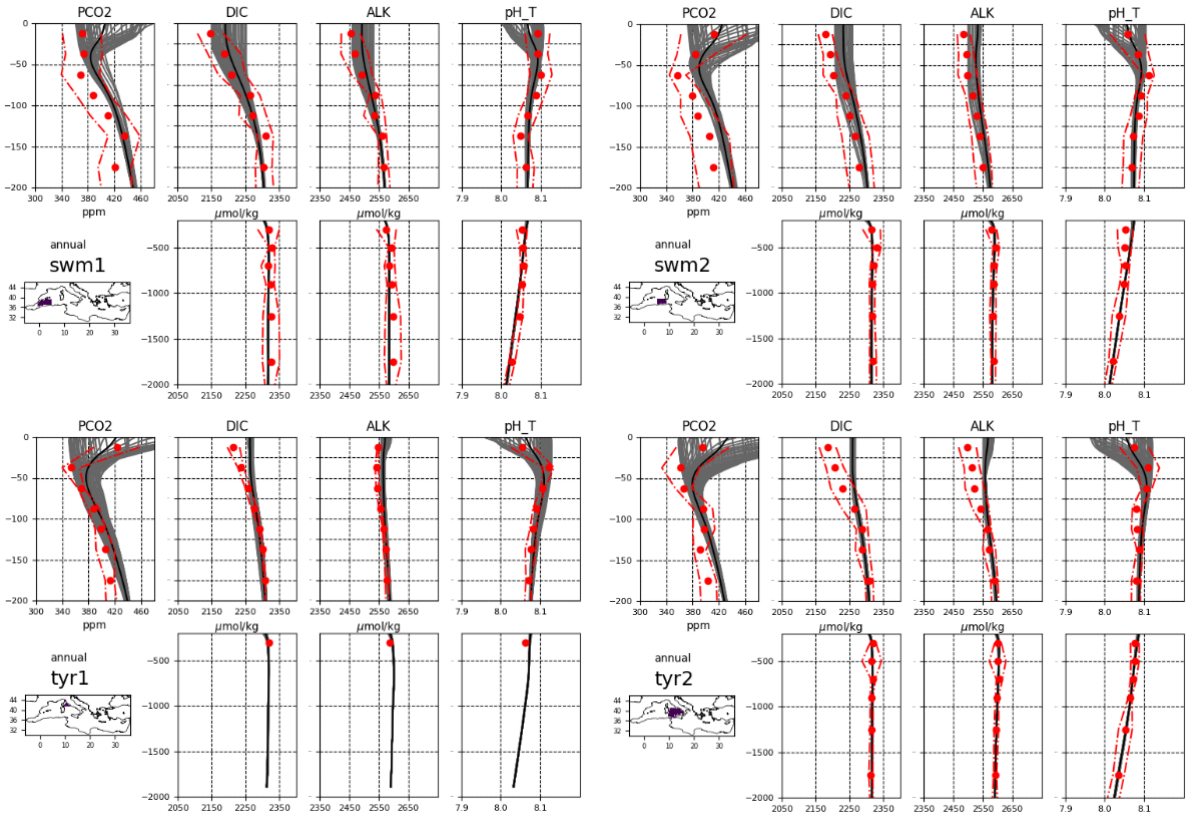

Figure IV.16.2 *(cont.) See above.*

V. SYSTEM'S NOTICEABLE EVENTS, OUTAGES OR CHANGES

Date	Change/Event description	System version	other
25/09/2017	First release of Mediterranean Sea biogeochemical analysis and forecast at 1/24° including assimilation of satellite chlorophyll over the entire domain	MedBFM2	V3.2 version
30/04/2018	Changes in the physical model (see CMEMS-MED-QUID-006-013 v1.1) and recalibration of boundary condition at the Atlantic buffer.	MedBFM2.1	V4.1 version
28/01/2018	Upgrade of the BFM model to the official version 5. Open boundary condition at the Dardanelles Strait consistently with the Med-PHY configuration.	MedBFM3.0	Q2/2019
06/12/2019	Upgrade of the 3DvarBio data assimilation scheme with assimilation of BGC-Argo floats data and daily forecast production cycle	MedBFM3.1	Q1/2020
15/01/2021	Upgrade of boundary condition in the Atlantic Ocean. Addition of new products (ammonium, silicate and zooplankton carbon biomass). Update of the off-line coupling with the physical system by considering tide and new physical data assimilation.	MedBFM3.2	Q2/2021
03/09/2021	Release of version Q4/2021 of the Med-biogeochemistry with the addition of the daily discharges of nutrients and carbonate system variables for the Po River (Adriatic Sea). No substantial changes in the quality of the NRT product.	MedBFM3.2	Q4/2021
31/08/2022	Release of version Q4/2022 of the Med-biogeochemistry with the addition of the optical component and the assimilation of BGC-Argo oxygen profiles. Increase of quality of oxygen. No substantial changes in the quality for the other variable.	MedBFM4.0	Q4/2022
16/6/2023	Release of version Q4/2023 of the Med-biogeochemistry with improved bio-optical component, and the addition of carbon biomass and chlorophyll concentration of 4 phytoplankton functional types (PFTs).	MedBFM4.0	Q4/2023

VI. QUALITY CHANGES SINCE PREVIOUS VERSION

The present version differs from the previous one for the following points.

- The present version of the Mediterranean Sea Analysis and Forecast BGC product includes 22 variables. Four new variables are validated: chlorophyll concentration of the four phytoplankton functional types (diatoms, dinoflagellates, nanoflagellates, and picophytoplankton).
- The new tuning of bio-optical component of the OGSTM-BFM model has improved light attenuation coefficient and the metrics related to vertical phytoplankton dynamics (i.e., vertical profile RMSD, DCM, …). Surface chlorophyll is not improved by the new bio-optical tuning. Changes in net primary production cannot be fully assessed due to lack of enough measurements.
- No substantial changes on product quality are observed in the other variables (i.e., nutrients and carbonate system variables) after the new tuning.

VII. REFERENCES

Álvarez, E., Cossarini, G., Teruzzi, A., Bruggeman, J., Bolding, K., Ciavatta, S., Vellucci, V., D'Ortenzio, F., Antoine, D., Lazzari, P., 2023. Chromophoric dissolved organic matter dynamics revealed through the optimization of an optical-biogeochemical model in the NW Mediterranean Sea. Biogeosciences Discussions 1–43. https://doi.org/10.5194/bg-2023-48

Álvarez, E., Lazzari, P., Cossarini, G., 2022. Phytoplankton diversity emerging from chromatic adaptation and competition for light. Progress in Oceanography, 204, 102789

Álvarez, M.; Sanleón-Bartolomé, H.; Tanhua, T.; Mintrop, L.; Luchetta, A.; Cantoni, C.; Schroeder, K.; Civitarese, G., 2014. The CO2 system in the Mediterranean Sea: a basin wide perspective, Ocean Science, 10(1), pp.69-92

Amadio, C., Teruzzi, A., Pietropolli, G., Manzoni, L., Coidessa, G., Cossarini, G., 2023. Combining Neural Networks and Data Assimilation to enhance the spatial impact of Argo floats in the Copernicus Mediterranean biogeochemical model. EGUsphere 1–28. https://doi.org/10.5194/egusphere-2023-1588

Antoine, D., & Vellucci, V. , 2021. BOUSSOLE project: HPLC dataset. Retrieved November 29, 2022, from http://www.obs-vlfr.fr/Boussole/html/boussole_data/other_useful_files.php

Artuso, F., Chamard, P., Piacentino, S., Sferlazzo, D. M., De Silvestri, L., di Sarra, A., et al., 2009. Influence of transport and trends in atmospheric CO2 at Lampedusa. Atmos. Environ. 43, 3044–3051. doi: 10.1016/j.atmosenv.2009.03.027

Bakker, D. C. E., Pfeil, B. Landa, C. S., et al., 2016. A multi-decade record of high quality fCO2 data in version 3 of the Surface Ocean CO2 Atlas (SOCAT). Earth System Science Data 8: 383-413. doi:10.5194/essd8-383-2016.

Behrenfeld, M., & Dall´Olmo, G. (2020). BOUM08 HLPC dataset. Retrieved January 28, 2021, from https://seabass.gsfc.nasa.gov/archive/OSU/VF/archive

Bergametti, G., Remoudaki, E., Losno, R., Steiner, E., Chatenet, B., 1992. Source, transport and deposition of atmospheric Phosphorus over the northwestern Mediterranean, J. Atmos. Chem., 14, 501–513.

Bittig HC, Maurer TL, Plant JN, Schmechtig C, Wong APS, Claustre H, Trull TW, Udaya Bhaskar TVS, Boss E, Dall'Olmo G, Organelli E, Poteau A, Johnson KS, Hanstein C, Leymarie E, Le Reste S, Riser SC, Rupan AR, Taillandier V, Thierry V and Xing X, 2019. A BGC-Argo Guide: Planning, Deployment, Data Handling and Usage. Front. Mar. Sci. 6:502. doi: 10.3389/fmars.2019.00502

Bellacicco, M., Vellucci, V., Scardi, M., Barbieux, M., Marullo, S., D'Ortenzio, F., 2019. Quantifying the Impact of Linear Regression Model in Deriving Bio-Optical Relationships: The Implications on Ocean Carbon Estimations. Sensors 19, 3032. https://doi.org/10.3390/s19133032

Bosc, E., Bricaud, A., & Antoine, D., 2004. Seasonal and interannual variability in algal biomass and primary production in the Mediterranean Sea, as derived from 4 years of SeaWiFS observations. Global Biogeochemical Cycles, 18(1).

Boss, E., & Claustre, H., 2012. *TARA-Oceans-Expedition HPLC dataset*. *SeaBASS*. https://doi.org/10.5067/SeaBASS/TARA_OCEANS_EXPEDITION/DATA001

Boss, E., & Claustre, H., 2014. *TARA-Mediterranean HPLC dataset*. *SeaBASS*. https://doi.org/10.5067/SeaBASS/TARA_MEDITERRANEAN/DATA001

Buga L., G. Sarbu, L. Fryberg, W. Magnus, K. Wesslander, J. Gatti, D. Leroy, S. Iona, M. Larsen, J. Koefoed Rømer, A.K. Østrem, M. Lipizer, A. Giorgetti, 2018: EMODnet Thematic Lot n° 4/SI2.749773 EMODnet Chemistry Eutrophication and Acidity aggregated datasets v2018 doi: 10.6092/EC8207EF-ED81-4EE5-BF48-E26FF16BF02E

Christaki, U., Giannakourou, A., Van Wambeke, F., & Grégori, G., 2001. Nanoflagellate predation on auto-and heterotrophic picoplankton in the oligotrophic Mediterranean Sea. *Journal of Plankton Research*, *23*(11), 1297-1310.

Colella, S., 2006: La produzione primaria nel Mar Mediterraneo da satellite: sviluppo di un modello regionale e sua applicazione ai dati SeaWiFS, MODIS e MERIS, Phd Thesis, Universita Federico II Napoli, 162 pp.

Colella S, Falcini F, Rinaldi E, Sammartino M, Santoleri R , 2016. Mediterranean Ocean Colour Chlorophyll Trends. PLoS ONE 11(6): e0155756. doi:10.1371/journal.pone.0155756

Copin-Montegut C., 1993. Alkalinity and carbon budgets in the Mediterranean Sea. Global Biogeochemical Cycles, 7(4), pp. 915-925.

Cornell, S., Rendell, A., Jickells, T., 1995. Atmospheric inputs of dissolved organic Nitrogen to the oceans, Nature, 376, 243–246.

Cossarini, G., Lazzari, P., Solidoro, C., 2015. Spatiotemporal variability of alkalinity in the Mediterranean Sea. Biogeosciences, 12(6), 1647-1658.

Cossarini, G., Mariotti, L., Feudale, L., Mignot, A., Salon, S., Taillandier, V., et al. , 2019. Towards operational 3D-Var assimilation of chlorophyll Biogeochemical-Argo float data into a biogeochemical model of the Mediterranean Sea. Ocean Model. 133, 112–128. doi: 10.1016/j.ocemod.2018.11.005

Crise, A., Solidoro, C., and Tomini, I. 2003.: Preparation of initial conditions for the coupled model OGCM and initial parameters setting, MFSTEP report WP11, subtask 11310.

de la Paz, M., Huertas, E.M., Padín, X.-A., Gónzalez-Dávila, M., Santana-Casiano, M., Forja, J.M., Orbi, A., Pérez, F.F., Ríos, A.F., 2011: Reconstruction of the seasonal cycle of air–sea CO2 fluxes in the Strait of Gibraltar, In Marine Chemistry, Volume 126, Issues 1–4, Pages 155-162.

DiCicco, A., Sammartino, M., Marullo, S., & Santoleri, R., 2017. Regional Empirical Algorithms for an Improved Identification of Phytoplankton Functional Types and Size Classes in the Mediterranean Sea Using Satellite Data. *Front Mar Sci*, *4*, 126. https://doi.org/10.3389/fmars.2017.00126

Dolan JR., Vidussi F. , Claustre H., 1999. Planktonic ciliates in the Mediterranean Sea: longitudinal trends Deep-Sea Research I 46 (1999) 2025}2039

D'Ortenzio, Fabrizio, David Antoine, and Salvatore Marullo, 2008; "Satellite-driven modeling of the upper ocean mixed layer and air–sea CO2 flux in the Mediterranean Sea." *Deep Sea Research Part I: Oceanographic Research Papers* 55.4: 405-434.

Dutkiewicz, S., Hickman, A.E., Jahn, O., Gregg, W.W., Mouw, C.B., Follows, M.J., 2015. Capturing optically important constituents and properties in a marine biogeochemical and ecosystem model. Biogeosciences 12, 4447–4481. https://doi.org/10.5194/bg-12-4447-2015

Foujols, M.-A., Lévy, M., Aumont, O., Madec, G., 2000. OPA 8.1 Tracer Model Reference Manual. Institut Pierre Simon Laplace, pp. 39.

Garcia, H. E., K. Weathers, C. R. Paver, I. Smolyar, T. P. Boyer, R. A. Locarnini, M. M. Zweng, A. V. Mishonov, O. K. Baranova, D. Seidov, and J. R. Reagan, 2018. World Ocean Atlas 2018, Volume 4: Dissolved Inorganic Nutrients (phosphate, nitrate and nitrate+nitrite, silicate). A. Mishonov Technical Ed.; NOAA Atlas NESDIS 84, 35 pp.

Gregg, W. W. and Casey, N. W., 2009: Skill assessment of a spectral ocean-atmosphere radiative model, J. Marine Syst., 76, 49–63, https://doi.org/10.1016/j.jmarsys.2008.05.007.

Guerzoni, S., Chester, R., Dulac, F., Herut, B., Loÿe-Pilot, M.-D., Measures, C., Migon, C., Molinaroli, E., Moulin, C., Rossini, P., Saydam, C., Soudine, A., Ziveri, P., 1999. The role of atmospheric deposition in the biogeochemistry of the Mediterranean Sea. Prog. Oceanogr., 44 (1-3): 147-190.

Herut, B. and Krom, M., 1996: Atmospheric input of nutrients and dust to the SE Mediterranean, in: The Impact of Desert Dust Across the Mediterranean, edited by: Guerzoni, S. and Chester, R., Kluwer Acad., Norwell, Mass., 349–358.

Huertas, I. E., Ríos, A. F., García-Lafuente, J., Makaoui, A., Rodríguez-Gálvez, S., Sánchez-Román, A., Orbi, A., Ruíz, J., and Pérez, F. F., 2009: Anthropogenic and natural CO2 exchange through the Strait of Gibraltar, Biogeosciences, 6, 647-662.

Kempe, S., Pettine M., Cauwet, G., 1991. Biogeochemistry of european rivers. In Degensempe & Richey eds, biogeochemistry of Major World Rivers, SCOPE 42 John Wiley 169-211

Kourafalou, V. H., & Barbopoulos, K., 2003. High resolution simulations on the North Aegean Sea seasonal circulation. In Annales Geophysicae (Vol. 21, No. 1, pp. 251-265).

Krasakopoulou E., Souvermezoglou E., Giannoudi L., Goyet C., 2017. Carbonate system parameters ad anthropogenic CO2 in the North Aegean Sea during October 2013. Continental Shelf Research, 149, 69-81.

Lazzari, P., Teruzzi, A., Salon, S., Campagna, S., Calonaci, C., Colella, S., Tonani, M., Crise, A. 2010. Pre-operational short-term forecasts for the Mediterranean Sea biogeochemistry. Ocean Science, 6, 25-39.

Lazzari, P., Solidoro, C., Ibello, V., Salon, S., Teruzzi, A., Béranger, K., Colella, S., and Crise, A., 2012. Seasonal and inter-annual variability of plankton chlorophyll and primary production in the Mediterranean Sea: a modelling approach. Biogeosciences, 9, 217-233.

Lazzari, P., Solidoro, C., Salon, S., Bolzon, G., 2016. Spatial variability of phosphate and nitrate in the Mediterranean Sea: a modelling approach. Deep Sea Research I, 108, 39-52.

Lazzari, P., Salon, S., Terzić, E., Gregg, W. W., D'Ortenzio, F., Vellucci, V., Organelli, E., and Antoine, D., 2021: Assessment of the spectral downward irradiance at the surface of the Mediterranean Sea using the radiative

Ocean-Atmosphere Spectral Irradiance Model (OASIM), Ocean Sci., 17, 675–697, https://doi.org/10.5194/os-17-675-2021.

Lazzari, P., Álvarez, E., Terzić, E., Cossarini, G., Chernov, I., D'Ortenzio, F., & Organelli, E., 2021. CDOM spatiotemporal variability in the Mediterranean Sea: a modelling study. Journal of Marine Science and Engineering, 9(2), 176.

Loÿe-Pilot, M. D., J. M. Martin, and J. Morelli, 1990. Atmospheric input of inorganic nitrogen to the western Mediterranean. Biogeochem., 9: 117-134.

Mazzocchi M. G., Siokou I., Tirelli V., Bandelj V., de Puelles M. F., Örek Y. A., de Olazabal A., Gubanova A., Kress N., Protopapa M., Solidoro C., Taglialatela S., Terbiyik Kurt T., 2014. Regional and seasonal characteristics of epipelagic mesozooplankton in the Mediterranean Sea based on an artificial neural network analysis. *Journal of Marine Systems*, *135*, 64-80

Meybeck M., Ragu A., 1995 River Discarges to the Oceans: An Assessment of suspended solids, major ions and nutrients UNEP STUDY

Melaku Canu, D., Ghermandi, A., Nunes, P. A. L. D., Lazzari, P., Cossarini, G., and Solidoro, C. , 2015. Estimating the value of carbon sequestration ecosystem services in the Mediterranean Sea: an ecological economics approach. Glob. Environ. Change 32, 87–95. doi: 10.1016/j.gloenvcha.2015.02.008

Mignot A., F. D'Ortenzio, V. Taillandier, G. Cossarini, S. Salon, L. Mariotti, 2017. Estimation of BGC-Argo chlorophyll fluorescence and nitrate observational errors using the triple collocation method. 6th Euro-Argo Users Meeting July 4-5, 2017 in Paris, France.

Deliverable D4.6: SES land-based runoff and nutrient load data (1980 -2000), edited by Bouwman L. and van Apeldoorn D., 2012 PERSEUS H2020 grant agreement n. 287600.

Olsen, A., R. M. Key, S. van Heuven, S. K. Lauvset, A. Velo, X. Lin, C. Schirnick, A. Kozyr, T. Tanhua, M. Hoppema, S. Jutterström, R. Steinfeldt, E. Jeansson, M. Ishii, F. F. Pérez and T. Suzuki,, 2016. The Global Ocean Data Analysis Project version 2 (GLODAPv2) – an internally consistent data product for the world ocean, Earth Syst. Sci. Data, 8, 297–323, 2016, doi:10.5194/essd-8-297-2016

Olsen, A., Lange, N., Key, R. M., Tanhua, T., Álvarez, M., Becker, S., Bittig, H. C., Carter, B. R., da Cunha, L., Feely, R. A., van Heuven, S., Hoppema, M., Ishii, M., Jeansson, E., Jones, S. D., Jutterström, S., Karlsen, M. K., Kozyr, A., Lauvset, S. K., Lo Monaco, C., Murata, A., Pérez, F. F., Pfeil, B., Schirnick, C., Steinfeldt, R., Suzuki, T., Telszewski, M., Tilbrook, B., Velo, A. and Wanninkhof, R., 2019: GLODAPv2.2019 -- an update of GLODAPv2, Earth Syst. Sci. Data, 11(3), 1437–1461, doi:10.5194/essd-11-1437-2019.

Oreskes, N., Shrader-Frechette, K., and Belitz, K. , 1994. Verification, validation, and confirmation of numerical models in the earth sciences. Science 263, 641–645. doi: 10.1126/science.263.5147.641

Organelli, Emanuele, et al., 2014. "Seasonal dynamics of light absorption by chromophoric dissolved organic matter (CDOM) in the NW Mediterranean Sea (BOUSSOLE site)." Deep Sea Research Part I: Oceanographic Research Papers 91: 72-85.

Peloquin, J. M., Swan, C., Gruber, N., Vogt, M., Claustre, H., Ras, J., et al. , 2013. The MAREDAT global database of high performance liquid chromatography marine pigment measurements. *Earth System Science Data*, *5*, 109–123. https://doi.org/10.5194/essd-5-109-2013

Ribera d'Alcalà M., Civitarese G., Conversano F., Lavezza R., 2003. Nutrient ratios and fluxes hint at overlooked processes in the Mediterranean Sea. Journal of Geophysical Research, 108(C9), 8106, doi:10.1029/2002JC001650.

Salon, S., Cossarini, G., Bolzon, G., Feudale, L., Lazzari, P., Teruzzi, A., Solidoro, C., Crise, A., 2019. Marine Ecosystem forecasts: skill performance of the CMEMS Mediterranean Sea model system. Ocean Sci. Discuss. 1–35. https://doi.org/10.5194/os-2018-145

Schmechtig, C., Poteau, A., Claustre, H., D'Ortenzio, F., Dall'Olmo, G., Boss, E., 2018. Processing Bio-Argo particle backscattering at the DAC level. https://doi.org/10.13155/39468

Schneider, A., Wallace, D. W. R., and Kortzinger, A., 2007: Alkalinity of the Mediterranean Sea, Geophys. Res. Lett., 34, L15608, doi:10.1029/2006GL028842.

Siokou-Frangou, I., Bianchi, M., Christaki, U., Christou, E. D., Giannakourou, A., Gotsis, O., Souvermezoglou, E., 2002. Carbon flow in the planktonic food web along a gradient of oligotrophy in the Aegean Sea (Mediterranean Sea). Journal of Marine Systems 33– 34 (2002) 335–353

Siokou-Frangou, I., Christaki, U., Mazzocchi, M. G., Montresor, M., Ribera d'Alcalà, M., Vaqué, D., & Zingone, A., 2010. Plankton in the open Mediterranean Sea: a review. Biogeosciences, 7, 1543–1586, https://doi.org/10.5194/bg-7-1543-2010.

Siokou, I., Zervoudaki, S., Velaoras, D., Theocharis, A., Christou, E. D., Protopapa, M., & Pantazi, M., 2019. Mesozooplankton vertical patterns along an east-west transect in the oligotrophic Mediterranean sea during early summer. *Deep Sea Research Part II: Topical Studies in Oceanography*, *164*, 170-189.

Somot, S., Sevault, F., Déqué, M., Crépon, M., 2008. 21st century climate change scenario for the Mediterranean using a coupled atmosphere–ocean regional climate model, Global and Planetary Change, 63, 2–3: 112–126.

Souvermezoglou, E., Krasakopoulou, E., Pavlidou, A., 2014. Temporal and spatial variability of nutrients and oxygen in the North Aegean Sea during the last thirty years. Mediterranean Marine Science, 15/4, 805-822.

Teruzzi, A., Dobricic, S., Solidoro, C., Cossarini, G. 2014. A 3D variational assimilation scheme in coupled transport biogeochemical models: Forecast of Mediterranean biogeochemical properties, Journal of Geophysical Research, doi:10.1002/2013JC009277.

Teruzzi, A., Bolzon, G., Salon, S., Lazzari, P., Solidoro, C., Cossarini, G., 2018. Assimilation of coastal and open sea biogeochemical data to improve phytoplankton simulation in the Mediterranean Sea. Ocean Modelling, 132, 46-60

Teruzzi, A., Di Cerbo, P., Cossarini, G., Pascolo, E., Salon, S., 2019. Parallel implementation of a data assimilation scheme for operational oceanography: the case of the MedBFM model system. Computers & Geosciences 124, 103-114.

Tugrul, S., Besiktep,e T., Salihoglu, I., 2002. Nutrient exchange fluxes between the Aegean ad tBlack Seas through the Marmara Sea. Mediterranean Marine Science, 3/1, 33-42.

von Schuckmann, K., Le Traon, P.Y., Smith, N., Pascual, A., Brasseur, P., Fennel, K. and Djavidnia, S., et al., 2018. Copernicus Marine Service Ocean State Report. Journal of Operational Oceanography, 11 (sup1), pp.S1-S142.

Wanninkhof 2014, OCMIP2 design document & OCMIP2 Abiotic HOWTO. Limnol. Oceanograph. Methods, 12, 351-362.

Weiss, R., 1974. Carbon Dioxide in Water and Seawater: The Solubility of a Non-Ideal Gas. Marine Chemistry, 2, 203-215. http://dx.doi.org/10.1016/0304-4203(74)90015-2

World Ocean Atlas, 2013 database, https://www.nodc.noaa.gov/OC5/woa13/

Yalcin B., Artuz M.L., Pavlidou A., Cubuk S., Dassenakis M., 2017. Nutrient dynamics and eutrophication in the Sea of Marmara: data from recent oceanographic research. Science of the Total Environment, 601-602, 405-424.

Zeebe, R.E. and Wolf Gladrow, D., 2001. CO2 in seawater: equilibrium, kinetics, isotopes, Elsevier oceanography series. Elsevier.